PULSED LASER EXCITED FLUORESCENCE OF FLUORANTHENE

A Dissertation

by

Dan Lassiter Philen

Submitted to the Graduate College of
Texas A&M University
in partial fulfillment of the requirment for the degree of

DOCTOR OF PHILOSOPHY

May, 1975

Major Subject: Chemistry

PULSED LASER EXCITED FLUORESCENCE OF FLUORANTHENE

A Dissertation

by

Dan Lassiter Philen

Approved as to style and content by:

R. M. Hedges
(Chairman of Committee)

G. E. Martell
(Head of Department)

Dean Pearce
(Member)

D. C. Conway
(Member)

Philip J. Green
(Member)

May, 1975

ABSTRACT

Pulsed Laser Excited Fluorescence of Fluoranthene (May, 1975)

Dan Lassiter Philen, B.S., Auburn University

Chairman of Advisory Committee: Dr. Richard M. Hedges

A pulsed laser spectroscopy system has been designed, constructed, and applied to the study of the dual fluorescence of fluoranthene. The apparatus incorporates a pulsed molecular nitrogen gas laser, or nitrogen laser pumped dye laser, associated electronics spectrometer, and data processing electronics. The completed experimental arrangement allows for the measurment of energy (wavelength) resolved spectra as well as the determination of decay times - time resolved spectra. The experimental system allows for the detection of fluorescence with higher spectral resolution than is generally possible with conventional excitation sources.

The time resolved and energy resolved spectra of the dual fluorescence of fluoranthene have been characterized. The energy resolved spectrum consists of two easily discernable regions. The s region ($S_2 \rightarrow S_0$) at 3700A to 3950A where the major contribution to the fluorescence originates from transitions $\phi_s \rightarrow \phi_o^{o\omega}$ to totally symmetric vibronic components of the ground state $\phi_o^{o\omega}$, and the ℓ region ($S_1 \rightarrow S_0$) at 4050A to approximately 5400A which represents to contribution to the emission which arises from transitions

$\{\phi_\ell\} \rightarrow \{\phi_\ell^{\ell\omega}\}$ to nontotally symmetric components $\{\phi_\ell^{\ell\omega}\}$ of the ground electronic state.

The decay characteristics of the vibronic lines in the two regions have been determined. Typical of the s region is an anomalously long 140 nsec lifetime compared to a theoretical lifetime of approximately 20 nsec, and typical of the ℓ region is a lifetime of 58 nsec. These results are in good agreement with theoretical predictions for the intermediate level spacing, strong coupling situation.

In each region there are observed short lived lines (lifetimes of from 5 to 34 nsec) which come from unrelaxed excited vibrational levels of the excited electronic states.

The anomalous phosphorescence (wavelength resolved only) of fluoranthene has also been observed.

To

Rossanne

ACKNOWLEDGMENTS

The author would like to express his gratitude to his parents for their encouragment and assistance during his time in school. I am indebted to Robert H. Dinius for his initial encouragement and support as an undergraduate. I would also like to thank Richard M. Hedges for his patience and understanding during the course of my graduate studies. I would like to acknowledge the Robert A. Welch foundation for financial support of this project; and finally I would like to thank Rossanne for her interest, faith, and patience with me during the course of this work.

TABLE OF CONTENTS

LIST OF TABLES

LIST OF FIGURES

CHAPTER I

INTRODUCTION

In the past few years there has been considerable interest, both theoretical and experimental, in fluorescence from higher excited singlet states of molecular systems. In 1950 M. Kasha[1] proposed that regardless of the singlet state initially excited, the fluorescence occurs from the lowest excited π-electronic singlet state. That is, fluorescence emission is independent of excitation energy, and until recently; exceptions to this generalization, now called "Kasha's rule", were limited to azulene and its derivatives. Azulene, however, has its first excited singlet state, S_1, 14,000 cm^{-1} above the ground state and the second excited singlet, S_2, 14,000 cm^{-1} above that; so it does not represent the typical case found in most aromatic hydrocarbons. Normally the $S_0 \rightarrow S_1$, ground to first excited singlet state, energy gap is large compared to the energy separation of the higher singlet states. As a result, internal conversion from a higher singlet state to S_1 takes place on a much shorter time scale than fluorescence emission and Kasha's rule is obeyed.

Fluorescence from higher singlet states is difficult to record experimentally, not only because it is expected to be of low intensity, but there may be interference from the background exciting

---

The journal used as a pattern for style and format is the Journal of Chemical Physics.

light in the region where one would expect to observe fluorescence. Also, self absorption of the $S_2 \rightarrow S_0$ fluorescence into the $S_0 \rightarrow S_1$ absorption band and reemission as $S_1 \rightarrow S_0$ fluorescence ordinarilly is indistinguishable from $S_2 \rightarrow S_1$ internal conversion followed by $S_1 \rightarrow S_0$ fluorescence. (See Figure 1.) Compounds which have a strong first absorption band obviously disqualify themselves as subjects for such a study.

Compounds of interest for the study of $S_2 \rightarrow S_0$ fluorescence should have the common feature that the first band in the absorption spectrum is very weak, and hence the lowest singlet state carries only a small transition moment with respect to the ground state, which usually means that it has a low rate constant for radiative transitions. Close to it in energy should lie the second excited singlet state with an absorption that is strongly allowed.

With these criteria in mind, several theoretical explanations of dual fluorescence[2-7] have been formulated, but further development of a general theory has been hampered by insufficient supportative experimental evidence.

Historically, studies of fluorescing systems have been ones of extremes. The simplest case is the atomic system (See Figure 2.) in which the electronic energy states are widely separated, relaxation between states is slow, and radiative transitions between states (fluorescence) is readily observed. Prime examples of this

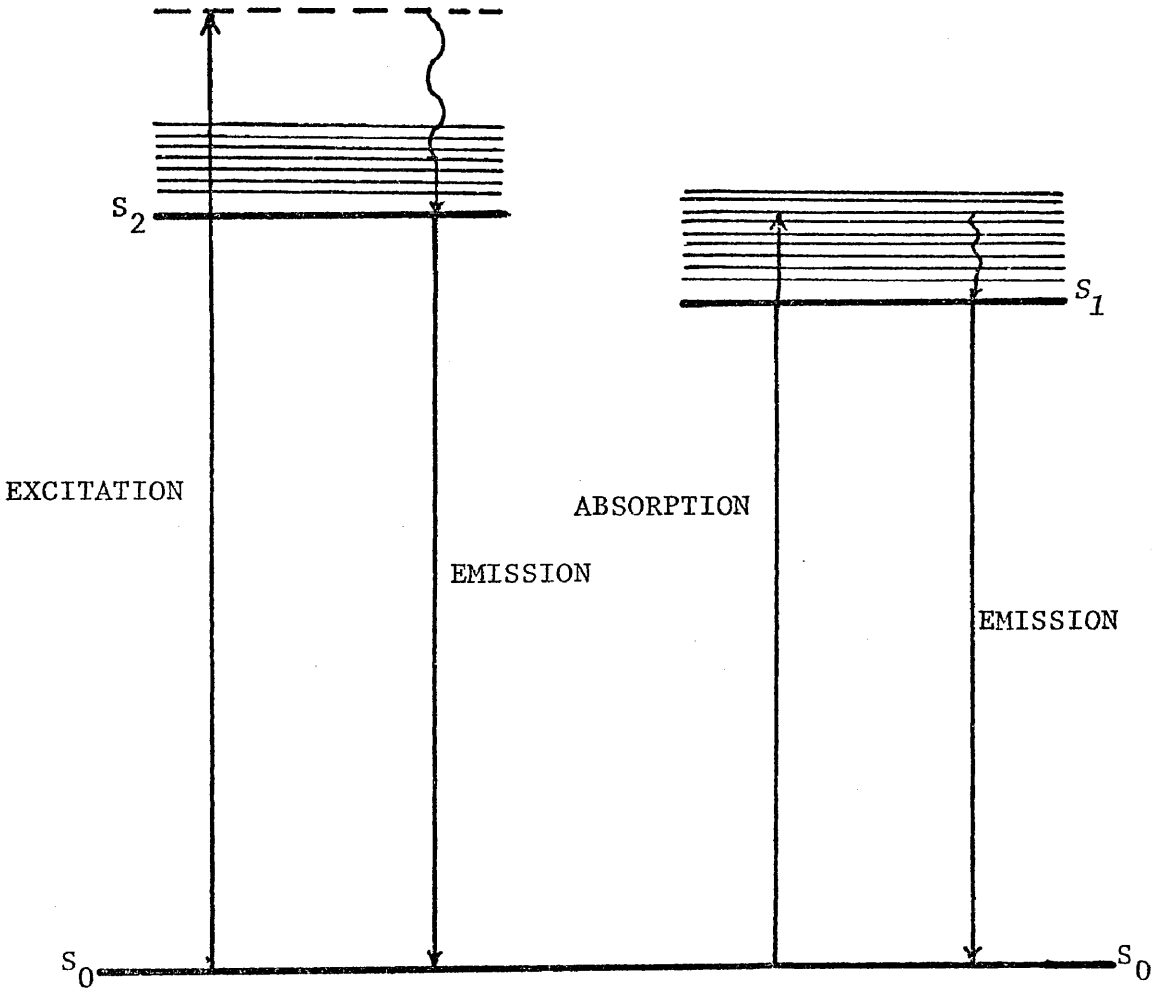

Figure 1. Absorption of emission from the second excited singlet state.

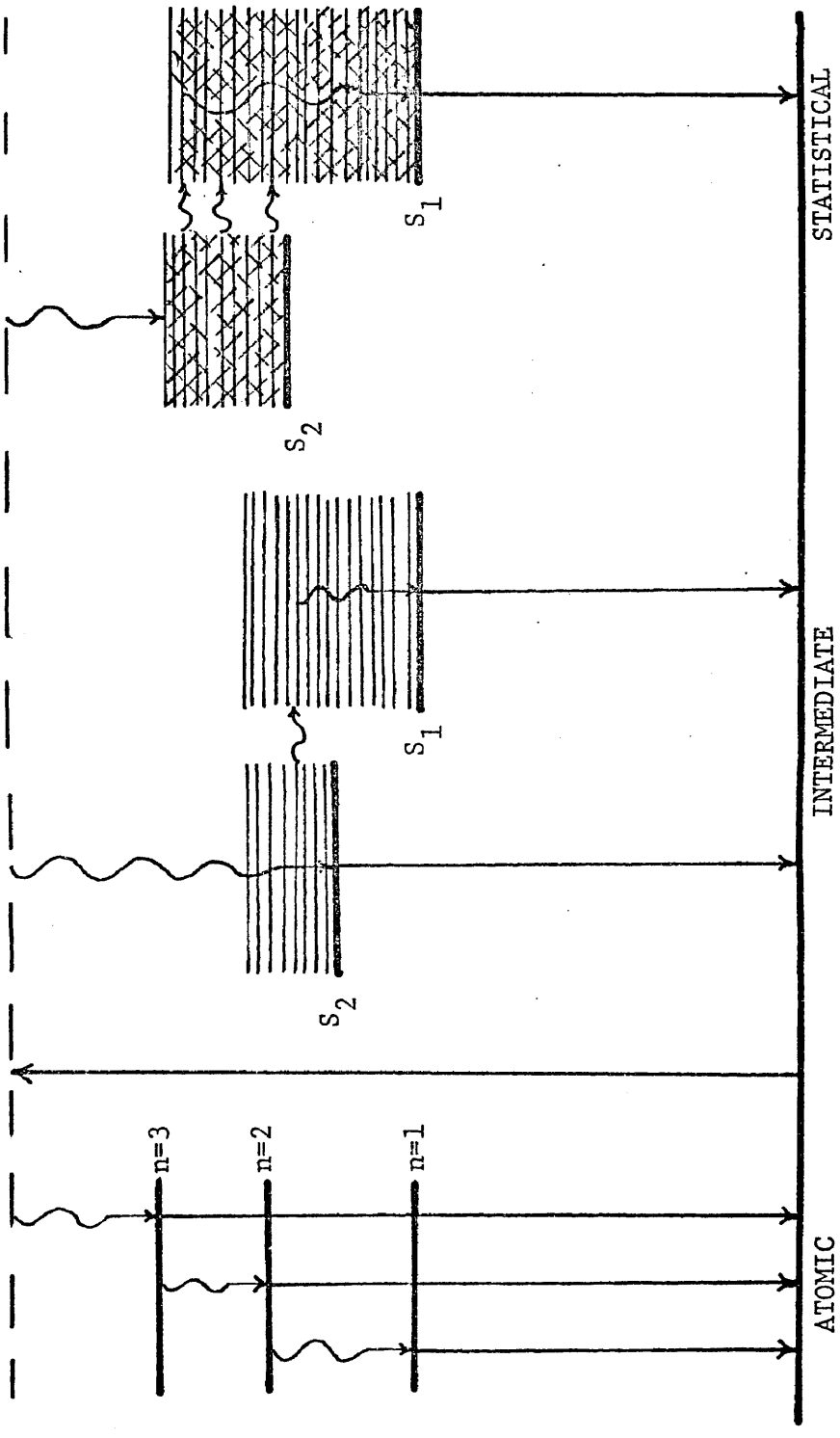

Figure 2. Radiative characteristics of fluorescence from atomic and molecular systems.

are the Lyman, Balmer, etc. series in hydrogen; and argon-ion and helium-neon lasers use this effect in the principle of their operation.

The other extreme, which exists in molecular systems, is the so-called "statistical limit" case[7] (See Figure 2.) in which each electronic state contains a large number of vibrational and rotational energy states. The density of states is sufficiently large such that relaxation from higher electronic states is faster than the time required for fluorescence, and consequently, the molecular system relaxes to the lowest lying excited electronic state. Fluorescence occurs from this state to the ground state and Kasha's rule is obeyed.

The situation involving dual fluorescence is intermediate between these two extremes and is generally referred to as the "dense intermediate case". In this situation the vibrational energy levels of the electronic state are more widely spaced than in the statistical limit but obviously more dense than the atomic case. Energy levels of a higher excited state may be coupled to energy levels of other overlaping states allowing relaxation to occur; but due to the lower density of states, the interstate coupling is less extensive, relaxation is slower, and radiative transitions may also occur from the higher excited state as fluorescence.

While direct experimental observations of dual fluorescence have been slow, there is nevertheless a small but growing list

of compounds which have been shown to exhibit $S_2 \rightarrow S_0$ fluorescence. A list of compounds which have been observed to show dual fluorescence is in Table 1.

Part of the problem in observing dual fluorescences has been in the development of new techniques and processes for spectroscopy. Indeed, the application of lasers to problems in chemistry seems to coincide with the experimental observation of dual fluorescence. To this end, it has been necessary in these experiments to construct the appropriate lasers and assemble the proper processing electronics to carry out a detailed study of dual fluorescence.

It is reasonable to ask whether a laser is necessary for the observation of fluorescence. The following simple calculation indicates that this effect probably would have been very difficult, if not impossible, to observe prior to the development and application of high power nitrogen gas and tunable dye lasers to spectroscopy. Presently available pulsed dye lasers are capable of producing an average spectral irradiance of 0.2 watt per square centimeter per angstrom, whereas intense white-light sources, such as a 1000-watt xenon lamp, can only produce 2 microwatts per square centimeter per angstrom at a distance of 50 cm from the excitation zone. Hence, visible tunable lasers are at least 10^5 times brighter than conventional white-light sources and pulsed molecular nitrogen gas lasers are at least ten times brighter still. That is, they are one million times brighter than white-light sources. Moreover, this comparison does not include the large losses incurred in passing the

Table 1. Compounds which have been shown to exhibit dual fluorescence.

Compound	Reference
Pyrene	8, 9, 11, 14
3,4-benzpyrene	6, 8, 9, 13, 14
1,12-benzperylene	8, 10, 13
1,2-benzanthracene	8, 15
Ovalene	15
Naphthalene	12
20-methlycholanthrene	8
Coronene	8*

* The data on coronene is not conclusive.

white light through a monochromator in order to narrow the bandwidth[16].

In addition to the obvious power advantage of lasers, they are already monochromatic so that no power is lost in having to use a monochromator to narrow the bandwidth. Even if white-light sources could be made to be as bright as lasers, and as spectrally narrow, lasers would still have the advantage when time resolution is needed. The time duration of a molecular nitrogen gas laser pulse in typically 10 ns., which approaches the theoretical delta pulse assumed by spectroscopists for many applications. Thus, the pulsed nitrogen laser is ideally suited for lifetime measurments where a highly intense light pulse is needed for a short time only, and then the resulting fluorescence may be analyzed without the interference from the background of the exciting light. Typical flashlamps have pulse durations on the order of milliseconds which is about the limit of mechanical choppers. Therefore, the nitrogen laser with its very narrow spectral line-width, short pulse duration, and high power output (photon flux) is well suited to spectroscopic applications where precise measurments of fluorescence characteristics are needed.

A very detailed description of the theory, design and construction, and performance parameters of the molecular nitrogen gas laser and the organic dye laser is given in appendices I and II respectively.

CHAPTER II

THEORY OF DUAL FLUORESCENCE

The thermal back population as a principle mechanism of excitation for dual fluorescence has been largely disproved; however, the early experiments were discussed in this light, and it would be helpful to investigate this background.

Birks[15] states that the reason that compounds which exhibit dual fluorescence have a small ($<3000cm^{-1}$) energy separation between S_2 and S_1, is so that efficient thermally activated $S_1 \rightarrow S_2$ internal conversion can occur during the excited lifetime of S_1. The thermal activation of the S_2 fluorescence in 1,12-benzperylene and 3,4-benzpyrene has been proposed by Easterly, Christophoru, and Carter,[13] and they concluded that the $S_2 \rightarrow S_0$ fluorescence of 3,4-benzpyrene was thermal in origin, originating by back population from S_1. They note that the S_2 fluorescence spectrum has very distinct transitions with the same energy spacings present in the S_1 spectrum. To support this observation, they state that, "Since the $S_2 \rightarrow S_0$ transition must, moreover, end at the same upper vibrational levels of S_0 as do the $S_1 \rightarrow S_0$ transitions, we assume that the low energy part of the $S_2 \rightarrow S_0$ emission spectrum resembles the general shape of the low energy part of the $S_1 \rightarrow S_0$ emission spectrum." The ratio of F_2 to F_1 (fluorescence from $S_2 \rightarrow S_0$ and $S_1 \rightarrow S_0$ respectively) was also determined, as any thermal population of S_2 would make F_2 more intense and steal intensity from S_1. However, they measured the intensity of S_1 to decrease from 1.4 to 0.5 in relative units on

going from -90°C to +90°C. The S_2 intensity increased from 0.06 to 0.2 in relative units over the same temperature range. Thus, the ratio, F_2/F_1 becomes a slightly increasing function, and the resulting ratio appears to give an excessive emphasis. That is, any real increase in F_2 intensity is blown out of proportion by the also decreasing F_1 intensity.

Easterly et al., thus assigned the S_2 level in 3,4-benzpyrene to a level 1240 cm^{-1} above S_1, and it seems that thermal population may be a plausable argument in this case. To summarize Easterly's paper[13] he states that, "From the data and the analysis presented, it is reasonable to conclude...the fluorescence quantum yield from S_2 is primarily due to an indirect fluorescence originating from thermal repopulation of S_2 from S_1."

In a later paper, van den Bogaardt[17] showed that at least part of the emission attributed to S_2 emission by Easterly was due to a "hot" band emission of the first excited singlet state. The term "hot" used throughout this discussion is not the general meaning of "hot" but is intended to denote an excited vibrational level of an electronic state S_n', which has not undergone relaxation or which is vibrationally unrelaxed. Van den Bogaardt et al., studied the relative yields and fluorescence lifetimes of the S_2 and S_1' emissions of 3,4-benzpyrene from 77°K to 293°K and concluded that the population of these states was not according to thermal equilibrium. It was also shown that upon excitation into

S_2 at lower temperatures, the total S_1' emission exceeded the amount obtained by thermal population from S_1; and, at temperatures where the thermal component was negligible, the S_1' intensity approximated a constant value. This points to a direct emission from S_1' levels after population by internal conversion from the excited S_2 levels. Thus, it is concluded that after excitation into S_2 and internal conversion into the first excited electronic singlet state, a small fraction of molecules is found in a "hot" S_1' state for which the vibrational deactivation is rather slow. Van den Bogaardt et al. very convincingly proved that the anomalous fluorescence of 3,4-benzpyrene consists of two parts: a hot $S_1 \rightarrow S_0$ fluorescence at $h\omega$=520 cm^{-1} and the $S_2 \rightarrow S_0$ emission.

Hoytink [18] showed that the same mistake was made for 1,12-benzperylene and that the larger part of the anomalous fluorescence was from a "hot" $S_1 \rightarrow S_0$ emission. Hoytink did not collect new data as van den Bogaardt had done, but used Easterly's data and determined that the main modes which contribute to the vibrational pattern are: $h\omega_1 \simeq$ 600 cm^{-1}, $h\omega_2 \simeq$800 cm^{-1}, and $h\omega_3$, the symmetrical C-C stretching mode at 1400 cm^{-1}.

Since $h\omega_1 + h\omega_2 = h\omega_3$ and the gap between S_1 and S_2 in 1,12-benzperylene is practically equal to 1400 cm^{-1}, the spectrum can easily be unravelled. The procedure used by Hoytink was to add up the 1400 cm^{-1} symmetrical progressions of the main peaks in the spectrum. These progressions are known to dominate the Franck-Condon

pattern, and by adding up all the contributions, a very good qualitative illustration of the observed spectrum was obtained.

Van den Bogaardt et al.[17] found that above 200°K the "anomalous" fluorescence was the same whether the molecules were excited into the zero level of S_1 or at higher frequencies. This indicates that the "anomalous" emission is entirely due to thermal population from S_1. Since Easterly et al.[13] investigated the hot fluorescence of 1,12-benzperylene in the temperature region 183°K-363°K, we can safely assume that their observations are also due to a thermal equilibrium between S_1 and the "hot" states.

Hoytink[18] also commented on the assumption made by Easterly et al.,[13] that both the S_1 and S_2 emissions terminate in the same upper vibrational levels of S_0. It was shown that the major part of the $S_1 \rightarrow S_0$ fluorescence is of vibronic origin whereas the strongly allowed $S_2 \rightarrow S_0$ transitions give rise to familiar symmetric progressions. Even if the vibronic contribution to $S_1 \rightarrow S_0$ were negligible, the statement would still hold because the $S_1 \rightarrow S_0$ transition is of L_b type symmetry whereas the $S_2 \rightarrow S_0$ transition is of the L_a type. In concluding Hoytink's paper[18], he remarks that, "Unfortunately...all data derived by Easterly et al. from the analysis of their spectra have no real physical significance and a careful reinspection is required."

It was thought that if S_2 were thermally populated from S_1, then it should be possible to excite into S_1 just below S_2 and observe emission from S_2. The dye laser (See appendix AII.) was set up

using α-NND[19] as a dye which lases at 3900A. The object was to look for emission from S_2 which had originated by thermal population from S_1. Unfortunately, no such emission was observed, but this is in line with the findings of van den Bogaardt[17] and Hoytink[18]. It thus seems that the process of thermal population of S_2 from S_1 is not as generally applicable as had been supposed, and thus, it should not be assumed to be a general explanation for the observation of dual fluorescences.

Jortner[3] has taken another approach to studying the processes involved in dual fluorescence in which the vibronic coupling of adjacent energy states is considered. Attention has been focused on the interesting situation where a small electronic energy gap exists between two electronic states of a large molecule. Typical examples in this class are acene aromatics[11] and naphthalene[12] where the spacings between the S_1 and S_2 states is less than 3000 cm^{-1}.

In considering the effects of intramolecular coupling, between nearly degenerate zero-order vibronic levels, which correspond to different electronic configurations within a polyatomic molecule, one should realize that the occurrence of interstate coupling provides a necessary but by no means sufficient condition for intramolecular relaxation. The anomalously long radiative lifetimes of the lowest spin allowed excited states of some triatomic molecules result from the redistribution of the intensity of an optically active zero-order state among a large number of

molecular eigenstates, which are well separated relative to their radiative widths, and which are active in both absorption and emission. However, no intramolecular relaxation occurs in this case[6].

The irreversible intramolecular decay occurs in the statistical limit, (Figure 2) and is characterized by an excited electronic state of a large molecule separated by a large energy gap from lower lying states.

The intermediate level structure situation is characterized by two excited electronic states of a large molecule which are separated by a small (less than 4000 cm^{-1}) energy gap. One expects that strong coupling will exist between a zero-order level ϕ_s (corresponding to a vibronic level of S_2) and a small number of zero-order vibronic levels $\{\phi_\ell\}$, which represent a subset of the vibronic levels of S_1.

As the S_2-S_1 electronic energy gap is small, the interstate coupling matrix elements are determined by appreciable Franck-Condon vibrational overlap factors and are thus expected to be large ($\simeq$10 cm^{-1})[6]. Thus, it is expected that the radiative decay of the second excited singlet state of a large molecule which corresponds to this "dense intermediate case" will exhibit the characteristics of the small molecule limit encountered within a large molecule.[3]

The intermediate situation is characterized by the following features:

1. No intramolecular relaxation between the S_2 level and the S_1 manifold is expected to occur.

2. Two spectral regions in the radiative decay spectrum, resulting from excitation into the S_2 state can be distinguished: a) the "s" region where the major contribution to the fluorescence decay originates from transitions $\phi_s \rightarrow \phi_o^{o\omega}$ to totally symmetric vibronic components $\phi_o^{o\omega}$ of the ground electronic state; b) the "ℓ" region where the contribution to emission arises from transitions $\{\phi_\ell\} \rightarrow \{\phi_o^{\ell\omega}\}$ to nontotally symmetric vibronic components $\phi_o^{\ell\omega}$ of the ground electronic state. Resonance fluorescence from the second excited singlet state is amenable to experimental observation in the s region.

3. As the decay time of the s states are much shorter than the ℓ states, the short decay time of the zero-order state ϕ_s is now diluted among n+1 levels. That is to say, the resonance yield is inversely proportional to the number, n, of effectively coupled levels.

4. The experimentally observable radiative decay times in the strong coupling intermediate level situation should be approximately equal in the s and ℓ regions, while the oscillator strength for the $S_0 \rightarrow S_2$ transition exceeds that for the $S_0 \rightarrow S_1$ excitation by about one to two orders of magnitude. Also, one should notice that the decay time in the s region will be appreciably lengthened in respect to what one might expect on the basis of the oscillator strength for the $S_0 \rightarrow S_2$ transition.

That is, as the radiative lifetime, τ, is much greater than $\hbar$ divided by the radiative width of the ϕ_s state ($\tau >> \hbar/\Gamma_s$), the experimental decay time in the s region is appreciably lengthened relative to the pure radiative lifetime. (In 3,4-benzpyrene Wannier et al.[6], observe that the energy resolved radiative lifetime in the s region which corresponds to "resonance fluorescence" from the second excited singlet state is appreciably longer, by a factor of $\simeq 5$, than expected on the basis of the integrated oscillator strength for the $S_0 \rightarrow S_2$ transition.)

5. The relative contributions to the quantum yields for emission in the s and ℓ regions are expected to be $R = Y_s/Y_\ell = \Gamma_s/n\langle\Gamma_\ell\rangle$, thus providing a method for estimating the numbers of strongly coupled levels. Here Γ_s and Γ_ℓ are the radiative widths for the s and ℓ regions respectively, n is the number of coupled levels, and $\langle\ \rangle$ denotes an average over the $\{\phi_\ell\}$ manifold.

These predictions for the strongly coupled intermediate case are drastically different from the features of the radiative decay in internal conversion when the $\{\phi_\ell\}$ manifold is "statistical", whereupon the experimental decay in the s region is appreciably shortened relative to the pure radiative lifetime[3]. The intermediate and statistical situations can be experimentally distinguished by measurements of the energy resolved decay times and fluorescence intensity originating from excitation into the lower vibronic components of the second excited singlet state of a large molecule.

In light of this, Wannier et al.[12] investigated the resonance fluorescence from the second excited singlet state of naphthalene. They observed dual fluorescence in which the experimental decay times vary only mildly (by less than a factor of 2) from the s region to the ℓ region. Thus the s region, which exhibits the $S_2 \rightarrow S_0$ decay, is characterized by an anomalously long radiative decay time, which is longer by about one order of magnitude from what might be expected on the basis of the integrated oscillator strength (f=0.1) for the $S_0 \rightarrow S_2$ transition. It was also noted that the ϕ_s level will also be weakly coupled to a large number (10^4-10^5 cm) of vibronic levels of the S_1 electronic configruation and that this weak coupling may contribute a decay channel for the intramolecular relaxation of the ϕ_s state. A part of the observed emission in the ℓ region may originate from this weak coupling. The submanifold $\{\phi_\ell\}$ of strongly coupled S_1 levels leads to the dramatic effect of anomalously long radiative decay time of the second excited singlet state.

In the case of 3,4-benzpyrene[6], naphthalene[12], and benzophenone[20] some "wiggling" of the decay curves was observed which may arise from radiative interference effects between closely spaced levels. The models for the radiative decay of coupled electronic states are an exact analog to the coupled harmonic-oscillator problem in mechanics. In the harmonic-oscillator problem, if just one of the oscillators of a coupled pair is excited initially, the excitation will move from one oscillator

to the other and back again with a frequency which depends on the frequency of the uncoupled oscillators. This periodic amplitude change has an analogy to the coupled states and should be observable for the strong and weak coupling cases.

Whether or not the "beats" arising from these oscillations will be observable in the radiative decay of the excited electronic state is both a theoretical and an experimental problem. That interference effects should be present on some level seems plausible[20]. That they will be sufficiently large compared to the purely exponential portion of the emission and amenable to experimental observation depends of the molecular system studied, the coupling between the levels, and the density of states.

The optimum situation for observation of "quantum beats" should occur when the period of oscillations is on the same time scale as the damping or lifetime. If the period is considerably longer than the lifetime, then the signal will be essentially gone before a single oscillation can be observed. When the period is considerable shorter, the total light emission during the time scale of a few oscillations is small, leading to reduced signal to noise ratio. The second situation is preferable to the first, because one can fit a locally noisy set of data to a long train of oscillations and still obtain a relatively high overall S/N ratio.

Busch et al.[20] observed a wiggling of the decay curves in benzophenone and suspected that this might arise from quantum beats.

Hochstrasser and Wessel[21] undertook a study of the oscillations in the fast decay of benzophenone, but were unable to obtain reproducible oscillations in their decay curves under conditions as close to those of Busch as possible. Thus, Hochstrasser et al.[21] attribute those oscillations that were observed to an experimental artifact rather than to quantum interference; so that the experimental observation of quamtum beats is still in question, but their possibility should not be ruled out. One possibility is that the coupled levels have such a breadth of states that the beats would be expected to damp out after a single oscillation, making their observation difficult.

The theoretical possibilities regarding quantum beats has also been investigated by Rhodes[5]. Rhodes noted that the interaction between a molecule and light leads to a time dependent correlation between the frequency of the absorbed photon and the excitation frequencies of the molecule. The effect of such correlations is that the excited state of the molecule prepared by interaction with a stationary beam of light may strongly depend on the duration τ, of the interaction as well as the frequency distribution of the light.

To illustrate this, consider a beam of light, $I(\omega)$, with intensity I and frequency ω, which has a band width of $\Delta\omega$. Assume that a molecule is initially in its ground state whose transition frequencies lie in the interval $\Delta\omega$. Any two of these states which lie closer than $2\pi\tau^{-1}$ are excited coherently; i.e., as a

superposition of states, however, any state whose nearest neighbor lies farther away than $2\pi\tau^{-1}$ tends to be excited statistically; i.e., with a definite probability, but not as a member of a coherent superposition of states.

The coherence width is defined as $\Delta\omega_c = 2\pi\tau^{-1}$, and if $\Delta\omega$ is the width of $I(\omega)$ then $\Delta\omega_c \leq \Delta\omega$. Suppose the spacing between every pair of levels lying within $\Delta\omega$ is greater than $\Delta\omega_c$; then the excited state at τ is a statistical mixture and the excited states will undergo rediative decay independent of each other and there will be no interference of amplitudes between states. An ensemble of molecules so excited will behave as though a given fraction of the molecules are in each excited state.

The opposite case is one in which all of the allowed excited states lie in a frequency interval smaller than $\Delta\omega_c$; then they are all excited as a coherent superposition with respect to the molecular hamiltonian. It is the time dependence of this non-stationary state with respect to the molecular hamiltonian that is referred to as a radiationless transition.

As an example of the coherence width effect, consider the effects of exciting the vibronic levels of a given electronic state of a molecule. The electronic energy surfaces are taken to be purely harmonic, with the same force constant and the Franck-Condon principle (Condon approximation) is assumed to be valid. The overall width of the electronic absorption band is denoted by $\Delta\omega_a$, the intensity $I(\omega)$ is assumed to be sufficiently

weak so that the total excited state probability is small, and the interval between excited states is simply the vibrational frequency, $\Delta\omega_v$. Consider the following two cases:

1. Small τ: $\Delta\omega > \Delta\omega_c > \Delta\omega_a > \Delta\omega_v$. This corresponds to pulse excitation, whereby τ is so small that the Born-Oppenheimer (vibrational) hamiltonian of the molecule has not had time to change the vibrational state. Thus the vibrational state at time τ is the same as that in the ground electronic state. The electronic state of the molecule at τ is a statistical mixture of the ground and excited electronic states, while the vibrational state is the pure ground vibrational state belonging to the lower electronic surface. If we follow the vibrational state with time ($>\tau$) we find that it oscillates with frequency $\Delta\omega_v$. This is the quantum mechanical analog of the original classical version of the Franck-Condon principle which states that, because the number coordinates tend to remain unchanged during an electronic transition, the transition tends to be vertical from the minimum of the lower potential surface to the side of the upper potential surface.

Now consider that part of the radiative decay of the excited state resulting from transitions back to the initial ground state. This is proportional to the time-dependent excited vibrational state and the ground vibrational state. Therefore, the total intensity due to this transition will oscillate with frequency $\Delta\omega_v$ as the excited state wave packet oscillates back and forth. Since this oscillatory wave packet is actually a superposition of

vibrational states of the excited electronic surface, the oscillatory decay may be regarded as arising from interferences of the time-dependent transition amplitudes from the upper levels.

2. Large τ: $\Delta\omega > \Delta\omega_a > \Delta\omega_c$. In this limit the duration of the exciting light is large compared to the vibrational period, and considering that the latter is on the order of $10^{-13} - 10^{-14}$ sec, this is certainly the practical limit attained in all conventional experiments. Since the coherence width is less than the interval for both frequencies, the excited state time τ is a mixture of vibrational states belonging to the upper potential surface rather than a pure coherent superposition. An ensemble of molecules in this state should be interpreted as having a certain fraction in each excited vibronic state, with a distribution determined by the Franck-Condon factors.

The statistical description of the excited state arises because τ is sufficiently large that a close correlation develops between each molecular frequency and the frequency of the absorbed light component. Thus, there tends to be developed a one-to-one correspondence between photon frequences and excited vibronic states.

Another way of expressing this is to say that τ is sufficiently large that the vibrations of the molecule have time to adjust themselves within the interval of time during which absorption is taking place. That is, the nuclei do have time to move during the time of electronic absorption. The Franck-Condon principle simply gives the probability distribution of the excited vibronic

levels, with the most probable level resulting in a classical turning point corresponding to a vertical transition.

Since the state of the molecule is a statistical mixture of eigenstates of the molecular hamiltonian, its time dependence arises solely from coupling with the radiation field. This means that there are no interferences of radiative transition amplitudes from the various excited levels, so the fluorescence decay of the molecule is a weighted mixture of exponential decays from the various excited vibronic states, in contrast to the oscillatory decay of case (1).

These descriptions are not necessarily limited to the isolated molecule, because if solvation leaves the vibronic structure of the absorption spectrum intact, then the description of the excited state at time τ would be essentially the same. However, the dynamics of the excited state following absorption would be different due to the fact that solvent interaction with the molecule leads to vibrational relaxation which competes with radiative decay and excited state oscillations.

Because of the short time required for pulse excitation, the value of the above model experiment is merely instructive. However, if the concept of coherence width is to have any real significance, it should enable us to make predictions about the fluorescence behavior of molecules which can be tested experimentally. Now consider a real case in which the exciting pulses range in duration, τ, from 10^{-12} sec to 10^{-6} sec. Also assume that the

intensity, $I(\omega)$, is essentially constant over the interval $\Delta\omega$ and is the same for each value of τ. (This last condition implies that the light is stationary.) The intensity is small so that the probability of the molecule being excited at τ is small and thus, the effective interaction time of the experiment covers the range of τ.

Suppose that the region $\Delta\omega$ contains only two stationary states of the molecule which are separated by $10^{-2}cm^{-1}$. The radiative widths of each state are taken to be much less than the spacing between them. For the picosecond excitation time, the coherence width of the interaction is $200cm^{-1}$, which is far greater than the state separation. Thus, the excited state character of the molecule at τ, which may be referred to as the spectroscopic state, is a coherent superposition of the two excited states with amplitude given by the radiative absorption amplitude. Since this state is not an eigenstate of the molecular hamiltonian, its probability will depend on time (for $t>\tau$). As a result of both the action of the hamiltonian of the molecule (intramolecular reactions) and interaction with the radiation field (radiative decay), the resulting time dependence of the fluorescence has an oscillatory decay. The oscillations in the fluorescence arise from an alternating constructive and destructive interference of the radiative transition amplitudes from the two excited states. An equivalent description of the oscillation is that the spectroscopic state at τ is an eigenvector of some zeroth-order molecular

hamiltonian, H_0 = H-V, and that the effective intramolecular interaction, V, drives transitions between the spectroscopic state and another zeroth-order molecular state.

In the microsecond experiment (10^{-6} sec duration pulse), the coherence width is 10^{-4} cm^{-1}; and as a result the two excited states are not excited coherently, but as a statistical mixture (i.e., the spectroscopic state is not a pure state). This means that an ensemble of such molecules behaves as though given fractions are in the ground state and each of the two excited states. Such a statistical mixture of molecular eigenstates is stationary with respect to the molecular hamiltonian and subsequent time dependence is due entirely to radiative interactions, and is the sum of exponential decays of the two states.

Even though the light intensity can be controlled to give the same excited state probabilities for the two experiments, the fluorescence intensity at τ would not be the same. The difference is that the coherent spectroscopic state ($\tau = 10^{-12}$ sec) behaves kinetically as one species at τ, and the mixed spectroscopic state behaves kinetically as several species decaying to the same product.

The main reason that these effects have not been observed is probably due to the small number of pulse excitation experiments which have been done under isolated conditions and also, the time dependence of fluorescence is not usually measured. In addition, these effects have not been predicted until recently[5], because theoretical spectroscopists have generally thought of

pure states rather than the more general class of statistical states described by density operators.

CHAPTER III

SUMMARY OF FLUORANTHENE SPECTRA

Fluoranthene, in addition to the compounds in Table 1, has also been suggested[15] as a possible compound which may exhibit dual fluorescence. Fluoranthene is an aromatic hydrocarbon with the following structure:

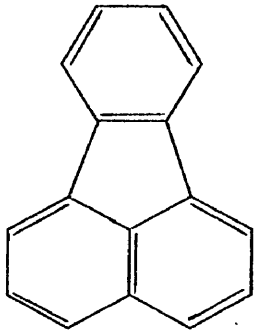

It has a molecular weight of 202.26 g/mole, crystalyzes into pale yellow needles or plates and melts at 110.5°C.

The earliest reported dual fluorescence of fluoranthene was by Nauman and co-workers[22] in 1957 in a series of unpublished studies in which they report observing two fluorescence band systems at 77°K. The F_1 band ($S_1 \rightarrow S_0$) originated at 24,860 cm^{-1} (4022 A) and extended to 17,500 cm^{-1} (5714 A); while a weaker F_2 ($S_2 \rightarrow S_0$) emission was observed from 28,310 cm^{-1} (3532 A) to 25,430 cm^{-1} (3932 A). Two phosphorescence band systems were recorded, P_1 originating at 18,550 cm^{-1} (5391 A) and extending to 16,610 cm^{-1} (60,205 A), and P_2 originating at 21,440 cm^{-1} (4664 A) and extending to 19,000 cm^{-1} (5263 A). They noted that the F_1 emission was the approximate mirror image of the weak $S_0 \rightarrow S_1$ absorption spectrum, and P_1 is the mirror image of the $S_0 \rightarrow T_1$ absorption. Excitation

below 28,000 cm^{-1} gave only F_1 and P_1, while excitation above 30,000 cm^{-1} yielded all four emmissions (F_1, F_2, P_1, and P_2).

Nauman also calculated a lifetime for fluoranthene of 212 nsec in cyclohexane at room temperature and noted that this exceeded the theoretical value of 16.4 nsec as derived from the integrated first absorption band system. He concluded that this showed that F_1 originated from the S_1 state which was "hidden" in the room temperature absorption spectrum by the adjacent absorption to the S_2 state. The weak $S_0 \rightarrow S_1$ absorption may be resolved in the low temperature solution spectrum. In this case the S_1 level is assigned to a ^1L_b state and the S_2 level is assigned to a ^1L_a state.

These symbols, ^1L_a and ^1L_b, are designations of the perimeter free electron model (PFEO), which is Platts theoretical model for the classification of the π-electronic states of the cata-condensed hydrocarbons. In the cata-condensed hydrocarbons, every carbon atom (and every π-electron) is on the periphery of the molecule, and in the PFEO model the π-orbitals are treated as orbitals of free electrons traveling in a one-dimensional loop around the molecular perimeter.

In this model, the orbital ring quantum number, q, is a measure of the angular momentum and describes the number of nodes in the wavefunction. When the circular perimeter is distorted to conform to the molecular perimeter, and the periodic potential due to the carbon atoms is introduced, q no longer describes the momentum, but remains a good quantum number, since it still

determines the number of nodes. If there are n rings in the molecule there are a total of 2(2n+1) π-electrons, since each carbon atom contributes one π-electron.

The total ring quantum number, Q, of the multi-electron system is the algebraic sum of the q's of the individual electrons. the nomenclature A, B, C is introduced to describe the states of the system with Q = 0, 1, 2, respectively and K, L, M to describe the states with Q = 2n, 2n+1, and 2n+2, respectively. If the potential were constant around the perimeter of the molecule, all the states, except A, would be doubly degenerate since the total momentum can be in either direction around the perimeter. The introduction of the periodic potential due to the carbon atoms removes this degeneracy, so that each state splits into two components represented by subscripts a and b.

The nodes in the electronic wavefunction occur at planes of symmetry perpendicular to the molecular plane. The subscripts a and b refer to the two alternative positions for the nodes relative to the molecule: a) where the nodal planes bisect the C-C bonds; and b) where the nodal planes pass through the carbon atoms. Wavefunctions of type b may be formed from a, by the interchange of nodes and antinodes, and each nodal plane cuts the molecule twice, so that for the L states (Q = 2n+1) there are 2(2n+1) cuts. The number of cuts equals the number of carbon atoms and the number of C-C bonds, and the L_a and L_b states correspond to weaker dipole transitions with polarizations

perpendicular and parallel to the long molecular axis respectively.

In some molecules, fluoranthene included, in which $S_1 = {}^1L_b$; the $S_0 \rightarrow S_1$ transition is not readily observed in the absorption spectrum because of its proximity to the more intense absorption band system, corresponding to the $S_0 \rightarrow S_2$ ($S_2 = {}^1L_a$) transition.

In such cases the radiative lifetime τ and the fluorescence spectrum can provide a useful mode of identification of S_1. For example, the experimental value of τ for biphenyl in cyclohexane is 89 nsec[22]. This may be compared to the theoretical value of 2.9 nsec, evaluated from the integrated "first" absorption band, which is broad and structureless. The assignment of $S_1 = {}^1L_b$, $S_2 = {}^1L_a$, with the fluorescence corresponding to the $S_1 \rightarrow S_0$ transition and the observed "first" absorption band to the $S_0 \rightarrow S_2$ transition, removes this discrepancy, which is common to the other biphenyl derivatives including fluoranthene. Thus, the state assignments for fluoranthene should be $S_1 = {}^1L_b$ and $S_2 = {}^1L_a$.

All of the compounds shown in Table 1 have several common characteristics which are:

1. $S_1 = {}^1L_b$
2. $S_2 = {}^1L_a$
3. S_2-S_1 energy separation is equal to or less than 3000 cm^{-1}

The first criterion ensures that S_1 has a long radiative lifetime and the second ensures that S_2 has a high radiative transition probability, while the third satisfies the requirement for the proper density of states in the dense intermediate model.

The proximity in energy (wavelength) and large difference in intensity in the absorption spectrum of the $S_2 \rightarrow S_0$ transitions in compounds like fluoranthene, seem to have added to the difficulty in interpreting dual fluorescences. This was pointed out in a paper on fluoranthene by Berlman, Wirth, and Steingraber[23] in 1967.

In this work, they measured the lifetime of the F_1 region as 53 nsec, and its quantum yield as 0.30. The theoretical lifetime was calculated to be 16.4 nsec. Their data indicates that the fundamental relationship of; theoretical lifetime equals the radiative lifetime divided by the quantum yield ($\tau_0 = \tau/QY$), does not hold for fluoranthene where τ_0 is obtained by integrating over the absorption bands.

They pointed out that usually when $\tau_0 \neq \tau/QY$, that the discrepancy can usually be traced to an improper evaluation of τ_0 in which absorption bands not related to the fluorescence have been included in the integration. Since the data available on the work by Nauman is somewhat vague, this may have been part of his problem. In systems where $S_1 = {}^1L_b$ and $S_2 = {}^1L_a$, the $S_2 \rightarrow S_0$ transition is very intense and the $S_0 \rightarrow S_1$ transition can usually only be resolved as a shoulder in the intense $S_0 \rightarrow S_2$ absorption even in the low temperature spectra at 77°K. Clearly then, it is very difficult to evaluate the proper absorption band for a correct estimate of τ_0. Berlman et al.[23] using their observed data,

calculate a natural fluorescence lifetime, τ_o, of 177 nsec, and using an assumed electronic level width equal to that for most molecules, estimate the extinction coefficient of the $S_0 \rightarrow S_1$ transition to be 270 ± 40. This low value is consistent with the designation that $S_1 = {}^1L_b = A_1$ in C_{2v} symmetry.

Probably the first real definitive study of the transitions in fluoranthene was carried out by Josef Michl [24] in 1968. Michl pointed out that as a result of semiempirical calculations by the Pariser-Parr-Pople (PPP) method, that, "It has become increasingly apparent that the traditional interpretation of the electronic spectrum of fluoranthene is oversimplified." Corroborating experimental evidence of this was provided by measurments of polarized emission and of dichroism of molecules on stretched polyethylene films[25]. He noted that it is a very poor approximation to regard fluoranthene as a loose combination of almost non-interacting naphthalene and benzene subunits.

A portion of the room temperature absorption spectrum measured by Michl is shown in Figure 3, with the small lines representing the positions of the calculated transitions. The room temperature spectrum in non polar solvents starts with several indistinct shoulders near 25,000 cm^{-1} just on the onset of a seemingly simple absorption band located between 25,000 cm^{-1} and 35,000 cm^{-1}. Little attention had been paid to these shoulders until the PPP-type calculations of Michl predicted that there should be three electronic transitions in the region of the apparently simple band.

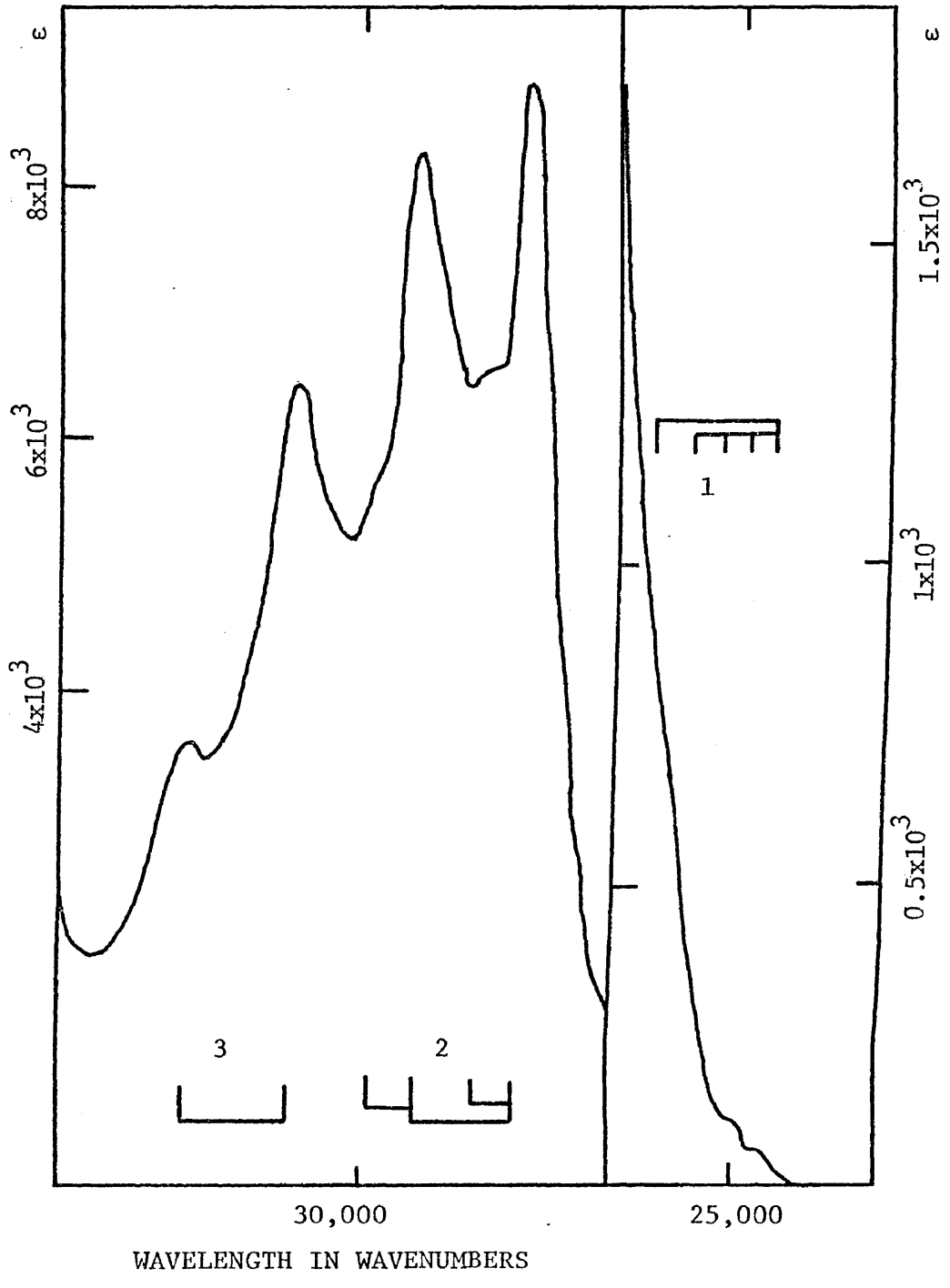

Figure 3. Room temperature absorption spectrum of fluoranthene[24] in 3-methylpentane. Lines indicate the suggested separation into individual transitions.

It was then suggested that the shoulders are due to a separate transition into the lowest excited singlet state, S_1. This assignment was also supported by the fact that there is a large difference between the wavelength of the first well-developed maximum in the absorption spectrum (27,800 cm^{-1}) and the first maximum in the fluorescence spectrum (24,900 cm^{-1}).

Low temperature spectra at 77°K partially resolved the fine structure of the shoulder and allowed a simple vibrational analysis to be made (Figure 4). Again, the calculated transitions are indicated by the small lines at the top of the figure. The first (0-0) vibrational component coincides almost exactly with the first (0-0) vibrational component of the fluorescence, and the fine structure of the fluorescence bears an approximate mirror image relationship to that of the "shoulders" up to the point where a more intense absorption band sets in. However, it is not related to the vibrational structure of the intense band.

This seems to be the first conclusive proof of the weak nature of the $S_0 \rightarrow S_1$ absorption and explained the nature of many compounds which showed anomalous fluorescence. Many compounds had been noted which had a large stokes shift, and Berlman et al.[23] rationalized the large stokes shift by having the fluorescence originate in a "hidden" band. Michl went ahead to resolve the band in fluoranthene, showed its relation to the fluorescence, and noted that it resembled a L_b transition in benzeniod hydrocarbons by its weak intensity ($\log \varepsilon \simeq 2$).

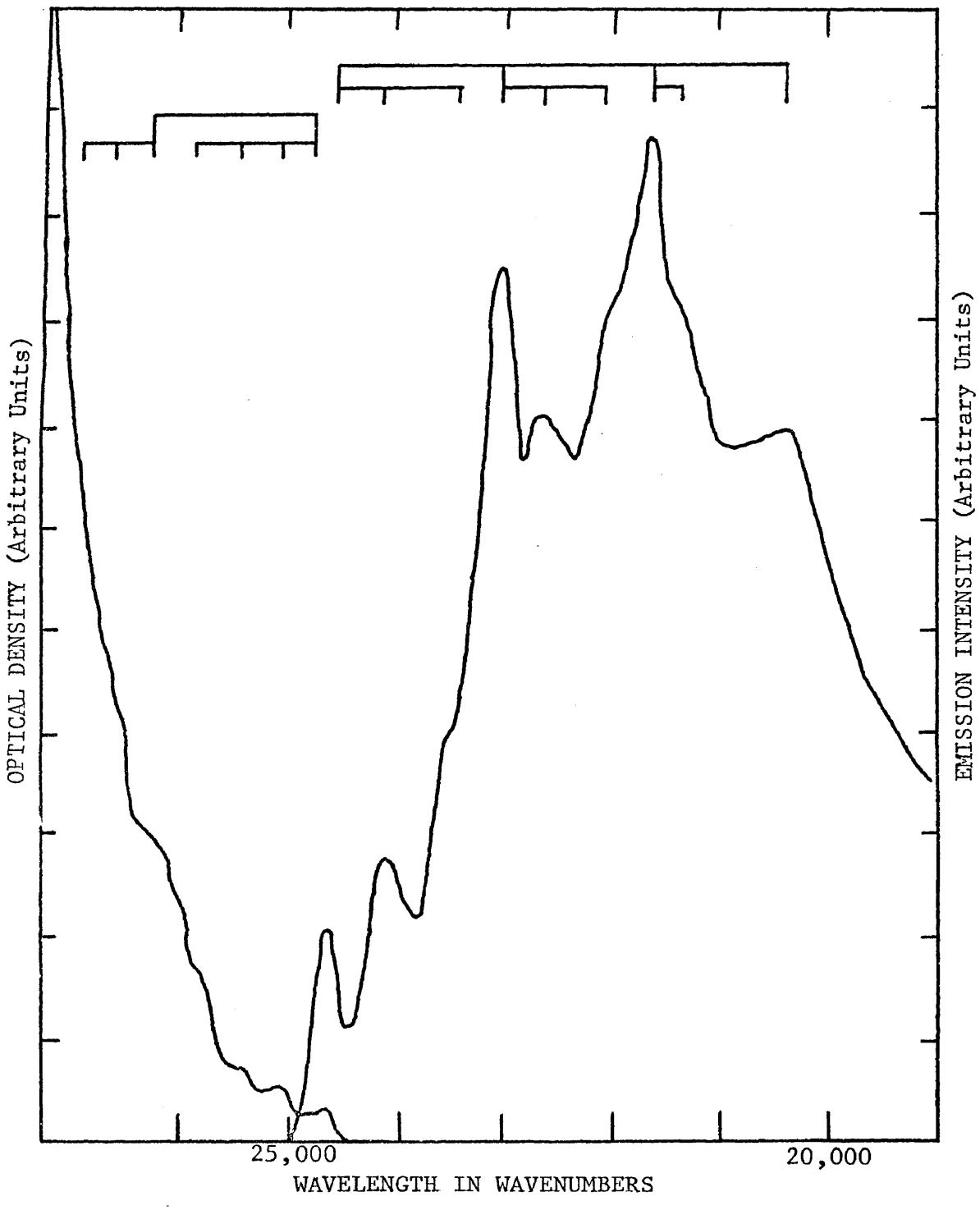

Figure 4. Part of the absorption (left) and fluorescence[24] emission (right) spectra of fluoranthene in 3-methlypentane glass at 77°K.

When the PPP-type calculations were performed, there were two electronic transitions predicted for the region of the apparently simple first absorption band. The peak at 27,800 cm^{-1} was taken as the (0-0) transition for one of these. Measurments of dichroism on stretched polyethylene foils[25] indeed showed that the intense absorption band is a composite and consists of two transitions of opposite polarizations.

Michl's paper provided additional strong evidence for the composite nature of what was originally thought to be the first absorption band of fluoranthene. The first two peaks, below 30,000 cm^{-1} belong to one transition while the two peaks above 30,000 cm^{-1} belong to the other.

However, it should be noted that in the experiments presented here, the nitrogen gas laser line at 3371 A corresponds to 29,664 cm^{-1}; which is sufficient to excite the first transition in the band, but not the one of different polarization above 30,000 cm^{-1}. Michl went on to do a complete analysis of the transitions in fluoranthene up to 50,000 cm^{-1} (2000 A), but since these are also above the limit of excitation with the laser, they are not presented here.

CHAPTER IV

EXPERIMENTAL METHODS

Materials

One of the problems in dealing with any compound which exhibits anomalous fluorescence, such as dual fluorescence, is to be certain that the effect under observation does not arise from impurities present in the sample. Birks[22] raised this possibility in regard to fluoranthene; and Nauman[22] used material which had been recrystalized, zone refined, and purified by chromatography to eliminate any possibilities of impurities. Berlman[23] bought samples from different suppliers and purified them by recrystalization from various solvents, zone refining and column chromatography. He then tested for impurities by exciting the solution with radiation of different wavelengths in succession, recording the fluorescence spectrum each time, and looking for major changes as a function of wavelength. This proceedure is very sensitive in highlighting the presence of an impurity which has a different fluorescence spectrum. Results of Berlman[23] tend to indicate that the observed fluorescence spectrum of fluoranthene is not due to an impurity, as may be the case in hard to purify compounds such as chrysene and coronene[8].

For the present studies, 99% pure fluoranthene purchased from Rutgerswerke-Aktiengesellschaft, was recrystalized three times from benzene. The recrystalized fluoranthene was put into a zone refining tube, degassed by the freeze-pump-thaw method three times,

and sealed off under vacuum. The sample was then zone refined for 72 hours on a Electronics Space Products multi-zone refiner, having five zones, at a rate of one cycle every two hours. For the final sample, the middle section of the zone refined column was taken, and a melting point range of 110.5-111.5 was determined on a Fisher-Johns melting point apparatus.

In order to achieve a transparent glass for low temperature studies, a solution of two parts ethanol, five parts diethylether, and five parts isopentane was made as the solvent. This mixture of solvents is generally referred to as EPA. Instrument grade isopentane from Phillips Petroleum was used without further purification. Analytical reagent grade ethyl ether from Mallinckrodt Chemical was also used without further purification. Ethyl alcohol (95%) was dried over magnesium for eight hours and distilled on a fractionating column to give greater than 99% water-free ethanol. Solutions were made at the concentration to be studied, placed in a quartz tube (4 mm O.D.) and degassed three times by the freeze-pump-thaw method to 20 microns.

The samples prepared in this manner were then ready for running on the appropriate apparatus in the laboratory. It is estimated that the change in concentration as a result of the freeze-pump-thaw cycle is less than ten percent.

Particular care must be taken in running freshly degassed samples which have been purged by the freeze-pump-thaw method. This technique is particularly amenable to the formation of regions

of high concentration of solute. This agglomeration results in regions of high concentration, which may allow solute-solute interaction and self absorption to occur with resulting quenching of the fluorescence. This is particularly severe at high initial concentrations (10^{-3} M) and has been responsible for some irratic behavior in the fluorescence of some samples. It is also suggested that in this light, and in the light of survey spectra run on the fluorimeter; that the extent of self absorption in compounds like fluoranthene has not been fully recognized.

To remedy this problem, degassed samples should be allowed to stand to warm to room temperature and then allowed to stand for a sufficient period or else mechanically shaken to disperse any areas of agglomeration. Likewise, it is especially important to insure that the initial concentration is low enough to prevent appreciable self absorption of the F_2 fluorescence.

Instrumentation

Preliminary survey spectra were run at 77°K on a Baird Atomic Fluorescence Spectrometer model SF-100 in order to establish the fluorescence spectrum and define the possible regions of interest.

The experimental arrangement for recording the dual fluorescence of fluoranthene by laser excitation is schematically represented in Figure 5. The apparatus shown in Figure 5 consists of a laboratory constructed molecular nitrogen gas laser which has a 160 KW output in a 10 nsec pulse at 3371 A. (See Appendix I for

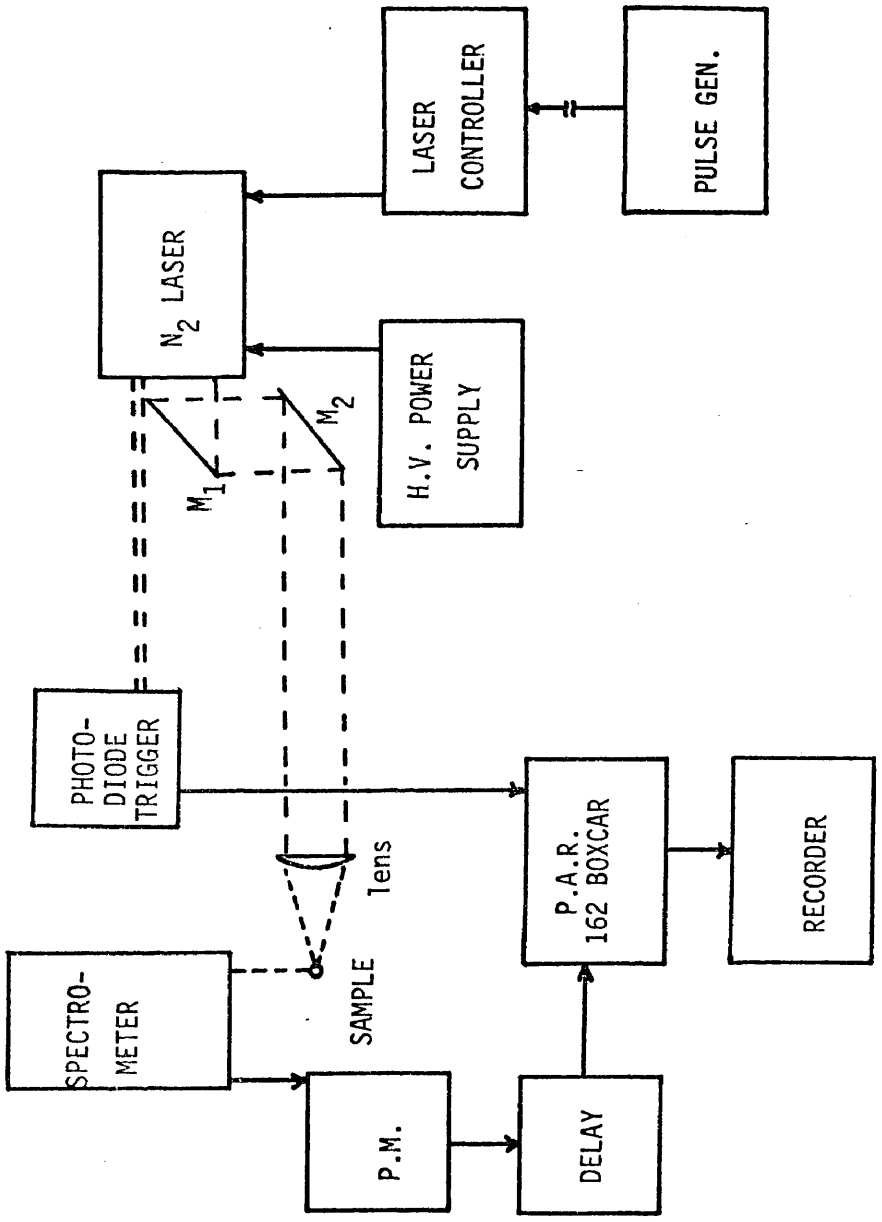

Figure 5. Schematic arrangement of the laser fluorescence apparatus.

construction details and performance characteristics.) The laser is powered by a 20 KV, 50 ma, 1 KW, power supply model 820-50 from Hipotronix Inc. and is controlled by a laboratory built control system (Figure AI-4) which allows a variable pulse rate from one pulse per second to 30 pulses per second.

As an added control device, a provision has been made to allow an external pulse generator to be used to fire the laser through the control box. This allows not only slower pulse rates, if necessary, but will also allow manual triggering of the laser for single pulse analysis, or allow only a few pulses to be averaged for power measurments.

The laser system consists of the laser channel, power supply, control system, and vacuum pump to supply a flow of nitrogen; all of which is sealed in a specially designed cage to screen out any radio frequency effects from the detection apparatus. The laser channel is sealed in a large copper box which completely encloses the laser. The power supply and control system are sealed in a cage made of aluminum wire screen. Power leads on the triggering apparatus feed through special high voltage diodes at the interface of the copper box to keep the RF energy from being radiated back down to the control system. All 110 V supply lines for the laser system are kept on a separate power line from the detection apparatus. For the use of the dye laser, the dye laser replaces mirror M_1. (See Appendix II for construction and performance details.)

The detection apparatus consists of a Jarrel Ash, one-half meter spectrometer, model 82-000, with a 0.2 A resolution in the first order; this is coupled to either a 1P28 photomultiplier or an Amperex 56UVP photomultiplier. The Amperex model 56UVP photomultiplier is powered by a Fluke High Voltage power supply model 408B and is useful for detection of very weak fluorescences because it has a much greater dynamic range than the 1P28. Its gain is 10^8 at 2200V and has a rise time of 2 nsec. For most applications, the 1P28 photomultiplier is used as it has a response time of less than 2 nsec and the voltage required for a 10^6 gain is only 750 volts[26]. Maximum voltages are 1050V for the 1P28 and 2500V for the 56UVP.

The heart of the detection apparatus is the Princeton Applied Research Model 162 Boxcar Integrator which is equipped with two model 164 gated integrators which render it as a dual channel integrator. In its simplest form, boxcar averaging is a process of controlled sampling and sample averaging. The process involves measuring the amplitude of a specific point on a repetitive waveform several times and then computing the average value of those measurments.

In some experiments it is necessary to examine the shape of a repetitive waveform. In the boxcar, this is done automatically by time-scanning a sampling aperture across the waveform. The sampling rate is made slow enough to permit a sufficient number of samples to be taken in each segment of the waveform to insure

accurate results. The output in the scanning operation is a dc level which follows the shape of the waveform under study.

In general applications the instrument synchronously samples the input signal by passing it through an aperture that can be fixed at any point on, or slowly scanned across, the input signal. The signal passed through the aperture is averaged by a variable time constant integrator, the output of which is the average of some number of repetitions of the input signal over the aperture duration. Because the average value of the noise over a large number of repetitions is zero, an improvement in the signal-to-noise ratio (SNR) occurs. If the aperture is fixed on a single point of the input signal, the output rises asympotically toward the amplitude of the synchronous portion of the input signal at the sampled point. If the aperture is scanned across the input signal, the synchronous waveform is reproduced at the output.

The boxcar integrator used in these experiments is equipped with a digital storage option which converts the analog voltage to a digital storage register and permits virtually infinite holding time to allow signals with extremely low duty factors to be averaged. A boxcar having two integrator modules functions as a dual channel integrator in that either channel may be processed by the 162 main-frame or the difference of the two channels may be processed. One of the more useful options available is the use of the ratio function which allows channel A to be compared to channel B and a ratio taken. This is especially useful in laser

experiments where channel B is used to monitor the slightly fluctuating laser power, and to normalize the signal of interest to the laser intensity. This is analogous to a double beam spectrometer which alternatively compares a reference beam to a sample beam, except that in this case both beams are sampled simultaneously. Prior to being made available at the output connector, the main-frame (162 module) output signal is smoothed by a low pass filter with a time constant that is continuously adjustable from 100 μsec to 100 sec.

Delay controls in the main-frame permit the aperture in each channel to be delayed independently from 1% to 100% of the Delay Range (time period of interest). The Delay Range is selectable in a 1-2-5 sequence from 0.1 μsec (100 nsec) to 50 msec. The scan time, the time required to scan the aperture across 100% of the selected Delay Range, can be set to any value from 10^{-2} sec to 10^{5} sec.

The Model 164 Gated Integrator module offers a choice of aperture widths ranging from 5 nsec to 50 msec. Pushbutton switches allow a choice of 50Ω or 1MΩ input impedance, ac or dc coupled, and the choice of linear (summation) or exponential averaging. Both the module gain and aperture duration may be trimmed to provide an exact match between modules if two Model 164's are to be used in dual-channel operation.

In manual operation, the aperture delay range time-base voltage is compared to the corresponding % initial delay control

voltage. The gate (aperture) opens at the time set by the % Initial Delay Control. Each channel is provided with a separate % initial delay circuit permitting the sampling switch of each channel to be closed at a different point on the aperture delay range time base if desired. Through the proper selection of the Aperture Delay Range and the setting of the % Initial Delay Controls, any point on the repetitive waveform under study may be sampled.

When the instrument is set for automatic scan, an internally generated scan ramp is also applied to the delay circuits. The % Initial Delay voltage and Scan Time ramp voltage are summed and sent to an aperture comparator which opens the gate. When the % Initial Delay control is set to its minimum position, the delay between the trigger and the aperture position is determined solely by the Scan Ramp. Figure 6 shows the time and amplitude relationships between the Aperture Delay Range time-base ramps, the Scan Ramp, and the aperture position. As the scan ramp ascends, the voltage applied to the comparator rises, and the aperture opens slightly later relative to the trigger time with each position. That is, the aperture is positioned slightly later on the Aperture Delay interval with each repetition.

When the % Initial Delay Control is adjusted to a setting other than minimum, the comparator input voltage is offset by the amount of the dialed Initial Delay. As a result, the beginning of the aperture scan is time shifted; and the resulting scan is

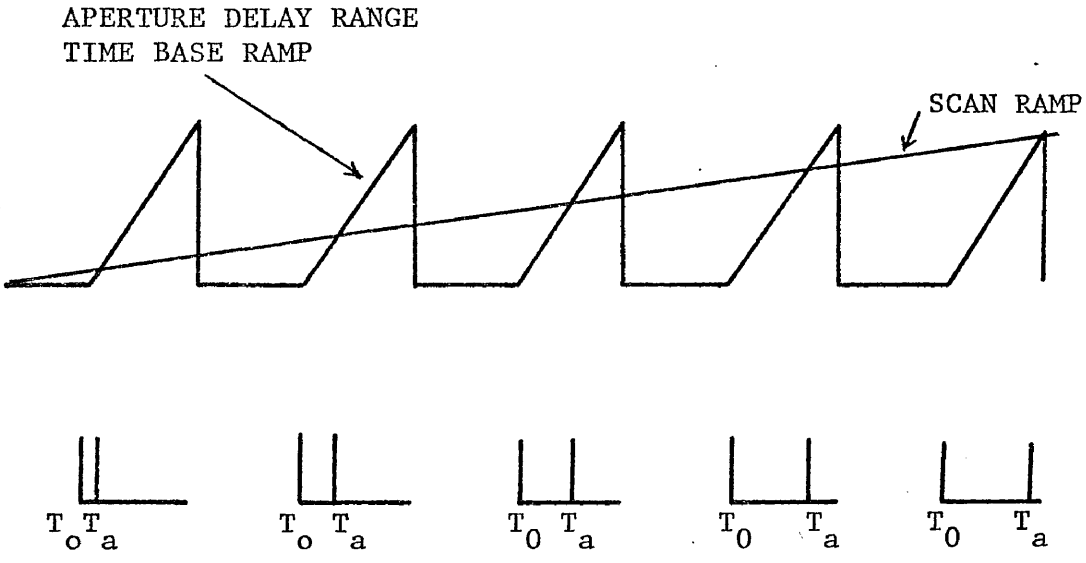

T_0 = Aperture delay range time base trigger.

T_a = Time when aperture opens.

Figure 6. Position of gated aperture and its relation to the boxcar trigger in the scaned mode of operation.

confined to an interval bounded at one end by the dialed Initial Delay, and at the other end by the selected Aperture Delay Range.

In all applications, the boxcar must be triggered either by the line voltage, or as is usually the case, by an external stimulus from the experiment under observation. In the experiments used to detect dual luminescence one must be concerned with the time-pulse fluctuations in the laser itself. Therefore, since each laser pulse, which is 10^{-8} sec in duration, causes fluorescence, the laser pulse itself was taken to be the point of zero time in order to initiate an aperture delay range time base ramp (Figure 6).

However, there is nominally a 20 nsec delay from the point of triggering until the onset of a time base, so the signal of interest must be delayed in order to have it fall within the selected aperture delay range. This is accomplished by the use of 50 feet of low loss coaxial cable from the photomultiplier to the boxcar and gives a resultant delay of 67 nsec.

The trigger used to initiate the time base is a Pin-Ten photodiode biased at +45 volts. Such an arrangement has a very fast rise time and a high, stable output for triggering. The output voltage is nominally +22 volts and triggering of the boxcar is adjustable over ±5 volts. Also, triggering on the positive going or negative going edge of the trigger pulse is possible. The experimental apparatus set up in this way, in no way interferes with the ability to recover information on the leading edge of the

input pulse.

Figure 7 illustrates the basic timing relationships in the boxcar and represents the process occuring in the previous discussion. Each time the boxcar is triggered (triggering on the positive edge of an externally derived trigger is indicated in the figure) there occurs a fixed trigger delay of nominally 20 nsec, at the end of which the selected Aperture Delay Range begins. (For convenience in illustration, the Aperture Delay Range is shown as a pedestal, although from an operating point of view, it is simply a selected time interval.) At some time after the beginning of the aperture delay range interval, but before the ending, an aperture (gate) opening occurs. The duration of the aperture opening can extend beyond the end of the aperture delay range normally does not. Usually, the aperture opening is very short relative to the selected delay range. In single point analysis (fixed Gate) the aperture opens at the same time after each trigger. In scanned operation it opens a bit later after each trigger, with the incremental increase in aperture delay each repetition normally being small relative to the duration of the aperture opening itself.

In examining dual fluorescences, two types of experiments are necessary. The first is a spectral (energy) distribution of the fluorescence, and the other is a time history of a portion, or portions, of the spectrum. The time history spectra are actually decay curves from which it is relatively easy to determine the

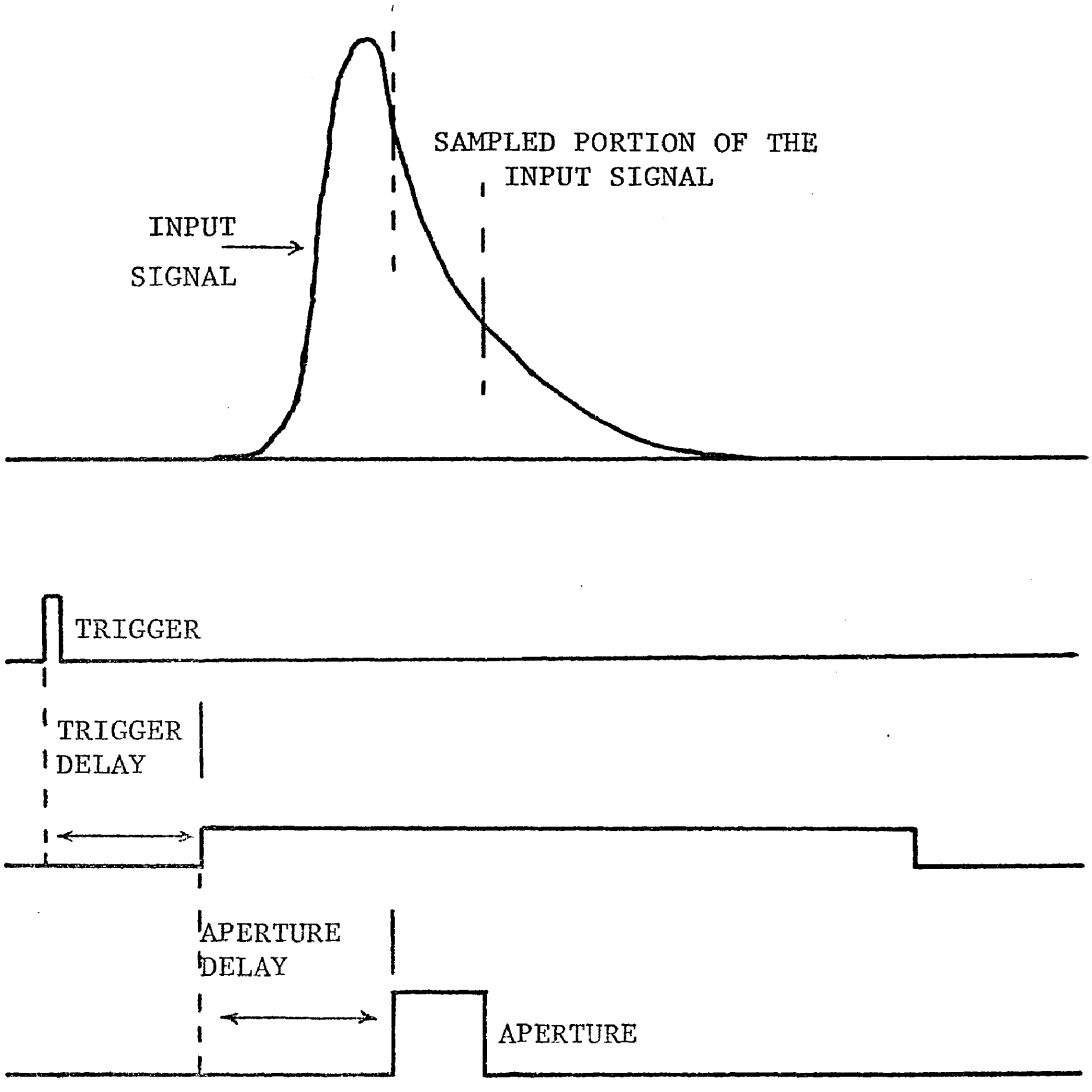

Figure 7. Basic timing relationships in processing a signal through the boxcar integrator.

decay time of the energy region under study.

Figure 8 represents the first type of experiment in which a narrow gate is fixed in time with respect to the laser pulse and the spectrum scanned with the spectrometer. The spectrum in Figure 8 is of the F_1 ($S_1 \rightarrow S_0$), and F_2 ($S_2 \rightarrow S_0$) regions of fluoranthene and represents the fluorescence profile 120 nsec after the laser pulse. By recording a spectrum at various fixed delays, with reference to the laser pulse, it is possible to compare spectra at different delay times and detect any changes in the intensity distribution - in effect obtain time resolved spectra.

On the other hand, Figure 9 illustrates the scanned mode of operation in which the spectrometer is fixed at some wavelength (energy) and the boxcar is scanned in time. This mode, as described earlier, provides a decay curve of the energy state in question. Figure 9 shows a time profile for the 3371A laser excitation and its relation to the 4050 A line of the F_1 fluorescence in fluoranthene which it is exciting.

Although the boxcar integrator provides an output of the scan ramp which is suitable for driving a X-Y recorder, in these experiments the output from the 162 main-frame is simply displayed on a Hewlett Packard strip chart recorder model 7101B equipped with a model 17500A plug-in module. This allows both types of experiments just described to be run with a minimum of adjustments to the apparatus.

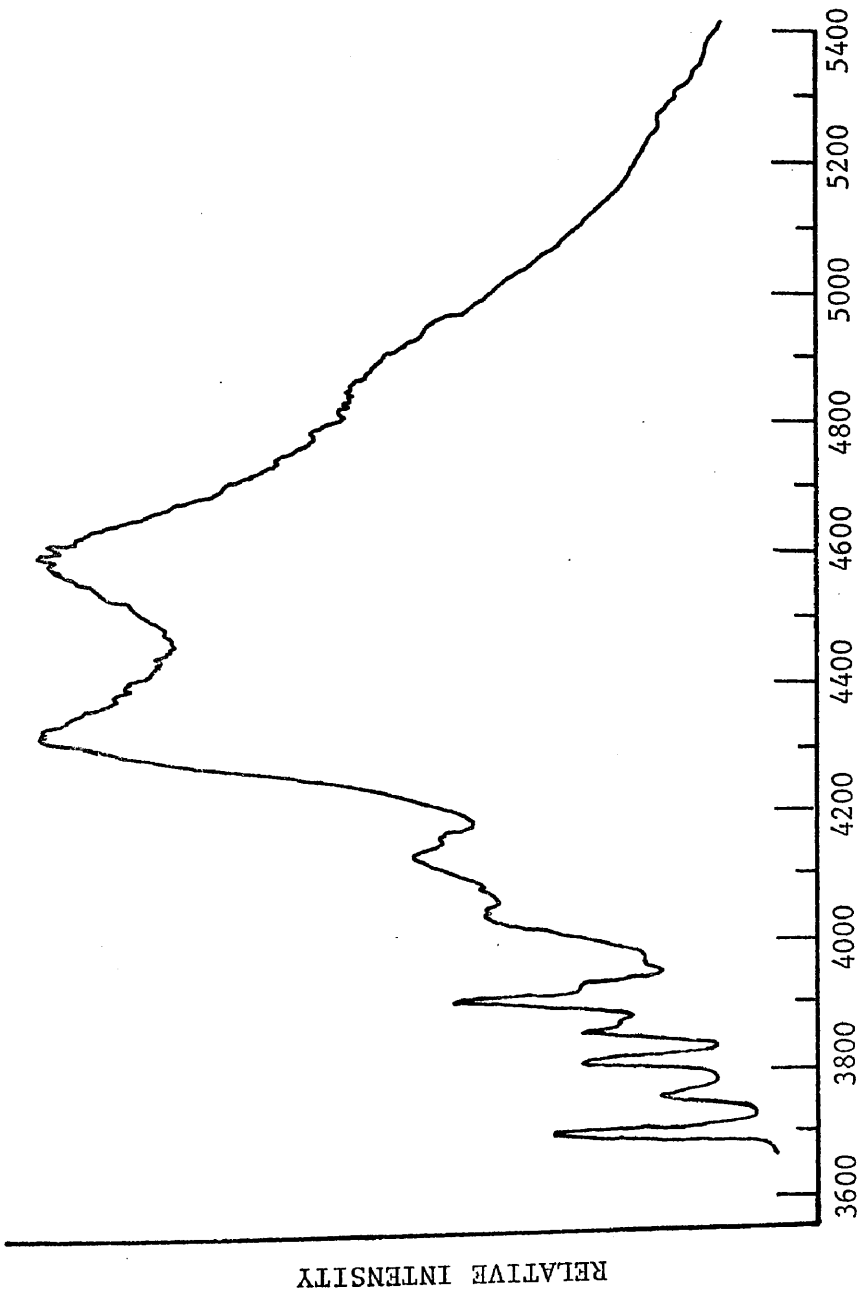

Figure 8. Energy (wavelength) resolved spectrum of the F_1 and F_2 regions in fluoranthene.

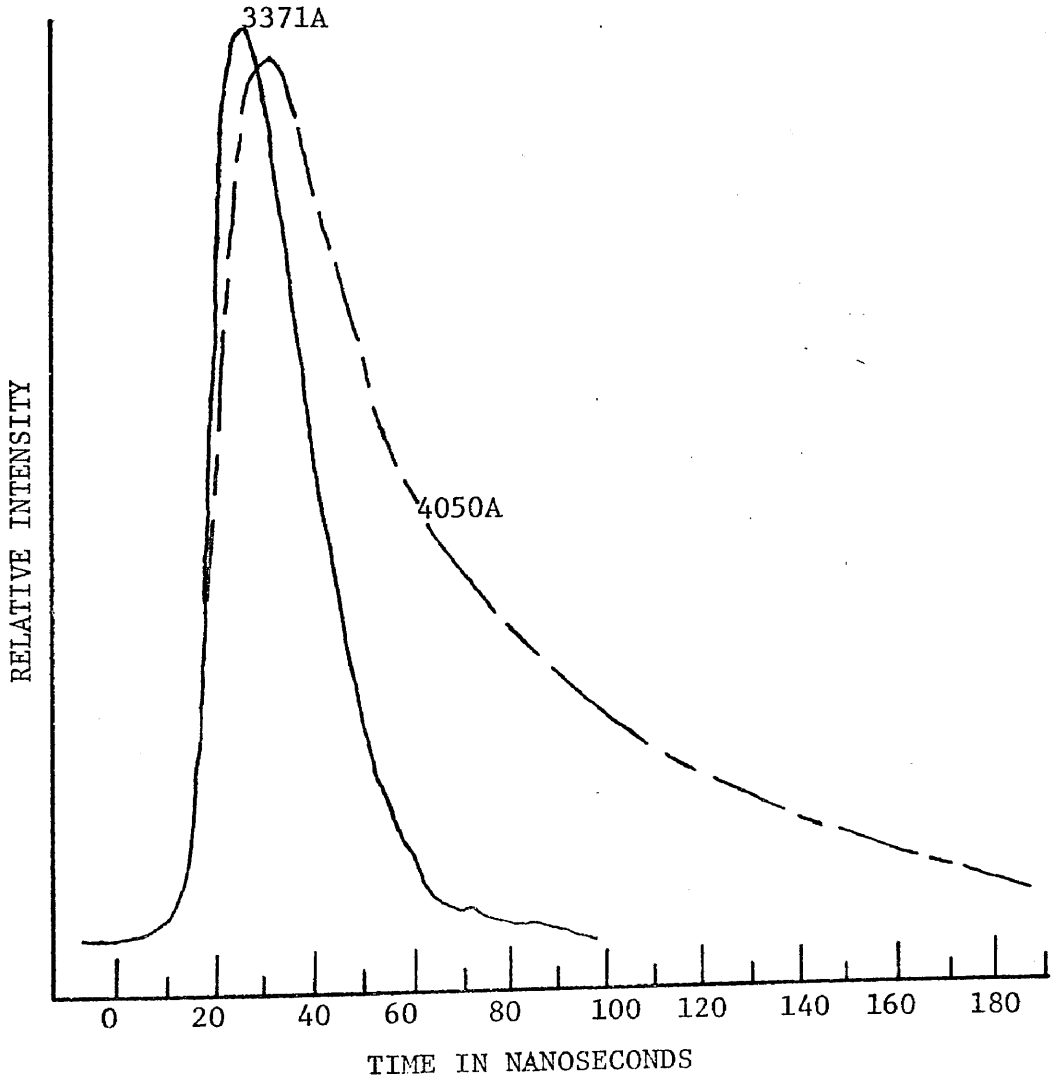

Figure 9. Time profile of the 4050A line of the F_1 fluorescence in fluoranthene, and its relation to the exciting pulse.

Due to the sensitive nature of the apparatus, it is very important to have the fluorescing sample properly aligned on the entrance slit of the spectrometer. In cases where the fluorescence yield is large and the 1P28 photomultiplier is used, it is possible to align and focus the fluorescence on the slit by use of an oscilloscope. The output from the photomultiplier is connected to a Tetronix model 564 dual trace, storage oscilloscope, and the position of the sample and the focusing lens are adjusted for a maximum signal on the scope. With the sample aligned, the photomultiplier is connected to the boxcar and the appropriate spectrum is run.

In cases where the fluorescence yield is low and where the 56UVP photomultiplier is used, a slightly different alignment proceedure must be used. The model 564 oscilloscope is not fast enough to record the weak pulses from the 56UVP, so the photomultiplier is removed and a Metrologic model 610 He-Ne laser is put in its place. The laser beam is aimed at the exit slit of the spectrometer, the spectrometer is set to the laser wavelength (6328A), and the beam is allowed to exit through the entrance slit of the spectrometer. The beam now emerging from the entrance slit is approximately 1mm in width, depending on the slit setting and the resulting diffraction, and defines a line along which the sample may be placed in order to be in proper alignment with the spectrometer. The sample is placed in the center of the exiting laser beam, the lenses focused, and the photomultiplier is replaced

with care so as to not distrub any of the previously set components. The sample is now correctly aligned and the spectrum may be run. This technique has been especially successful in studies where the dye laser was used to excite only F_1 fluorescence. The extinction coefficient at the excitation wavelength of 3900A is very small, thus the resulting fluorescence is quite weak. However, use of this alignment technique makes the observation of a selected fluorescence region experimentally much more feasible.

Recording and analysis of energy resolved spectra is fairly straight forward. Usually, the most intense peak in the region of interest is taken as a standard of intensity. That is, the gain of the electronic apparatus is set such that the most intense peak in a region is displayed with a full-scale deflection on the recorder. In other words, each spectrum is normalized with respect to one certain line. The 4600A line is used for F_1, and F_1 and F_2 spectra, while the 3820A line is used for F_2 spectra only. This allows a comparsion between spectra with different decay times to have a comparable resolution, and permits one to observe changes in the spectrum at long delay times where the intensity is low.

Data Processing

The process of obtaining real decay times from experimental curves is generally referred to as deconvolution. The purpose of deconvoluting optically induced transients is to free them from two sources of distortion: the finite rise time, width, and decay of the exciting pulse, and distortion introduced by the photon

detection and timing apparatus.

Several attempts to analyze such data have been made and may generally be put into three classes. The first is really a subtraction procedure in which the decay curve is first examined at times sufficiently long so that all but one of the decays become negligibly small. The slowest decay is thereby determined. The effect of this decay is then subtracted from the data and the next slowest decay determined. If the light pulse conformed to a delta pulse, all components of a decay could be determined in this way; in practice, however, the pulse is of finite duration and the proceedure involves the subtraction of quantities that are nearly equal, and the experimental errors become rapidly magnified and quickly dominate the procedure.

The second procedure relies on curve fitting methods. Such methods are in principle capable of analyzing data, but in practice curve fitting is sensitive to the choice of the number of components to be fitted, and extremely sensitive to even small errors in the data[27]. Ware[28,29] has made extensive use of this technique and suggested that it be termed an Exponential Series Method[29]. In his approach, the decay curve was represented by a series of the type

$$G(t) = \sum_{k=1}^{n} a_k e^{-t/\tau_k} .$$

That is, the decay curve data is reproduced by a series of exponential functions of the type $ae^{-t/\tau}$.

The problem then is to evaluate the a_k's and τ_k's. However, deconvolution with such a function, where one optimizes both

a_k and τ_k becomes awkward when n is large because one has the variable τ_k inside the integral that must be numerically evaluated for each data point. In practice the τ_k's are not varied but are preselected to span a suitable range and only the a_k's are varied. This reduces deconvolution to the solution of a set of n simultaneous equations, but the τ_k's are arbitrary and have no physical significance, nor is there any simple relationship between the τ_k's or the a_k's and the relaxation times of the system. In situations used by Ware[29], as many as 15 variables are used (n=15), and while the resulting solution reproduces the observed data, it has little significance in giving a physical interpretation of the results.

The third method, and the method used to analyze the experimental data generated here, is the "Method of Moments" which has been developed by Isenberg and Dyson[27]. The theory of analysis by the method of moments according to Isenberg and Dyson is briefly outlined in the following discussion.

Isenberg and Dyson set out by letting f(t) be the luminescence intensity from a sample excited by a Dirac delta function flash at t=0

$$f(t) = \sum_{n=1}^{N} a_n e^{-\lambda_n t}$$

where $\lambda_n = 1/\tau_n$. The problem is to determine the number of components N, the amplitude a_n, and the decay constants λ_n.

In practice, the flash of light used to excite the sample is of

finite duration, and may be comparable in duration to the fluorescence lifetime of the sample; consequently, the exciting light cannot usually be approximated by a delta function.

Let E(t) be the intensity of the exciting lamp and F(t) be the emission of the sample when excited by E(t). Then F(t) is given by the convolution

$$F(t) = \int_0^t E(t-u)f(u)du$$

where F(t) and E(t) constitute the experimentally determined data. The K^{th} moments of F and E are defined by

$$\mu_k = \int_0^\infty t^k F(t)dt$$

and

$$m_k = \int_0^\infty t^k E(t)dt$$

where the moments μ_k amd m_k may now be considered to be the given experimental information.

The K^{th} moment of F is,

$$\mu_k = \int_0^\infty t^k \int_0^\infty E(t-u)f(u)dudt$$

where μ_k is the double integral of $t^k E(t-u)f(u)$ in the u,t, plane, taken over the area bounded by u=0 and u=t. If the order of integration is reversed, one obtains

$$\mu_k = \int_0^\infty f(u) \int_0^\infty (u+v)^k E(v)\, dvdu$$

$$= k! \sum_{s=1}^{k+1} G_s (m_{k+1-s})/(k+1-s)!$$

where G_s is defined by

$$G_s = \sum_{n=1}^{N} \alpha_n/\lambda_n^s = \sum_{n=1}^{N} \alpha_n \tau_n^s \quad .$$

For successive values of k, a set of linear equations is obtained such that

$$\mu_0 = G_1 m_0,$$

$$\mu_1 = G_1 m_1 + G_2 m_0,$$

and

$$\mu_2/2! = G_1 m_2/2! + G_2 m_1 + G_3 m_0 .$$

These equations may be used to solve for the G's given the moments μ_i, m_i. A set of 2N G's completely characterizes a given sample. In other words, a knowledge of such a set is equivalent to a specification of $\alpha_1,\ldots\alpha_n$, $\lambda_1,\ldots\lambda_n$. For small values of N the α's and λ's may be determined from G_1, G_2, $\ldots G_{2N}$, by elementary algebra.

Because of experimental error it is often impossible to give an absolute meaning to N, the number of components. For example, if experimental data is obtained from a system that has but a single decay with a decay constant λ, it will always be possible to satisfy the experimental data by assuming that two components are present with decay constants $\lambda_1-\Delta_1$ and $\lambda_1+\Delta_2$, provided Δ_1 and Δ_2 are small enough. In other words, experimental errors preclude the possibility of resolving two components that have sufficiently close decay constants, or even of deciding if two species, rather than one, exist. Similarly, in multicomponent systems, it is impossible, in an absolute sense, to state how many components are present.

Unfortunately the emission data, F(t), extends only to some finite time, T, rather than to infinity as required in the

integration proceedure. Approximating the moments of F(t)

$$\mu_k = \int_0^\infty t^k F(t)dt$$

by

$$\mu_k \simeq \int_0^T t^k F(t)dt$$

may introduce significant errors, which become progressively worse as k becomes larger. No difficulty is encountered in the excitation data, E(t), however, since it rapidly approaches zero at early values of t.

This cut-off error is important because it appears that for reasonable sets of data, it is impossible to use the method of moments for a multicomponent analysis without a good correction. For such a correction, an iterative procedure has been proposed where μ_k is first approximated from the available data and then corrected by adding

$$\delta\mu_k = \int_T^\infty t^k \sum_{n=1}^{N} \alpha_n e^{-\lambda_n t}\, dt.$$

To calculate $\delta\mu_k$, approximate values of α_n and λ_n are used. The resulting moments are then used to find new values of α_n and λ_n which then allows a second estimate of $\delta\mu_k$. The process is repeated until an arbitrary small change in each of the parameters is achieved at each iteration.

The convergence of the iteration is followed by finding the root mean square difference between the values of μ_k calculated and estimates based on the equation,

$$\mu_k^{est} = \int_0^T t^k \sum_{n=1}^{N} \alpha_n \int_0^t E(t-\mu)e^{-\lambda_n t}\, d\mu dt \quad .$$

For rapid convergence $\delta\mu_k$ is desired to be as small as possible, and this requires that data be used at long enough times for the fluorescence to decay to low values. However, as the emission becomes smaller, the signal-to-noise ratio increases and the analysis becomes worse. It is therefore not feasible, in general, to make $\delta\mu_k$ arbitrarily small, and it is this feature that makes the cut-off correction important.

In the analysis scheme developed by Isenberg and Dyson[27] the computational scheme is as follows:

1. N moments are calculated from the excitation data, E, and an equal number from the fluorescence data, F.

2. An attempt is made to reconcile these moments with a single decay by fitting the fluorescence curve at long times to a single exponential. The constants α and λ for this hypothetical single component are determined from the fit.

3. The values of α and λ are used to calculate a cut-off correction, $\delta\mu_k$.

4. From the values of $\delta\mu_k$ and the experimental values of m_k, and μ_k a set of G's is determined.

5. The set of G's is then solved for the new values of α and λ.

6. These new values are used to calculate moments of F, which are then compared with the experimentally determined moments.

7. If the fit is unsatisfactory, the program returns to step 3.

8. If the fit is satisfactory, the number of components is

increased by one and excution is terminated.

Isenberg and Dyson also note that in cases where noisy two component data was analyzed for three components, that a common finding was a third component which showed a large value of τ_3 and a small value of α_3. Also cases were found which showed a third component with small negative values of α_3 and τ_3. Both of these situations were interpreted to be the result of a small base line drift.

The computer program used to process the data generated here is based on the method of moments by Isenberg and Dyson[27] and was supplied to us by Richard Hautala of the University of Georgia. The program was used initially without modification, but later a feature was added which plotted the shape of the calculated decay function. A sample plot of the experimental decay curve, calculated decay, and calculated decay function is shown in Figure 10.

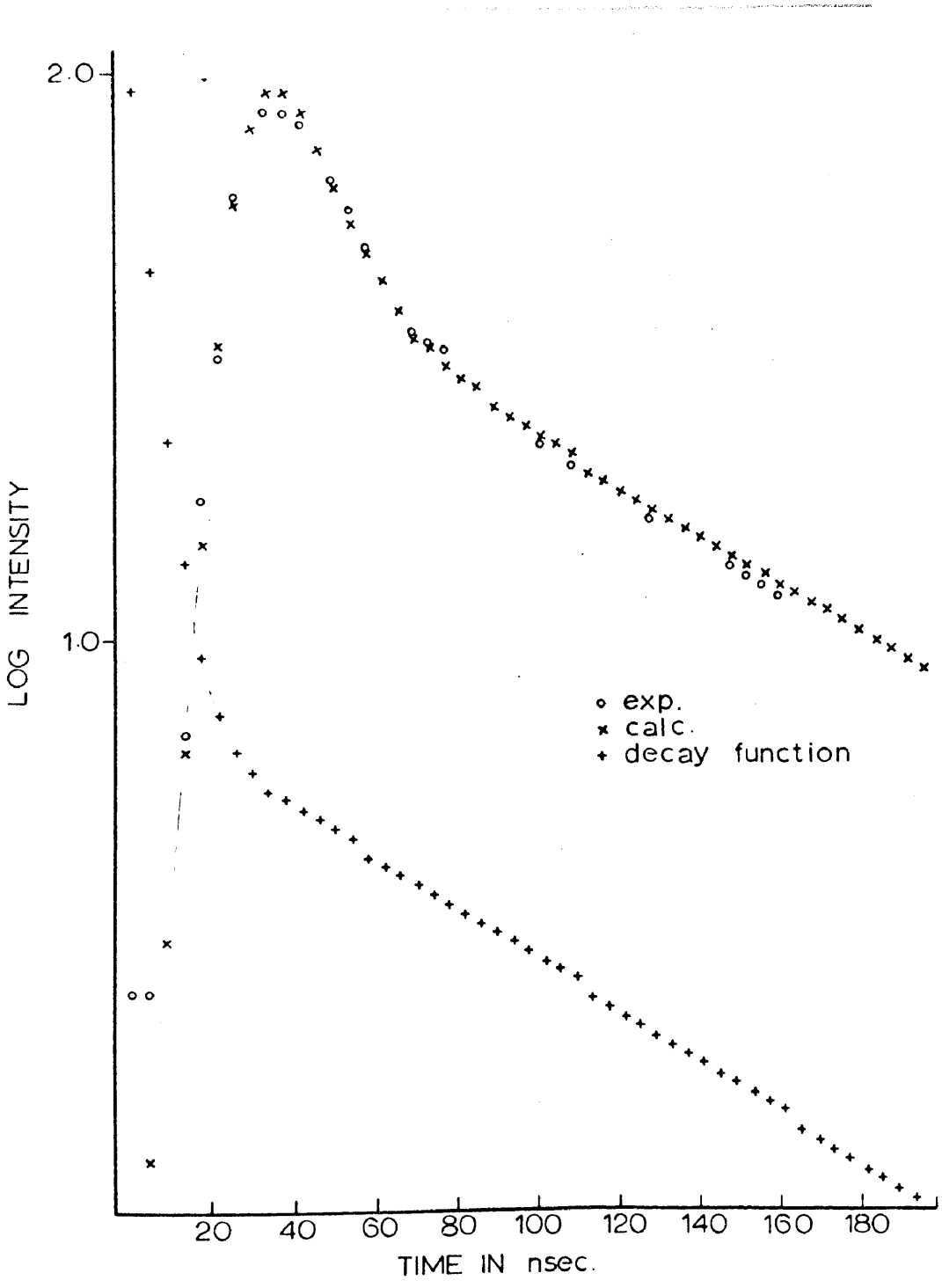

Figure 10. Sample plot of an experimental decay curve, calculated decay, and calculated decay function.

CHAPTER V

RESULTS

In order to test the data of Nauman reported by Birks[22], and in order the define the spectral regions of interest in fluoranthene, survey spectra were run on the Baird Atomic Fluorimeter. Figure 11 shows the fluorescence and phosphorescence emission of fluoranthene excited at 366 nm. The samples used were run at 77°K in EPA at a concentration of 10^{-4}M. The phosphorescence (dotted line) was measured using a mechanical chopper to screen out the shorter lived fluorescence and was normalized to full scale intensity for display. The relative magnitude of the phosphorescence can be seen from the shoulders on the fluorescence band in the 560 nm region.

Figure 12 shows the fluorescence and phosphorescence from the same sample excited at 314 nm and shows the new fluorescence F_2 and phosphorescence P_2. Again, the phosphorescence, shown by the dotted line, is normalized to full scale and bears no intensity relationship to the fluorescence. The transitions of interest thus defined are $S_2 \rightarrow S_0$ (F_2), $S_1 \rightarrow S_0$ (F_1), $T_2 \rightarrow S_0$ (P_2), and $T_1 \rightarrow S_0$ (P_1). The spectral results are in good agreement with those reported by Nauman with the exception of the P_2 portion of the spectrum. Nauman reported the P_2 phosphorescence as originating at 466 nm; however, we observe it to originate at a higher energy in the region of 400 nm. This is more in keeping with the process of phosphorescence in which one expects a triplet state ordinarily

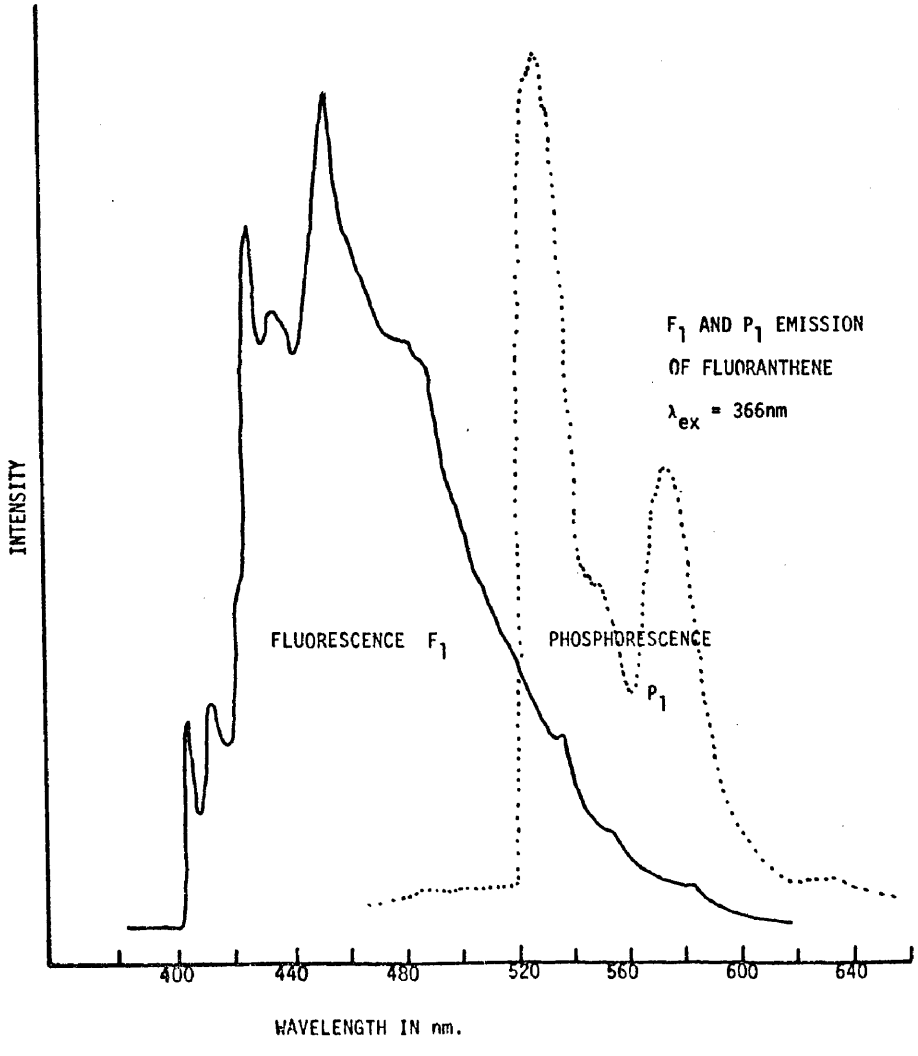

Figure 11. Fluorescence and phosphorescence of fluoranthene at 77°K, and excited at 3660 angstroms.

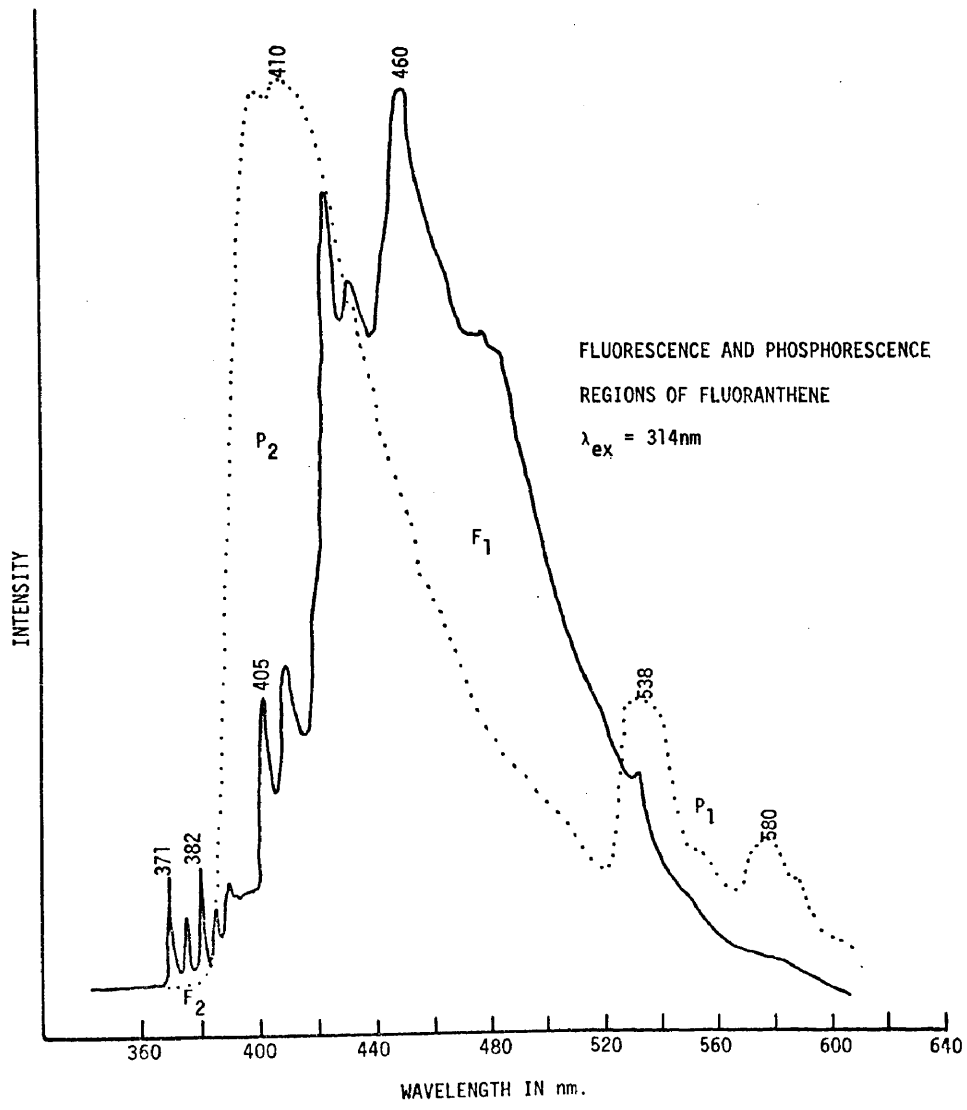

Figure 12. Fluorescence and phosphorescence spectrum of fluoranthene at 77°K, and excited at 3140 angstroms.

to lie slightly lower in energy than its corresponding singlet state. That is, T_2 should lie lower in energy than S_2, and T_1 will lie lower than S_1. This is the case that has been found experimentally in fluoranthene, indeed with T_2 between S_2 and S_1.

The observation of phosphorescence from T_2 to S_0 in fluoranthene presents a very interesting problem. The transition is, of course, spin forbidden and therefore rather long lived ($>10^{-4}$ sec). The internal conversion from T_2 to T_1 is spin allowed and would be expected to compete favorably with T_2 to S_0 phosphorescence even though the orbital symmetries of T_2 and T_1 are the same as those of S_2 and S_1, respectively. The indicated slowness or lack of internal conversion of T_2 to T_1 probably means that there is an insufficient density of vibronic states of T_1 in the energy range of T_2 and that there is inadequate Condon overlap of the vibronic states of T_2 with those of T_1.

With the areas of interest defined in the fluoranthene spectrum, samples were run on the laser-fluorescence system as shown in Figure 5. At first some difficulty was encountered in reproducing the spectra from sample to sample and in different solvents, however, it was later shown that self absorption has a greater influence than was first supposed. The difficulties encountered in the early spectral runs can now be attributed to agglomeration of the solute, as discussed earlier, or to having an excessively high initial concentration. The survey spectra of the fluorimeter were run at a concentration of 10^{-4}M and since the

spectra were reproducible and representative of the literature, some confidence was gained.

It was thought (since the magnitude of self absorption had not been recognized) that a 10^{-3}M sample would give a greater fluorescence intensity and would facilitate the detection of the F_2 fluorescence. However, due to the absorption of the $S_2 \rightarrow S_0$ emission back into the S_1 level, the opposite is true at high concentrations. Thus, while many normal fluorescence spectra may be run at concentrations of 10^{-3}M or higher, it is strongly recommended that in detecting dual fluorescences, that concentrations of 10^{-4}M or lower be used. Since the absorption is the product of concentration and transition probability, increasing the concentration increases the absorption and decreases the observed F_2 fluorescence intensity.

Figure 13 shows this effect over a concentration range of 10^{-6}M to 10^{-3}M. While the F_2 fluorescence intensity is larger relative to the F_1 fluorescence at 10^{-6}M, it should be remembered that this is a losing situation because lowering the concentration decreases the over-all intensity. Thus, a compromise must be reached between total intensity and the amount of F_2 fluorescence lost to self absorption. However, F_1 fluorescence could arise from coupling between levels and internal conversion to S_1. At best, neglecting all other effects, the minimum intensity obtainable in F_1 (assuming that it is pumped by F_2 fluorescence) would be found by computing the intensity from F_2 and then calculating

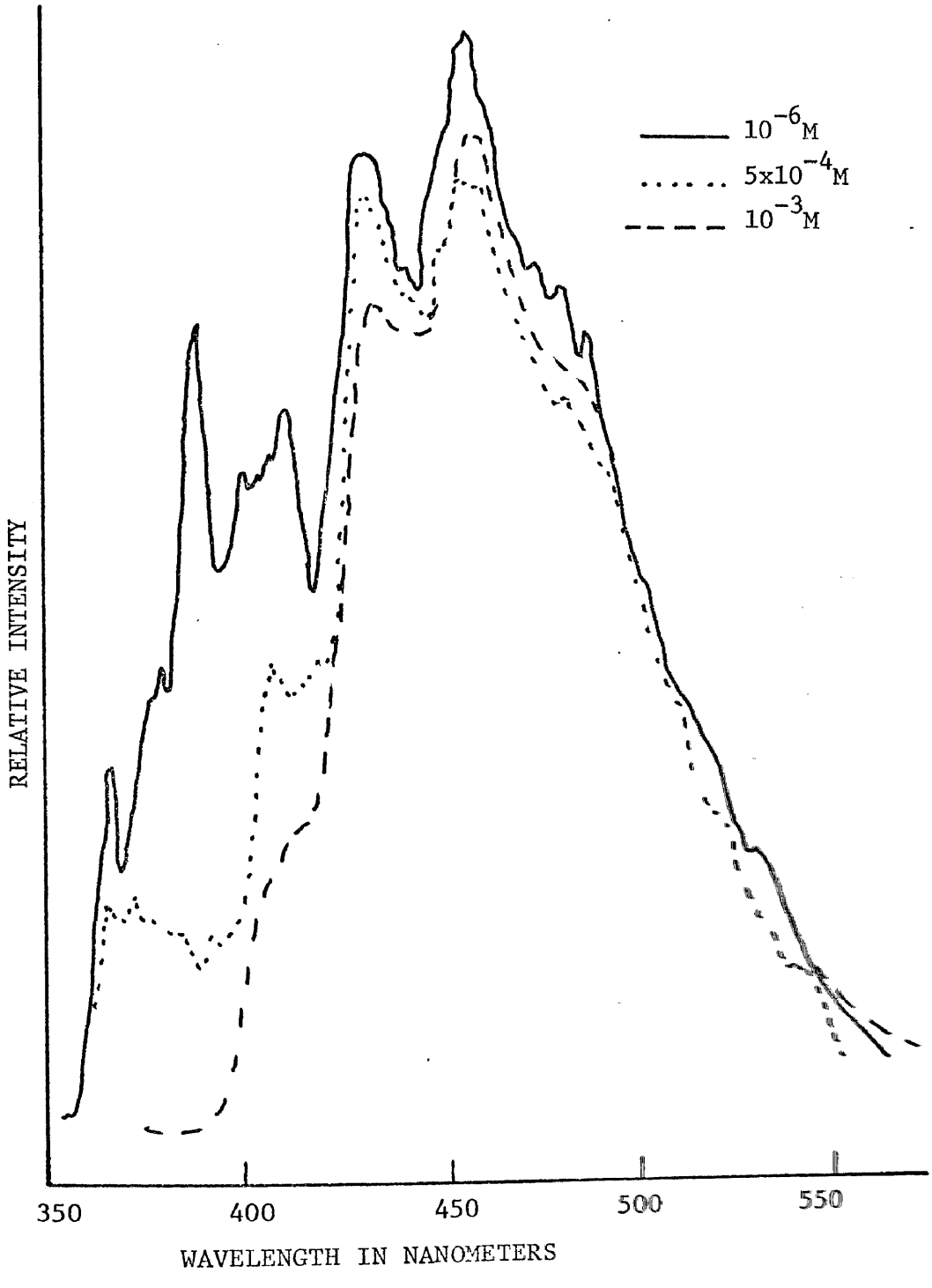

Figure 13. Effects of concentration on the absorption of F_2 emission in fluoranthene.

the resulting intensity of F_1 based on known concentrations, extinction coefficients, and quantum yields. It seems that it probably will be impossible to completely eliminate the F_1 fluorescence, but at least it should be possible to determine its origin and correct the intensities for that arising from self absorption.

It is also of interest to determine the relationship between fluorescence intensity and temperature. Figure 14 shows the fluorescence of fluoranthene at 77°K, at room temperature (298°K), and at intermediate temperature. All spectra were run at the same instrument sensitivity on the fluorimeter, and only the temperature of the sample was varied. Not only does the overall intensity decrease, but all structure in the F_2 region dissappears and the F_2 intensity decreases relative to the F_1 intensity in going from 77°K to 298°K. The relative intensities for the 3923A line are 64.5% of the F_1 intensity at 77°K and only 40% at 298°K.

Figure 15 shows the spectrum of fluoranthene run on the laser excitation apparatus at 77°K in EPA, and 10^{-4}M concentration. The regions of F_1 and F_2 fluorescence are clearly defined and are in good agreement with those run on the fluorimeter. From this spectrum, it was possible to identify the wavelengths of interest in each region of the spectrum for future reference. The F_2 region shows a good deal of structure and as a result, each band is easily labeled. However, in the F_1 region the bands are not as sharp and therefore each band was labeled

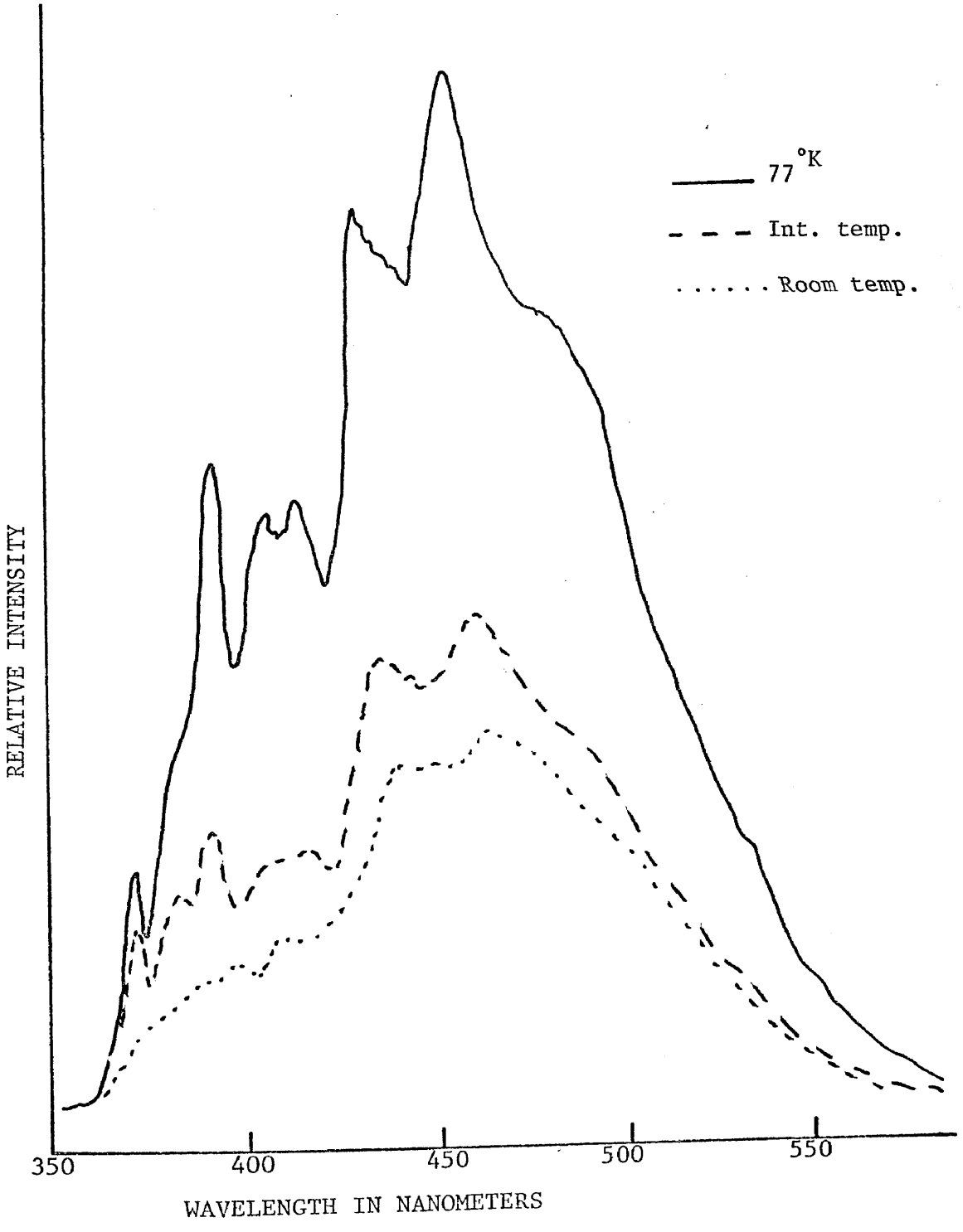

Figure 14. Effects of temperature on the fluorescence emission of a 10^{-6}M sample of fluoranthene.

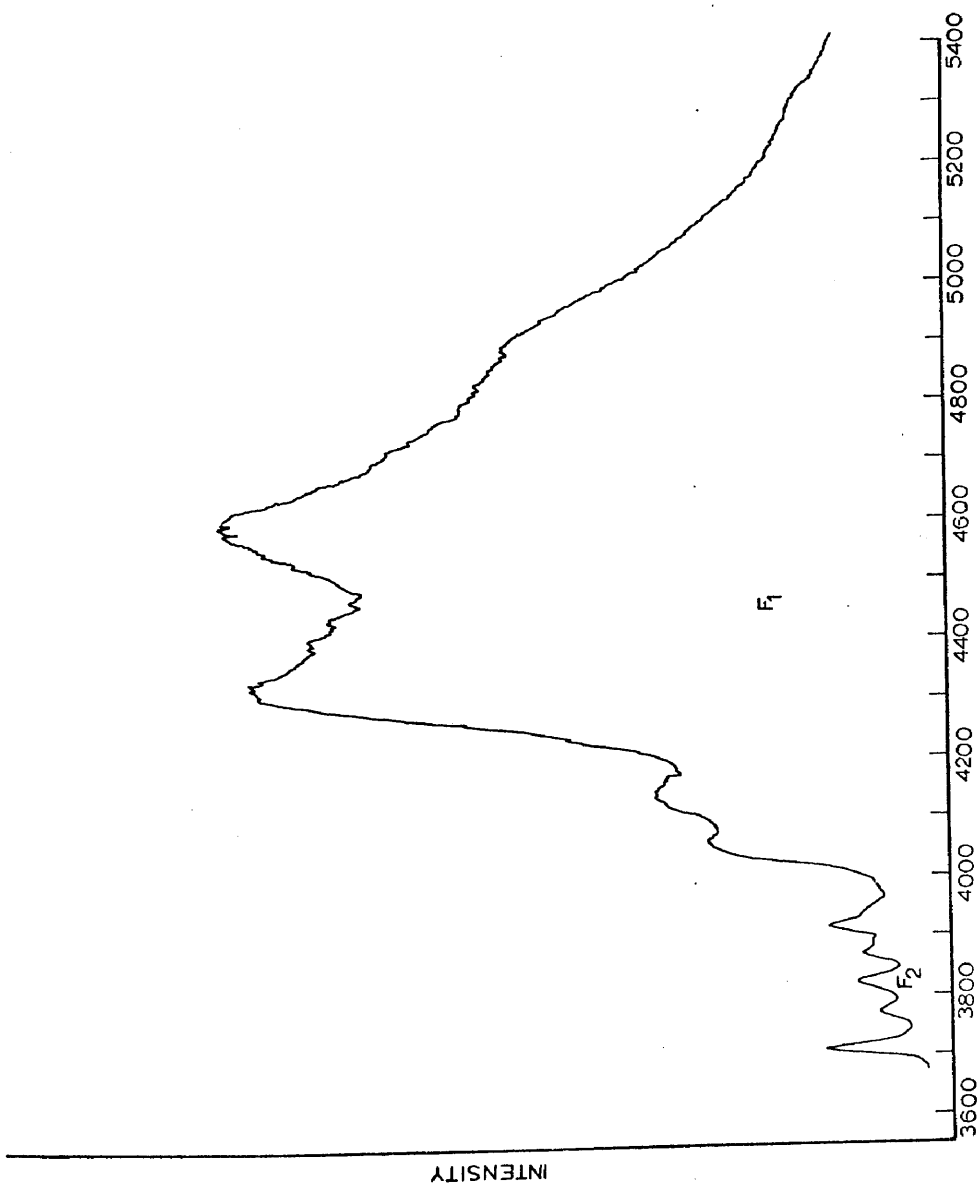

Figure 15. F_1 and F_2 fluorescence regions of fluoranthene run on the laser excitation apparatus at 77°K in EPA, and 10^{-4}M concentration.

at the midpoint of the band or the highest point, whichever was the easiest to distinguish. The resulting regions (now defined by line number - wavelength) are given in Table 2, with the 3710A line determined to be the 0-0 transition of $S_2 \rightarrow S_0$, and the 4050A the 0-0 transition of $S_1 \rightarrow S_0$.

On scanning the region from the laser wavelength (3371A) through the F_2 region, an interesting feature was observed in the vicinity of 3500A. Figure 16 shows a very broad structureless band in the region of 3500A which does not seem to be related to the F_2 fluorescence. The new band is located at 3535A, and is $1376 cm^{-1}$ lower in energy than the laser excitation line, and is $1334 cm^{-1}$ higher than the F_2 fluorescence.

In order to examine the intensity distribution of the F_2 region a time resolved spectrum was run in which the boxcar gate is positioned at some fixed point in time and the spectrometer scanned. (This method of energy resolved spectra has been described earlier.) The laser excitation was defined as the point of zero time. The resulting spectra are referenced relative to the laser pulse and the laser pulse can now be considered to be constant in time. (Since the laser pulse itself triggers the boxcar, any time fluctuations in the firing of the laser are compensated for by this method.)

Figure 17 shows the time resolved spectra of the region from 3450A to 4000A in 40 nsec increments from zero time to 120 nsec. This allows one to see intensity distributions and

Table 2. Wavelength regions in the fluorescence spectrum of fluoranthene.

Line in Angstroms	Energy in cm^{-1}
3535	28288
3710	26954
3768	26539
3820	26178
3865	25873
3923	25490
4050	24691
4130	24213
4325	23121
4600	21739
4900	20408

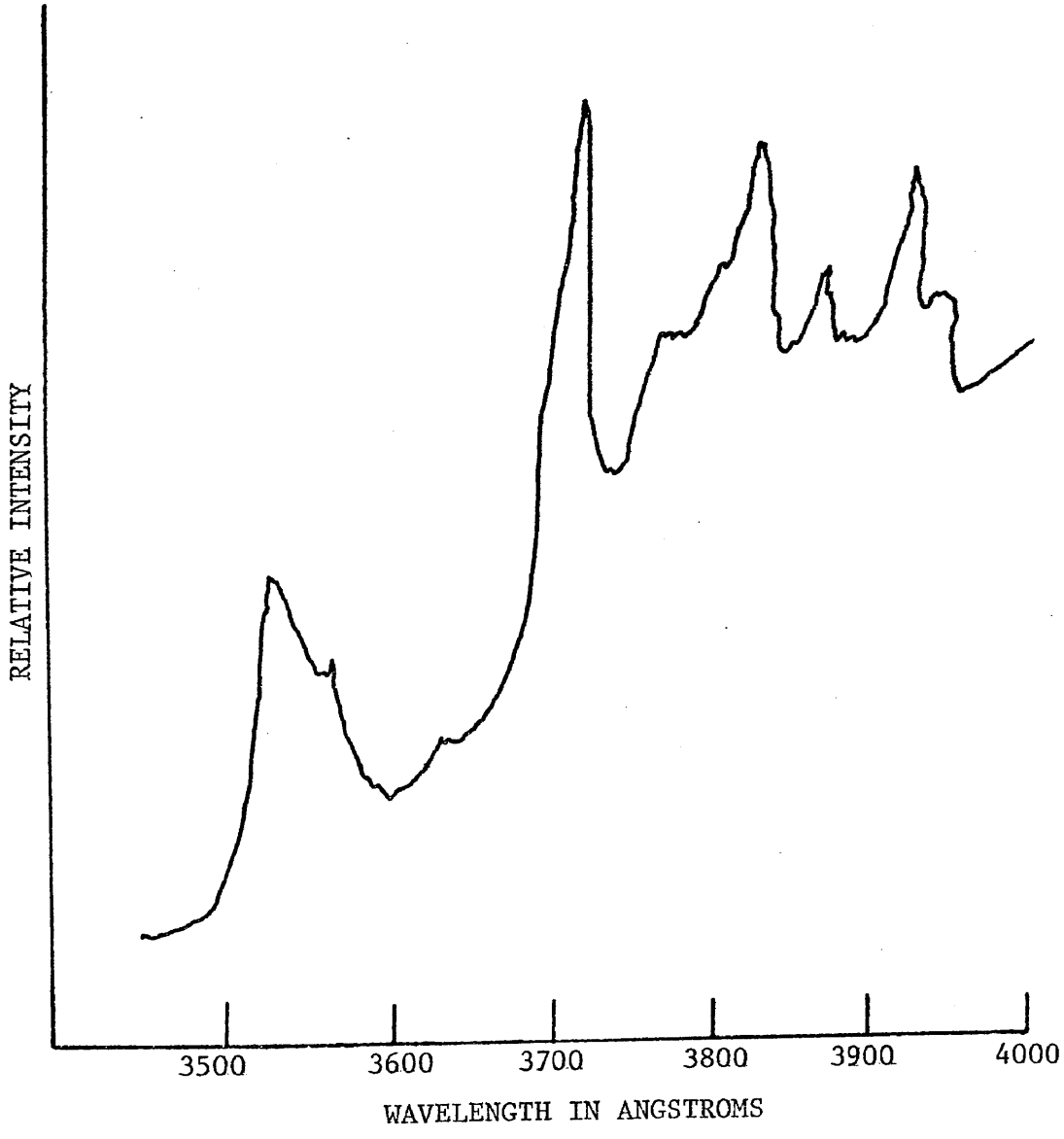

Figure 16. The F_2 fluorescence region of fluoranthene at 77°K in EPA and 10^{-4}M concentration.

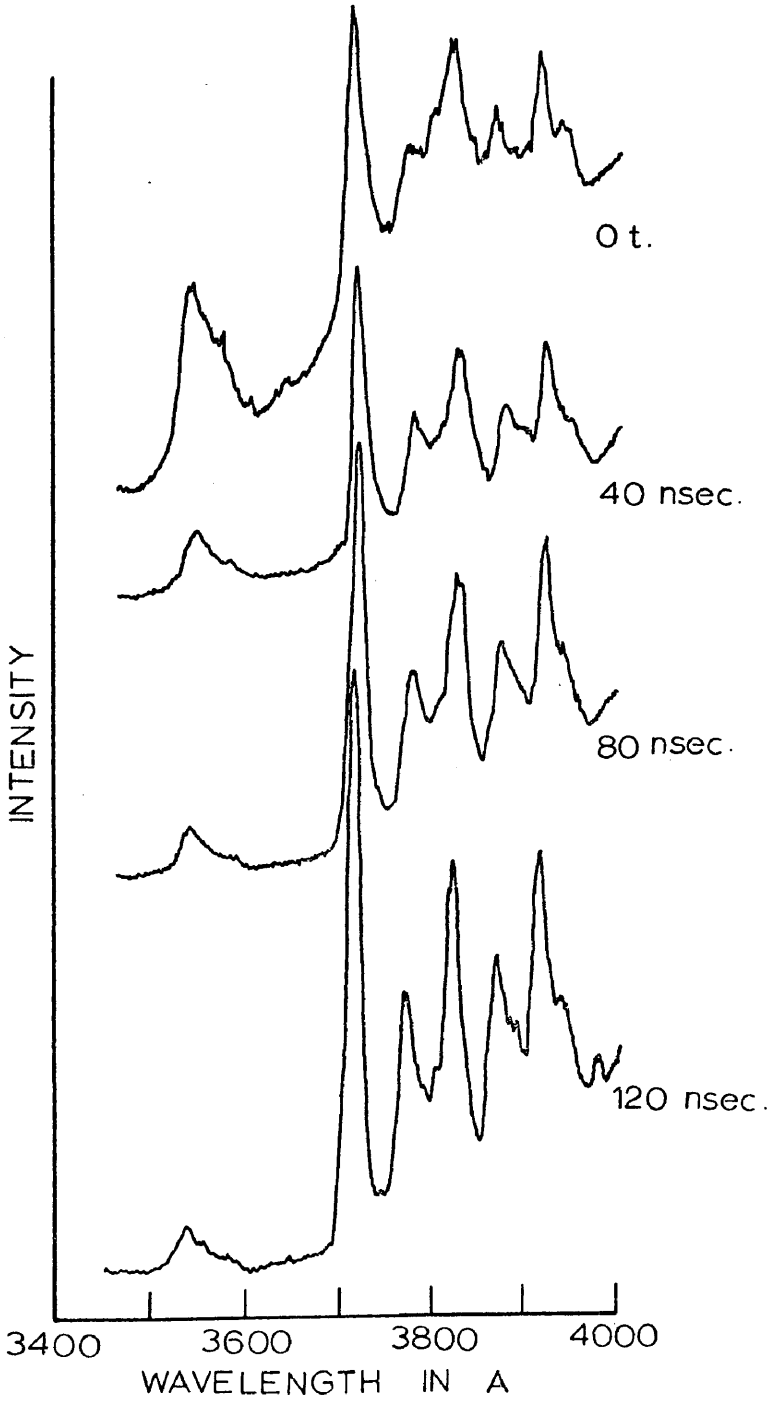

Figure 17. Time resolved spectrum of the F_2 region of fluoranthene in 40nsec increments from zero time to 120nsec.

changes in intensity as a function of time. The F_2 region from 3700A to 4000A shows a marked sharpening of the lines due to depopulation of levels of S_2, but more interesting is the band at 3535A. This band decays very fast to low intensity, has no structure, and is very broad. The spectra in figure 17 are all normalized to the F_1 maximum at 4600A and therefore the 120 nsec delayed spectrum seems more intense than the 0 nsec one. However, the instrument sensitivity is increased with each run to achieve normalization so that the 120 nsec delayed spectrum is very much weaker than indicated in the figure. Likewise the 3535A band is decaying very fast and does not remain constant from 80 nsec to 120 nsec as it seems.

Since this band is 1376cm^{-1} from the laser excitation, it could possibly be a Raman band of a C-C stretch (approximately 1400cm^{-1}). However, the absence of any other bands in this region seems to preclude this possibility. Geldof et al.[14] and Deinum[11] observed the same type of phenomena in pyrene and 3,4-benzpyrene. They attributed an observed short lived line, blue shifted by approximately 1400cm^{-1} to a "hot", S_2', band; i.e., an excited vibronic level of S_2. If this is a hot band, it should have a very fast relaxation time, which it does, but its intensity should also increase with increasing temperature.

Nauman[22] reported the F_2 fluorescence of fluoranthene as originating at 3532A, and extending to 3932A. However, in light of these more detailed experiments, it seems more reasonable to

assign the F_2 fluorescence to the region from 3710A to 3923A and the 3535A band to a hot band. It thus appears that the observation of hot bands in F_2 fluorescence may not be as unusual as one might suppose.

Figure 18 shows some of the primary photophysical processes which may occur following excitation of the second excited singlet state in an aromatic molecule. The different fluorescence decay steps are indicated by k_1 (F_1) and k_2 (F_2), and the location of a possible hot band is indicated by S_2'.

In order to examine the structure of the F_2 region and to define the location of the lines, a ratio spectrum was run in which another photomultiplier was inserted to monitor the laser power. This technique smoothes out the slight (1-5%) fluctuations in laser power and more precisely defines the location of a band since the ratio of the two signals is taken. This is the dual channel ratio mode described earlier, and, in a sense, is analogous to a dual beam spectrometer. Figure 19 shows the ratio spectrum of the F_2 fluorescence from 3700A to 4000A, and the wavelengths of the five distinct lines in the spectrum are listed in Table 2.

An interesting question now arises as to the time relationships between the F_1 and the F_2 fluorescence. The time resolved spectra of the total fluorescence (F_1 and F_2) were recorded in the same manner as the F_2 spectrum in Figure 17 and this is indicated in Figure 20. The F_1 spectrum is characterized by having broad structureless bands so that marked changes in the intensity

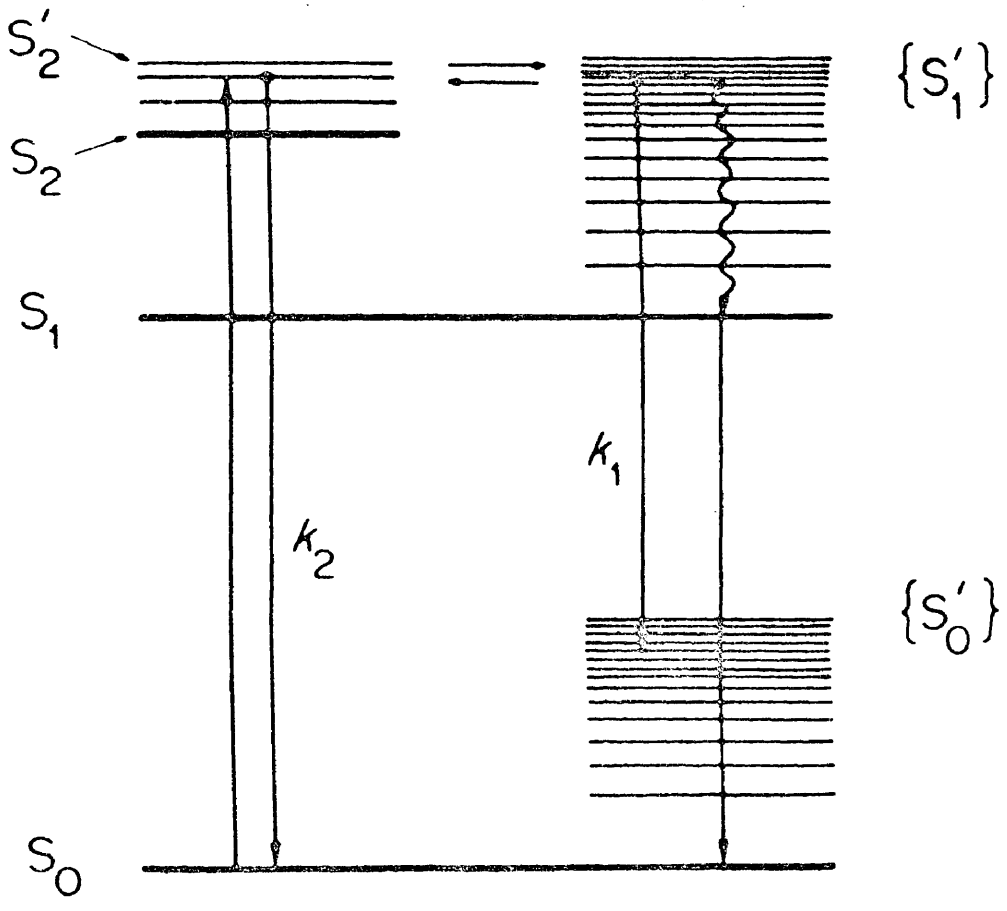

Figure 18.[22] Some primary photophysical processes which may occur following excitation into the second excited singlet state of an aromatic molecule.

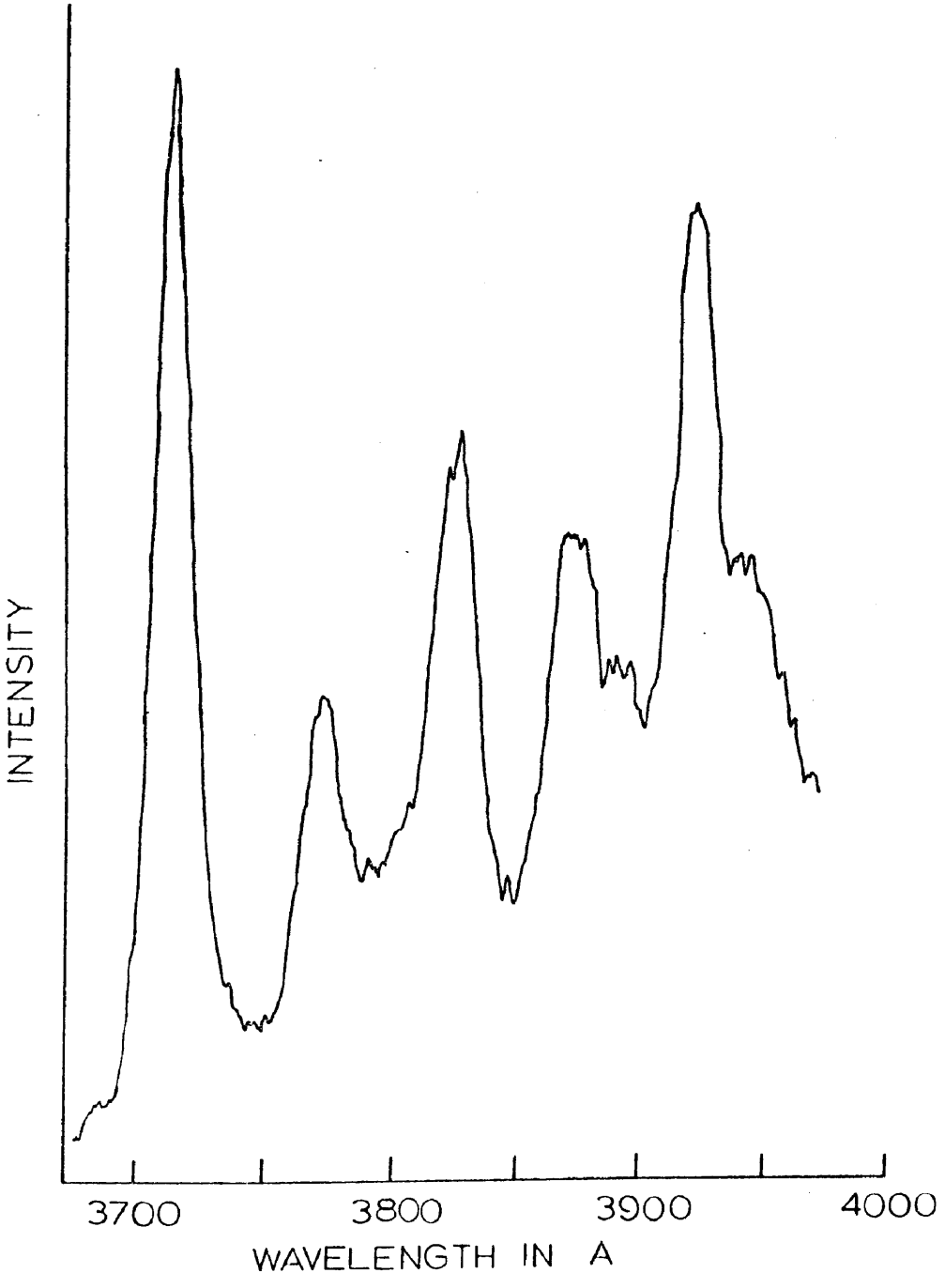

Figure 19. The ratio spectrum of the F_2 fluorescence of fluoranthene in EPA at 77°K and 10^{-5}M concentration.

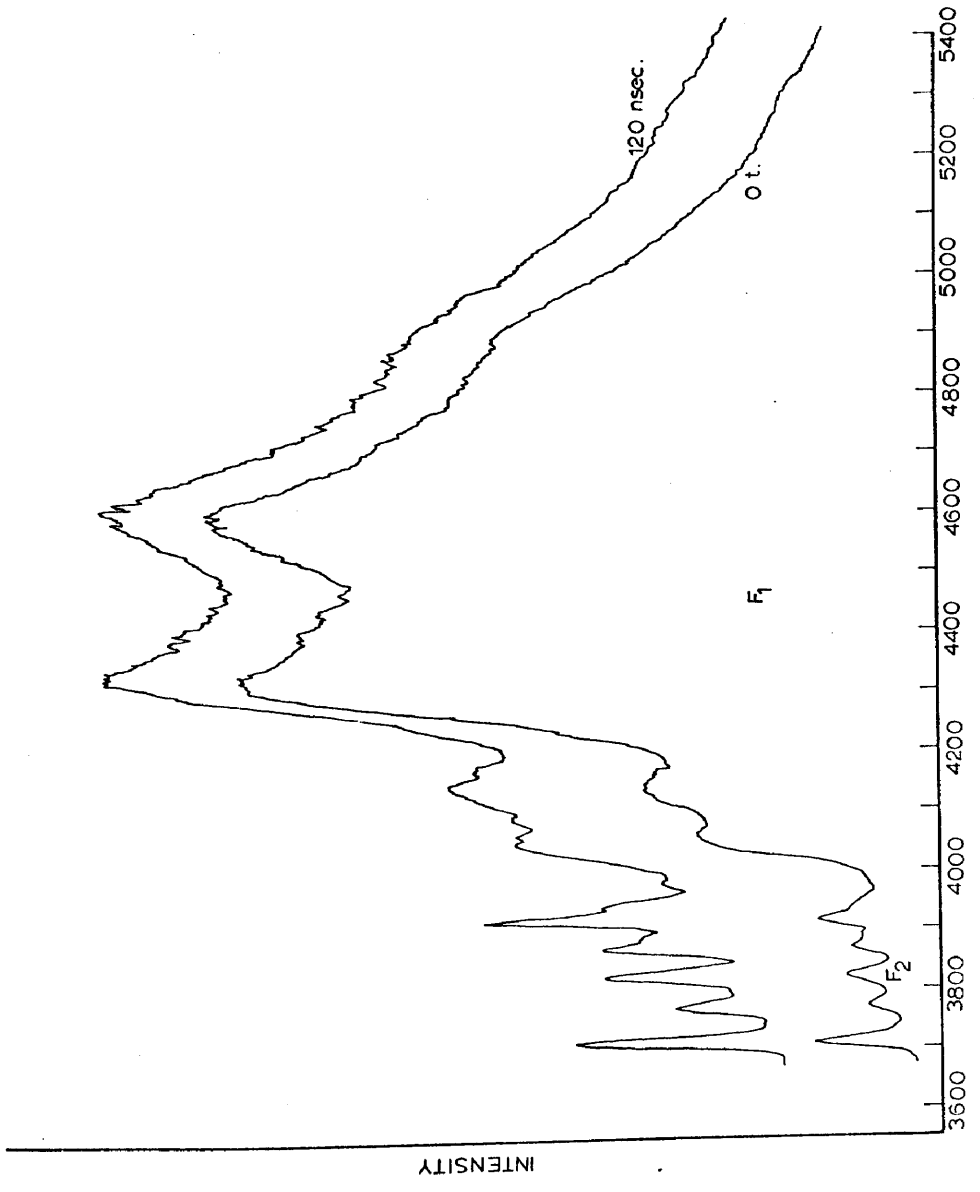

Figure 20. Time resolved spectrum of the F_1 and F_2 regions in fluoranthene in EPA at 77°K, and 10^{-4}M concentration.

distribution are generally not observed. However, an interesting feature of this is that the relative intensity of F_2 to F_1 appears to increase at longer times. This could be caused by the S_1 state feeding, or back populating, S_2. Since this is most improbable, the other possibility is that the S_1 state is decaying faster than S_2. The spectra in Figure 20 were normalized with the 4600A band of F_1 full scale (The spectra in Figure 17 were recorded in the same manner.). It is to be noticed in Figure 17 that the F_2/F_1 intensity is greater at 120 nsec delay than at 0 nsec delay, indicating that S_2 decays slower than S_1.

The actual lifetimes of the two states were then determined. The decay curves were plotted by setting the spectrometer to the line in question and scanning (in time) the gate of the boxcar averager. This is illustrated in Figure 7 and has been described in detail in the section on experimental methods. Figure 22 shows the overlay of several different lines and their relationship to the exciting pulse. Here, zero time represents the start of the time base, and the display of the decay curves represents their location in the time base range.

The laser line at 3371A is represented by the solid line, the 3535A hot band by the dotted line, the 4050A and 4600A band belong to S_1 and the dashed line represents the 3710A line. It is clear that the 3710A line of F_2 is longer lived than the F_1 fluorescence, but to determine the magnitude of the decay free from the laser pulse, the computer program using the method of moments,

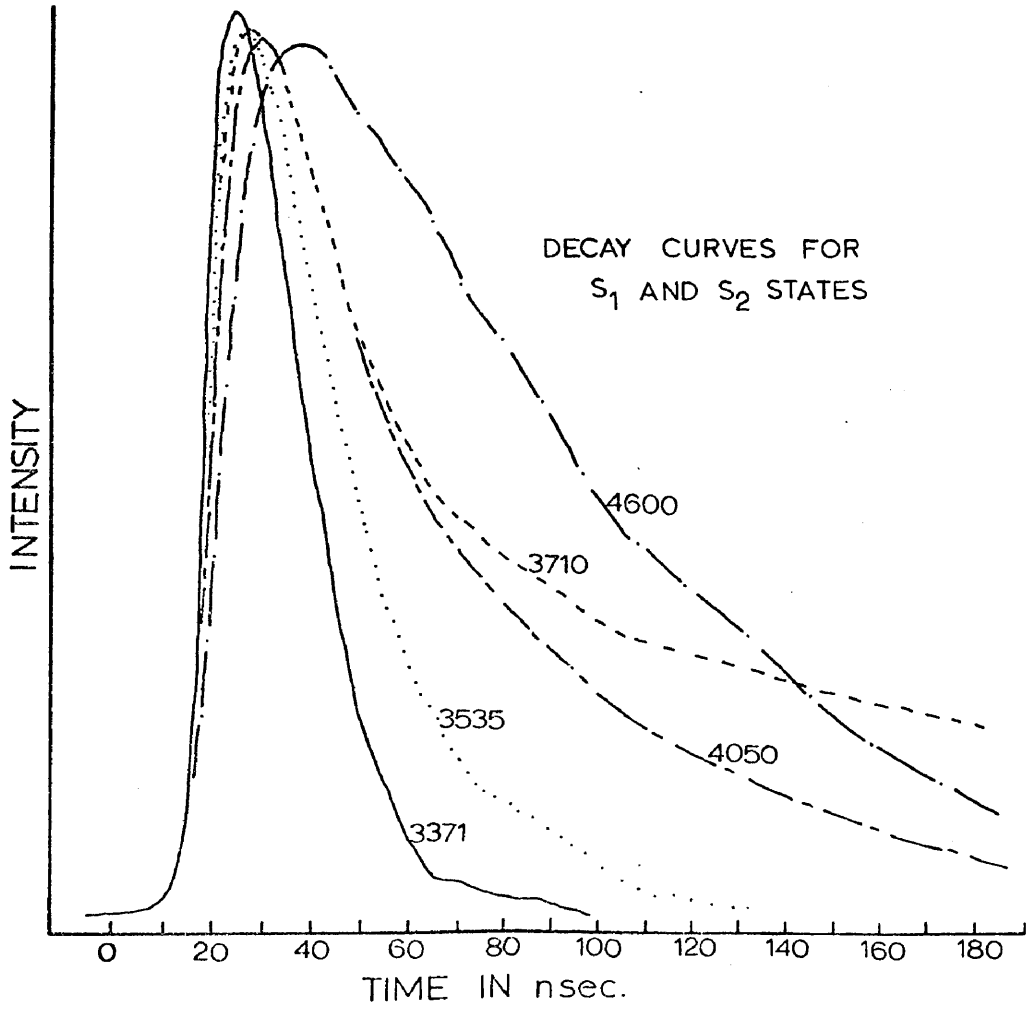

Figure 21. Experimental decay curves for the two spectral regions of fluoranthene and their relationship to the excitation pulse (solid line).

described earlier, was employed. This program, as modified by us, determines the best fit from fitting the calculated curve to the exponential data using one, two, or three exponentials. The resulting best fit, as determined by the smallest standard deviation of the moments, is plotted, and then the corresponding decay function is plotted. This is indicated in Figure 22 for the 3820A line of F_2. The fact that the slope of the decay function and the decay curve are the same means that the decay function represents a good interpretation of the decay curve.

For computational ease, the decay function is calculated to fit into the range covered by the experimental decay; and thus, while the two curves are not of the same magnitude, the relationship between their slopes indicates the closeness of the fit. The decay functions determined in this manner give a value for the observed decay time of the state and are presented in Table 3.

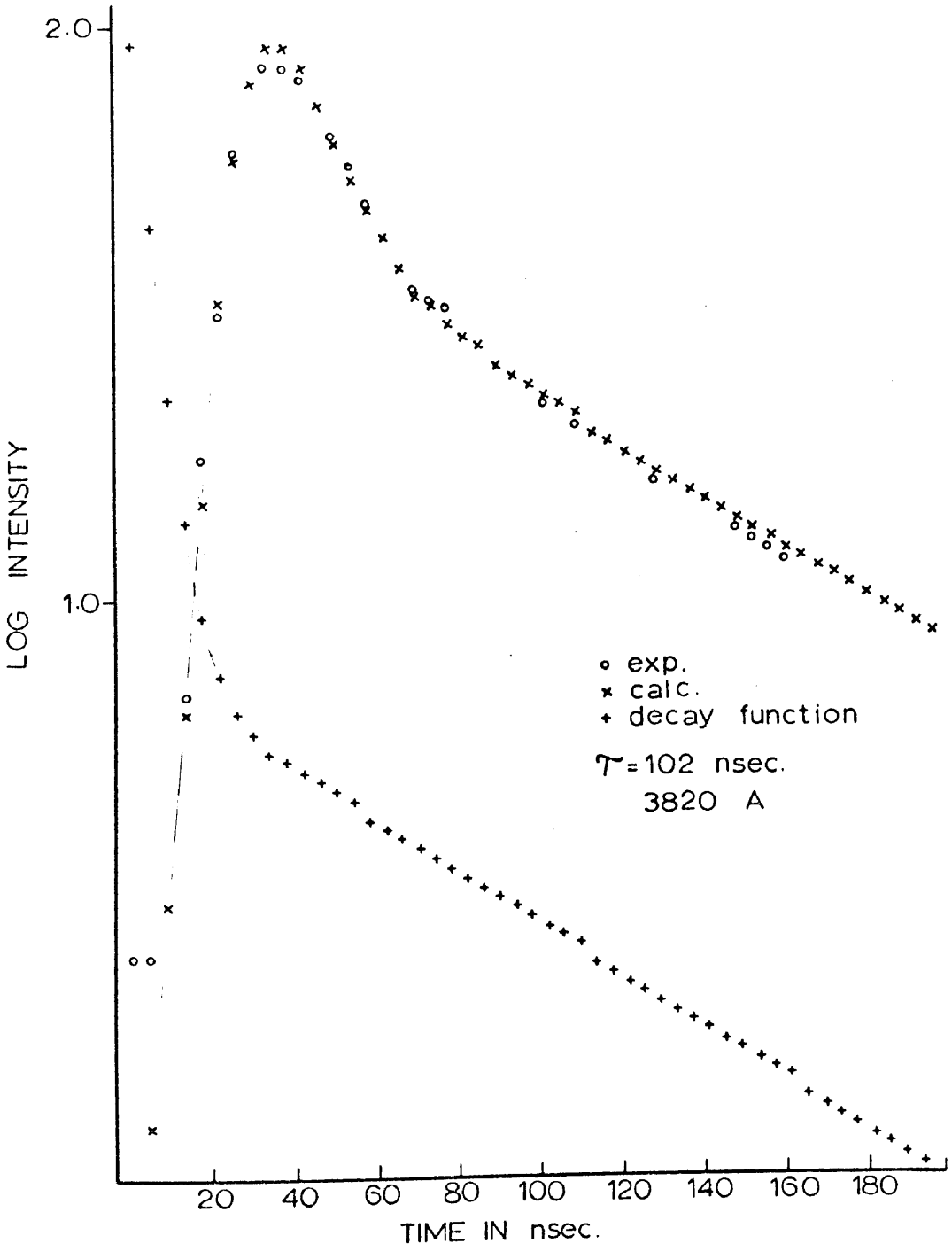

Figure 22. Computer calculated best fit to the experimental decay curve. The calculated decay function is plotted in the lower curve.

Table 3. Experimentally determined lifetimes for the various lines in the fluoranthene spectrum.

Line in Angstroms	Lifetime in nsec
3535	5
3710	140
3768	18
3820	102
3865	19
3923	45
4050	58
4150	28
4325	34
4600	58
4900	52

CHAPTER VI

CONCLUSIONS AND SUMMARY

A pulsed laser spectroscopy system has been designed and constructed and utilized to study the dual fluorescence of fluoranthene. The apparatus, as described, incorporates a pulsed molecular nitrogen gas laser and associated electronics, spectrometer, and data processing electronics. The completed experimental arrangement allows for the measurment of energy (wavelength) resolved spectra as well as the determination of decay times-time resolved spectra. The short pulse length and high intensity of the nitrogen laser allows these spectra to be recorded with higher spectral resolution than is generally available. Thus, the experimental system presented here is capable of being applied to a great variety of fluorescent compounds and is, in general, applicable to the study of fluorescence of most molecules. The high intensity of the nitrogen laser pulse also makes it possible to study compounds which have low quantum yields of fluorescence with relatively little difficulty.

Using the apparatus described in the experimental section, the time resolved and energy resolved (wavelength) spectra of the dual fluorescence of fluoranthene have been characterized. The energy resolved spectrum consists of two easily discernible regions: the s region ($S_2 \rightarrow S_0$), where the major contribution to the fluorescence originates from transitions $\phi_s \rightarrow \phi_0^{0\omega}$ to totally symmetric vibronic components of the ground electronic state

$\phi_0^{0\omega}$, covers the region from 3700A to 3925A, and the ℓ region ($S_1 \rightarrow S_0$) which contains the region above 4000A and represents the contribution to the emission which arises from transitions $\{\phi_\ell\} \rightarrow \{\phi_0^{\ell\omega}\}$ to nontotally symmetric components $\phi_0^{\ell\omega}$ of the ground electronic state.

The theoretical radiative lifetime of the states in the s region may be calculated from the relation given by the Mulliken approximation as follows:

$$\tau = 1.5/(f\nu^2)$$

where f = the integrated oscillator strength

and ν = the wavenumber of the transition.

Assuming a value of 0.1 for the oscillator strength (Michl[24] calculates an approximate value of 0.1, and Wannier[6] also assumes this to be a reasonable value for this type of transition.) of the s region one calculates a theoretical radiative lifetime of 20 nsec. However, the 3710A line has an experimental decay time of 140 nsec, and the 3820A line has a decay of 102 nsec. The complete listing of the descrete spectral regions and their corresponding lifetimes are given in Table 4, and the same lines are given with their decay functions (α's and τ's) in Table 5.

In the intermediate level spacing, strong coupling situation one expects that the radiative decay times in the s and ℓ regions should be approximately equal, while the oscillator strength for the $S_0 \rightarrow S_2$ excitation exceeds that of the $S_0 \rightarrow S_1$ transition by about one to two orders of magnitude. From the data it is indeed apparent that the experimental decay times vary very slightly (by about a

Table 4. Assignment of the lines in the fluoranthene spectrum.

Line in Angstroms	Lifetime in nsec	Origin
3535	5	S_2'
3710	140	S_2
3768	18	S_2'
3820	102	S_2
3865	19	S_2'
3923	45	S_2'
4050	58	S_1
4150	28	S_1'
4325	34	S_1'
4600	58	S_1
4900	52	S_1

Table 5. Calculated decay functions for a "best fit" to one or two exponential decays.

Line in A	One Exponential		Two Exponentials			
	α	τ	α_1	τ_1	α_2	τ_2
3535	0.3	4.44				
3710	0.03	55.9*	0.0066	143.5	0.25	3.68
3768	0.0828	17.7				
3820	0.0529	44.27*	0.0176	102.5	0.175	4.854
3865	0.0781	18.7				
3923	0.0363	45.4				
4050	0.0615	38.7*	0.0324	58.6	0.493	1.15†
4150	0.0702	27.9				
4325	0.0644	38.4				
4600	0.0619	58.4				
4900	0.0645	52.8				

* Not a "best fit".
† Reflects a small base line drift.

factor of two) from the s region to the ℓ region.

If coupling is involved in this case, one would expect that the decay time in the s region would be appreciably lengthened relative to that expected on the basis of the integrated oscillator strength for the transition. By comparing the observed and calculated radiative lifetimes, it is noted that the energy resolved radiative lifetimes in the s region, which correspond to "resonance fluorescence" from the second excited singlet state, are appreciably longer (by a factor of 5-6) than expected on the basis of the integrated oscillator strength for the $S_0 \rightarrow S_2$ transition ($f \simeq 0.1$). Thus, the experimental data are in good agreement with the theoretical predictions[28] for the intermediate level spacing strong coupling situation.

From Table 5 the decay functions as calculated from the experimental decay curves are listed. It is noticed that all of the lines (except two) have a single exponential decay. The 3710A line and the 3820A line both have a two component decay characterized by a very short (4 nsec) decay followed by a longer lived component. At the present time there seems to be no conclusive explanation of this phenomenon. Jortner[3] notes that the decay from a state in the s region should be a sum of exponentials. That is, a sum of the exponential decay from the upper state and the exponential decay from the lower state to which it is coupled. Rhodes,[5] however, says that the observed decay should be a sum of the exponential decays of the states involved in the region.

This two component decay is quite intriging; one possibility is that the short component is the result of the emission of a hot band of the same wavelength, thus overlaping the principle transition. If a hot level emitted to an excited ground vibronic level with the same energy (wavelength) as the normal 3710A or 3820A lines, it could give a fast component to the decay. However, that the two lines would be precisly the same energy is unlikely. Therefore, if this sort of process occured, it should be possible to discern a change in the line shape with time that parallels (in time) the decay. A shift in wavelength would also be observed. This would need to be checked by a much more careful time resolved spectrum of the lines because of any possible wavelength shift. Nevertheless, it seems that the full explanation of this phenomenon will have to await further theoretical developments or refinements in measurment, higher resolution time resolved spectra.

The 3768A and 3865A lines are characterized by a very short decay, and are even shorter than the theoretical predictions by a few nanoseconds. Thus, these lines are assigned to "hot" bands of the S_2 emission and do not represent true states of the s region. The 3923A line represents an interesting case in which it is also proposed that this is a hot band of S_2 but is also coupled to S_1. It is energetically in the s region but has a lifetime comparable to the ℓ region. It seems, therefore, that the 3923A line represents a coupled hot band of S_2.

However, the data presented here agree well with what is generally expected to be observed on a theoretical basis[3,5]. Thus, fluoranthene provides a very good case for the study of dual fluorescence and should be an interesting example for theoretical examination since its energy separation between S_2 and S_1 is fairly large, and there is less of a problem of the overlap of hot S_1 and S_2 emission which is the problem in the cases of 1,12-benzperylene and 3,4-benzpyrene.

There are further experiments on fluoranthene which may be suggested. Preliminary, but not conclusive, experiments with the fluorimeter have indicated that it might be possible to increase the F_2/F_1 ratio by increasing the excitation energy (shorter wavelength). If this turns out to be the case, then it would tend to definitely disprove the thermal population argument as well as show the magnitude of internal conversion from S_2 to S_1, if any. Since there will always be some F_1 observed (from self absorption of F_2), it would be impossible to completely eliminate the F_1 emission. However, the limiting magnitude of F_1 fluorescence can be calculated, and by exciting at higher energies, the ratio of F_2/F_1 may be obtained. In this way the experimental limiting value of F_1 intensity may be determined. The difference between this value and the theoretical intensity should yield an estimate of the magnitude of the internal conversion.

Of even greater interest is the phosphorescence. The theoretical implications of observing phosphorescence from more

than one state have not been fully developed largely because the observation of phosphorescence from T_2 is not expected to occur. It has been suggested that the spin allowed $T_2 \rightarrow T_1$ internal conversion should be much more favorable than the spin forbidden $T_2 \rightarrow S_0$ phosphorescence, and thus, only $T_1 \rightarrow S_0$ phosphorescence should be observed. However, Figure 12 clearly shows the dual nature of the phosphorescence in fluoranthene and the spectrum presented in Figure 12 should be compared to that of Figure 11. The mere observation of dual phosphorescence is in itself unexpected and, thus, warrants further study as it immediately offers a system consisting of four descrete radiating states (T_2, T_1, S_2, and S_1). In light of this, it can be speculated that internal conversion does not occur from S_2 to S_1. Since T_2 is of the same orbital symmetry as S_2, intersystem crossing might occur from S_2 to T_2. Likewise T_2 to S_1 does not occur, but T_2 to S_0 does.

A possible four level system might be envisioned as follows in Figure 23, with virtually no internal conversion occuring between the singlet states or between the triplet states.

Since the spectra in figures 11 and 12 were run on the fluorimeter and a mechanical chopper was used to discriminate against the short lived fluorescence, then the phosphorescence observed must be fairly long lived although no lifetimes have been measured on the laser system.

Busch et al.[20] have observed the fluorescence from F_1 and the phosphorescence from T_1 in benzophenone and analyzed the observed

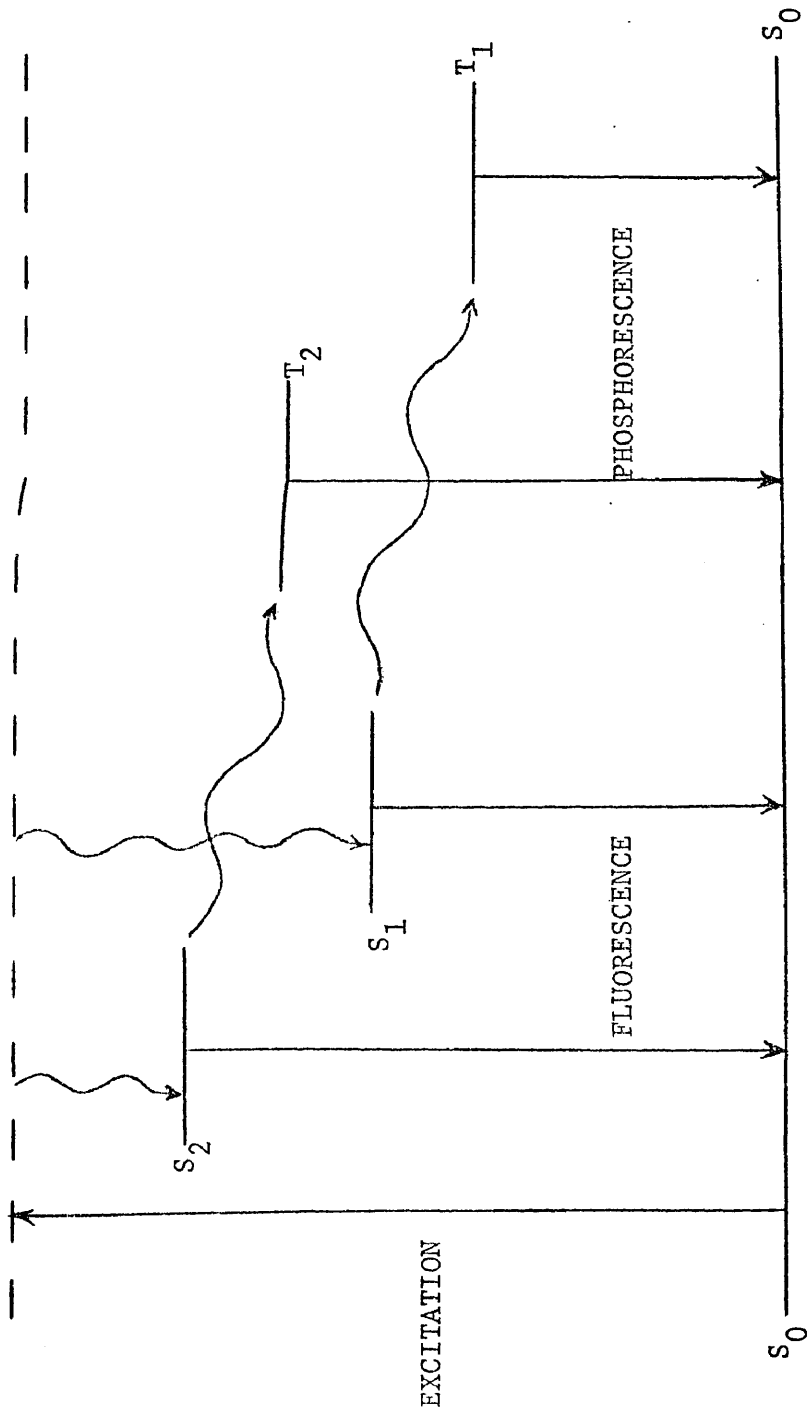

Figure 23. Possible four level sequence for the processes occuring in fluoranthene.

spectra in terms of the coupling models. Busch et al. concluded that the decay from the lowest singlet state of benzophenone exhibits predominantly the characteristics of strong interstate singlet-triplet coupling. It seems likely that in fluoranthene there may be some interstate coupling between S_2 and T_2, and between S_1 and T_1.

Thus, the triplet systems in fluoranthene offer some very interesting experimental possibilities which naturally have strong theoretical implications. The work carried out in this study on the fluorescence of the singlet systems offers a firm basis upon which to build future experiments. Certainly the understanding of this complex system will help refine the theoretical predictions put forth to date.

The experimental systems thus developed have provided a means for examining the dual nature of the fluorescence in fluoranthene and additional experiments have suggested future experiments which should be undertaken to fully understand this four level system. It is hoped that the data presented in this study will help towards the understanding of those processes involving emission from more than one excited singlet or triplet state.

APPENDIX I

DESIGN AND CONSTRUCTION OF A PULSED MOLECULAR NITROGEN LASER

Introduction

A molecular nitrogen gas laser is one of a class of self-terminating pulsed gas lasers that include neon[30-32], copper[33], and lead[34]. These lasers are typically excited by a fast-rising high voltage discharge and produce peak powers in the kilowatt to megawatt range, with pulse widths of the order of ten nanoseconds.

The energy level transition that takes place in a 3371 angstrom, pulsed molecular nitrogen laser corresponds to the (0,0) transition of the second positive band system of nitrogen, as shown in figure AI-1. The radiative lifetime of the C state is 40 nanoseconds, while the radiative lifetime of the B state is 10 microseconds. These lifetimes are in the wrong ratio for a steady state laser operation unless some selective collisional de-excitation process could be produced which would make the effective B state lifetime less than that of the C state. If the rate of excitation into the C state is larger than that for the B state, however, inversion and laser action can be obtained for a time like that required for transitions from C to B. This process has been observed experimentally[35]. Independent of gas density, electric field, and all other parameters that

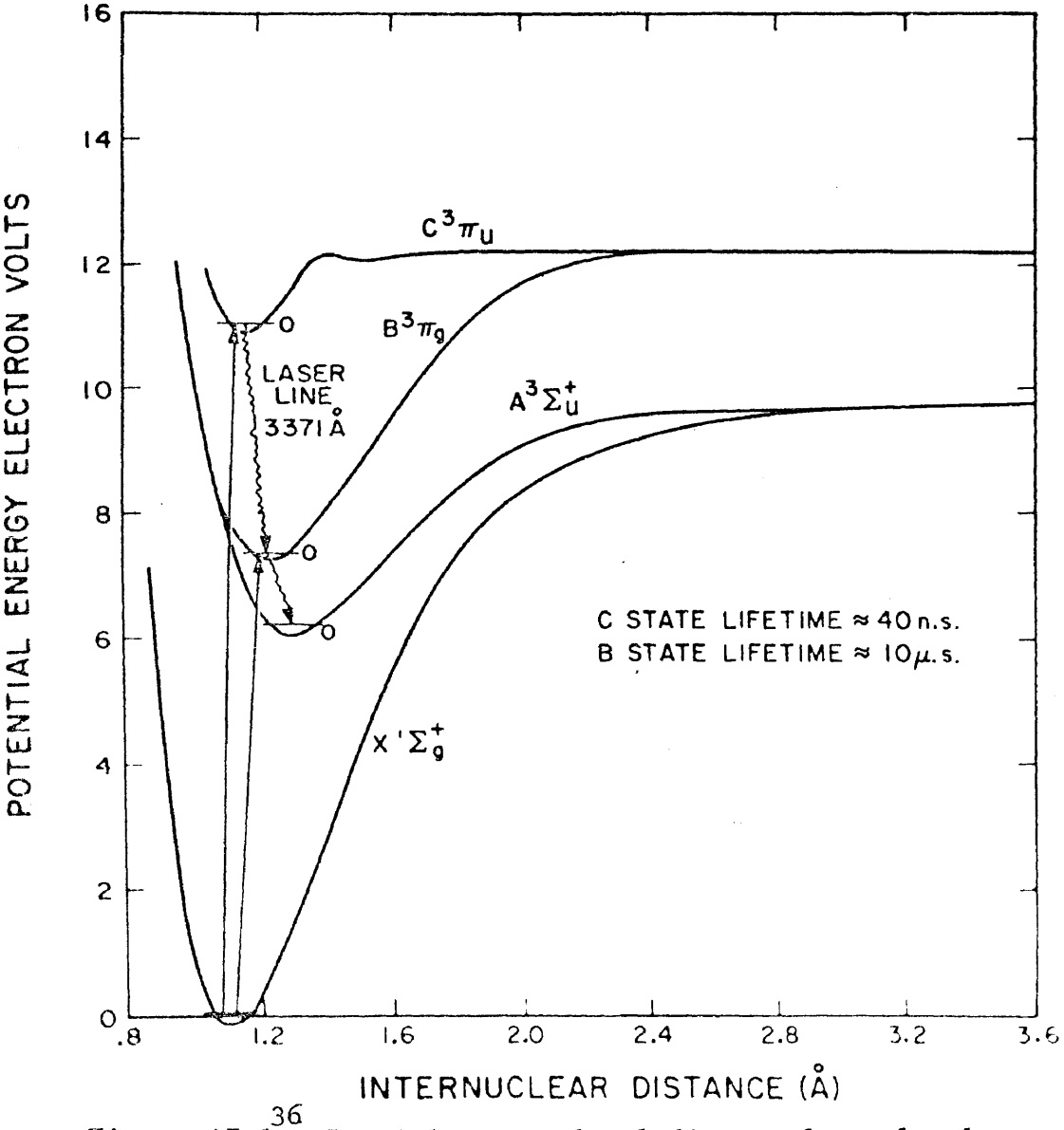

Figure AI-1.[36] Partial energy level diagram for molecular nitrogen showing the relevant energy levels of a laser operating on the second positive band at 3371 angstroms.

can be varied, the output of a pulsed nitrogen laser has been found to last for approximately 20 nanoseconds[36]. However, the length of the optical cavity (active medium) does have an effect on the observed pulse length, and pulse lengths are often reported as being about 10 nanoseconds[37].

A simple theory has been developed which appears to account for most of the observed features of the molecular nitrogen laser.[38] Direct electron impact excitation of the triplet states $C^3\Pi$ and $B^3\Pi$ is the excitation mechanism which has been used in theory[38] to overpopulate C with respect to B (inversion) for times of the order of the 40 nanosecond radiative lifetime of C.

There are several advantages to using a molecular nitrogen gas laser over conventional light sources. First of all, there is the definite synchronization characteristic. A laser pulse can be generated with less than one microsecond total delay time relative to a random input trigger signal. This is in contrast to optically pumped, solid state lasers in which the Q-switching must take place during the time the optical pumping in being performed, a time typically the order of a millisecond. The inherent short delay of the nitrogen laser allows its use in applications where a laser must remain in a continuous standby condition and yet be capable of reacting within less than one microsecond to some external stimulus.

The nitrogen laser offers excellent pulse to pulse stability,[36,37] and pulse to pulse uniformity is usually less than one per cent.[37] Also, tests have shown[36] that nitrogen laser systems are capable of over 25 million operations without degradation in the laser's output or failure of system components. Thus, this reliability allows the laser to be used in applications where long duration performance is essential. (In the test cited, the test was intentionally terminated at 25 million cycles of the laser system.)

Aside from the advantage of high peak power associated with nitrogen laser systems, the problem of removing waste heat and energy form the lasing medium appears to be a general limitation on the average power output of all lasers, both solid and gas. In the case of pulsed nitrogen lasers, the time required to diffuse the waste heat through the gas to the walls places a limit on the maximum pulse reptition rate attainable in a static laser.

Degradation of the laser's performance at high repitition rates is determined by the temperature of the nitrogen gas prior to the electrical pulse and the concentration of atoms and vibrationally or electrically-excited metastables. The effect of increased temperature is to increase the rotational excitation which will essentially broaden the transition and lower the gain. Increasing the proportion of vibrationally or electronically excited molecules reduces the population inversion because the

excitation cross section for these transitions are not as favorable. For a given input power, the gas temperature is determined both by diffusion cooling of the gas to the channel sidewalls and the rate of heat transfer through the sidewalls. This buildup of atoms and metastables is suppressed either by catalytic sidewalls or by flowing the nitrogen through the laser channel.

For a typical nitrogen laser configuration of a 3 mm wide gas channel operating at 20-30 torr, the time corresponding to the lowest order diffusion mode is approximately one millisecond. This sets a limit of approximately one thousand pulses per second on the repetition rate. Therefore, in the current design flowing nitrogen is used, and the pulse rate is limited to 30 pulses per second; however, in this case the pulse rate is determined by the power handling capability of the thyratron and not the laser itself.

Construction

The molecular nitrogen laser design incorporates a bandsaw blade as a multiple electrode structure to ensure an even transverse (cross-field) discharge in flowing nitrogen and produces superradiant emission at 3371 angstroms.

The laser head consists basically of two plates of glass supported on an aluminum base which serves both as a support and an electrical ground. (See figure AI-2.) The high voltage edge of the laser consists of a copper bus bar, which serves

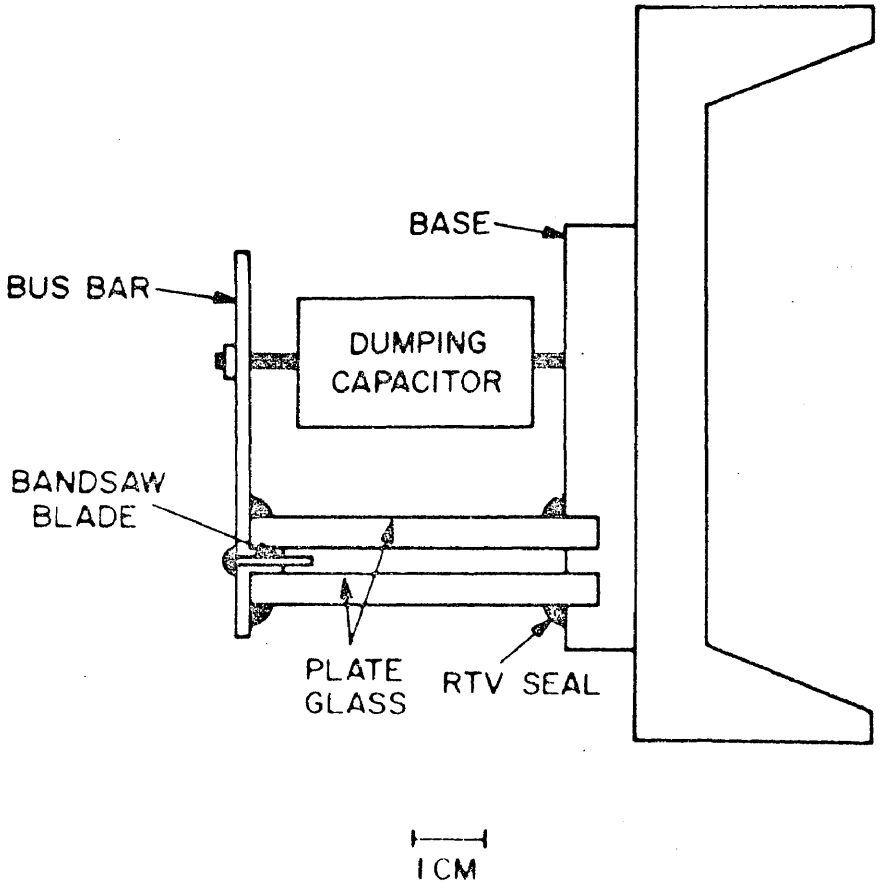

Figure AI-2.[37] Cross-sectional View of laser channel with aluminum support channel shown on the right.

both for distribution of the storage capacitor's charge to the dumping capacitors and as a mechanical support for the dumping capacitors, bandsaw blade, and copper spacer.

The schematic of operation of the nitrogen laser is illustrated in figure AI-3. Twenty dumping capacitors are mounted in parallel along the laser base and are connected together by the bus bar which in turn is connected to the low inductance storage capacitor. The storage capacitor is then charged to 10 KV. to 15 KV. and as the thyratron is triggered, the positive side of the floating storage capacitor is grounded, which then establishes the other side (bus bar) at a high negative potential (-10 KV. to -15 KV.). The charge, therefore, flows onto the bus bar to the dumping capacitors to provide the energy for the discharge in the nitrogen. This results in direct electron impact excitation of the triplet states of molecular nitrogen's second positive band, and superradiant lasing at 3371 angstroms.

The base of the laser channel is a section of channel aluminum 1.5 meters long and 12.7cm wide with two parallel grooves (0.63cm wide, 0.32cm deep, and 1.22m long) milled into it. The grooves are separated by a gap of 3mm and accomodate the plate glass strips which form the walls of the laser cavity. The glass plates are double strength tempered plate glass 6mm thick, 5cm wide, and 1.2m long, and are glued

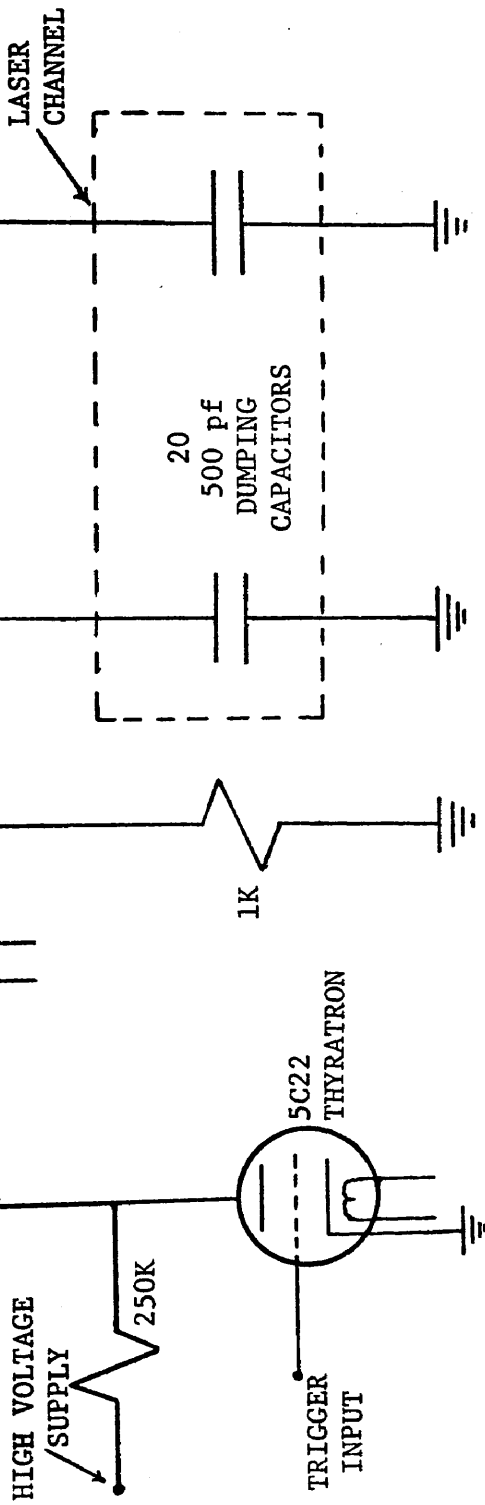

Figure AI-3. Functional diagram of the electronics for the discharge in a pulsed molecular nitrogen laser.[37]

into the grooves using General Electric Silicon Seal (RTV). This material provides adequate vacuum seal, is easily applied and alleviates mechanical problems since it is still flexible when cured. (High vacuum is not essential since the operating pressure of the laser is 10-25 torr.) The dumping capacitors are mounted in holes along the laser channel and are spaced 6cm apart. One 1.5mm hole is drilled in the ridge at each end to admit and withdraw nitrogen.

The bandsaw blade is about 1mm thick, 15mm wide, and has teeth about every 2mm (14 teeth per 2.54cm). Electrical connection to the dumping capacitors is through a bus bar made from 3mm copper stock and machined to shape (see figure AI-2). The blade is sandwiched between this and another machined piece of copper to complete the top of the channel, and positioned so that the teeth are 3.81cm from the aluminum base. The three pieces are glued in place with the silicon seal (fig. AI-2) and the ends of the laser cavity are then sealed with optical grade quartz windows 0.62mm thick. They are also attached to the plate glass by the silicon seal.

Use of the large aluminum channel allows the addition of leveling feet, electrical components, and an adjustable front silvered mirror at one end. The use of a mirror at one end increases the output power and reduces the beam divergence from several milliradians to one milliradian. No attempt at multiple reflections is necessary because the laser is

operating in a superradiant mode and also, the short pulse length limits the optical time path. Since light travels at 30cm per nanosecond, there would be a maximum of four passes through the laser.

The nitrogen flow system uses a standard fore pump to pump dry tank nitrogen through the laser, and pressure in the laser is monitored by a mercury manometer and regulated by a needle valve in the input line.

Electrical Circuitry

The electrical circuitry for the laser is shown in figure AI-4, and incorporates a 2N4852 unijunction oscillator and a plastic thyristor (2N4443) to fire the thyratron through a trigger pulse. The thyratron is a hydrogen fulled Amperex type 6279/5c22 that will switch the high voltage when provided with a 100 volt pulse to the grid, but to prevent high voltage grid flashback which will destroy the triggering circuitry, a negative voltage must be applied to the grid to shut off the thyratron. Therefore, a pi-filter is provided between the grid and triggering transformer so that the back voltage produced by its reactance turns off the thyratron. As an added precaution, a buffer amplifier and a thyrector protect the unijunction and the thyristor.

The storage capacitor has a very low self-inductance (less than 10 nanohenrys) since the transfer of charge must

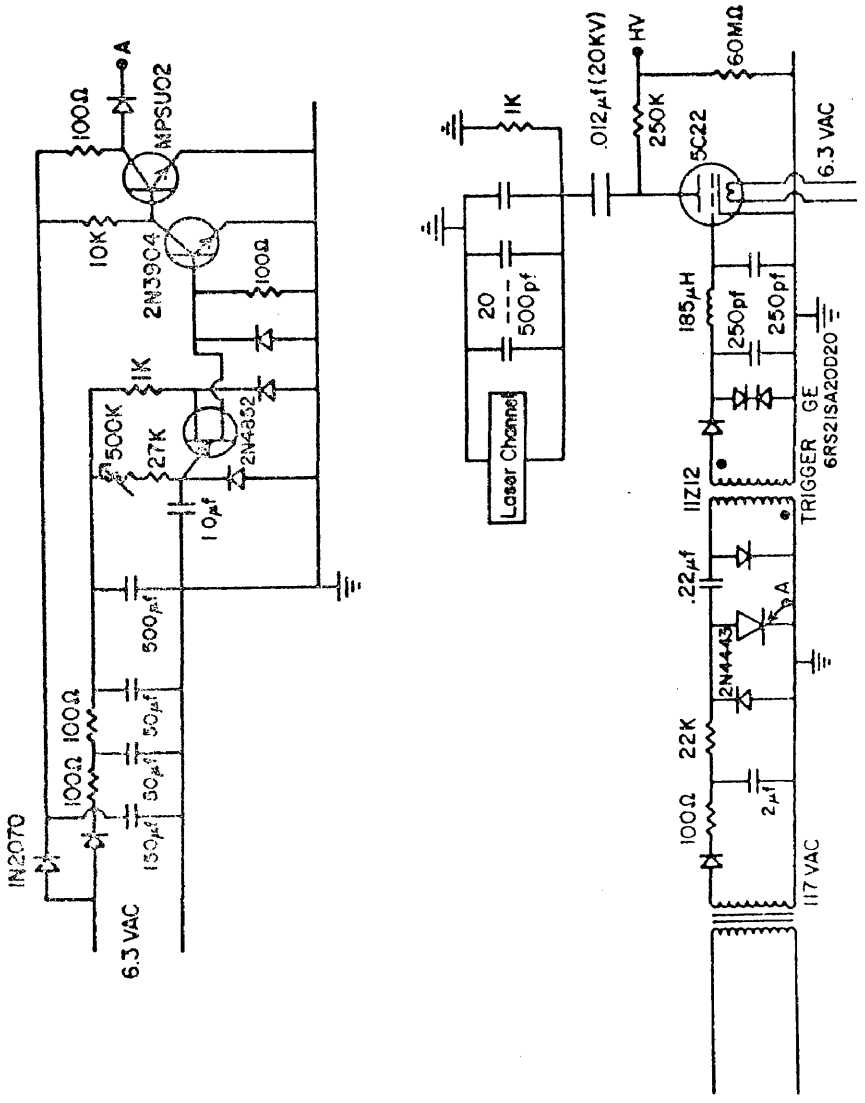

Figure AI-4. Schematic diagram of electronics for operation of nitrogen laser. Unijunction oscillator is at top, and trigger circuit for grid is at bottom.

be accomplished early in the breakdown of the nitrogen and is mounted on the bus bar for mechanical support and for electrical connection to the dumping capacitors.

The bulk of the circuitry is mounted in a box near the laser, but the current limiting resistor and the thyratron are mounted on the aluminum channel. This minimizes the path to ground for the thyratron and results in increased power output and efficiency.

The high voltage comes from an unregulated, one kilowatt supply capable of 20 KV. at 50 ma. However, the laser requires about 5 ma. when operating with this circuit design at 30 Hz, and the oscillator is limited to 30 Hz due to the power dissipation capability of the thyratron. The voltage requirement is also limited to 15 KV. by the thyratron and the current-limiting resistor is chosen to limit the current in the high voltage supply during its grounding by the thyratron.

The charging and discharging of the dumping capacitors has been observed with a fast high voltage probe[37] to charge for about 100 nsec. from the storage capacitor, then discharge in less than 20 nsec. (100% to 10%), a time comparable to the lifetime of the lasing levels of the second positive band in molecular nitrogen[35].

Laser Operating Parameters

The use of a bandsaw blade as a multiple point electrode

structure results in a very uniform discharge in the nitrogen in the laser cavity over a pressure range of 10 to 40 torr. The pulse to pulse uniformity of the laser at optimum pressure is better than 1%. A plot of pressure vs. relative power is shown in figure AI-5, and displays the dependence of the laser output power on the nitrogen pressure. In figures AI-5, 6, and 7, the laser power was recorded using a silicon photodiode as a detector. Therefore, these graphs represent the relative output power and not an absolute power, but since the photodiode output is directly porportional to the incident radiation, the photodiode output plotted against another variable has the same meaning as a relative laser output plotted against the same variable. The graph in figure AI-5 shows a minimum threshold pressure of 10 torr necessary to achieve laser action, and this agrees well with results obtained by Schenck[37]. This plot also establishes an optimum operating pressure of 20 to 25 torr for the most effecient results and smoothest performance. In the threshold region (10 torr) and the fall-off region (40 torr) the pulse to pulse uniformity is very poor and laser action is very unstable.

Having established the optimum pressure, a plot of applied voltage vs. output power at a pressure of 21 torr was made; and this shows very clearly the threshold condition imposed by the voltage requirement to be 9 KV. to 10 KV. This also agrees with Schenck's value of 9.5 KV.[37] (See figure AI-6.) At a nominal operating condition of 13.5 KV. it is observed

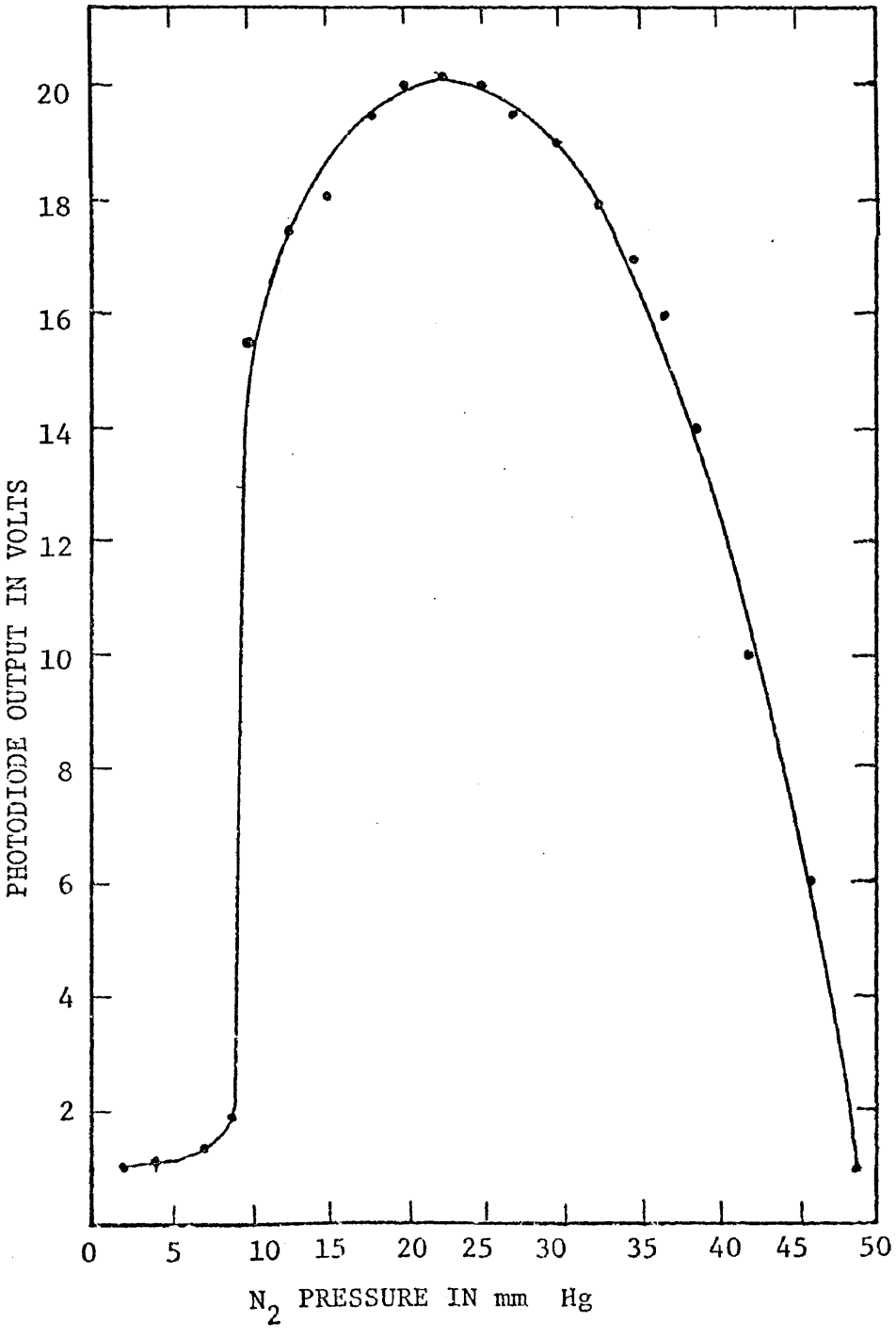

Figure AI-5. Laser output power as a function of nitrogen pressure.

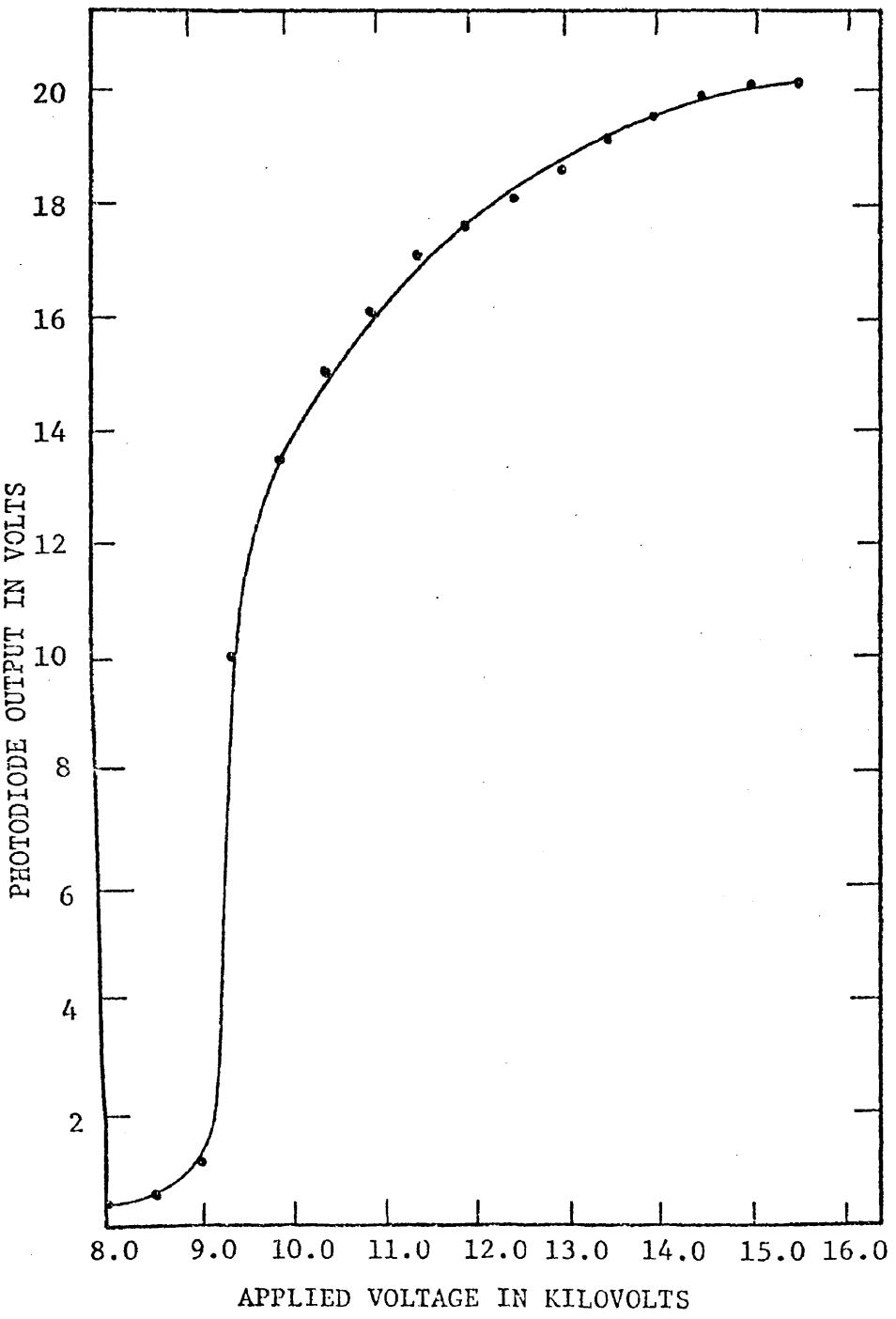

Figure AI-6. Laser output power as a function of applied voltage.

that the output power is very close to the maximum, so that it is possible to operate at this voltage with little loss in power, but with a higher switching capability of the thyratron[37] (rise time is 0.04 sec. at 13.5 KV.).

Figure AI-7 depicts the relationship between relative output power and pulse rate. Instead of using the internal oscillator circuit of the laser control system, a provision has been made to connect an external pulse generator to the thyristor as an added control over the timimg operations. This connection point is labeled "A" in the electrical schematic diagram in figure AI-4. From figure AI-7 it is observed that the peak power drops from 160 KW. to about 120 KW. (from absolute power measurments made later) as the pulse rate is varied from one pulse to thirty pulses per second, but it should be remembered that the average power is increased due to the increased pulse rate.

Figure AI-8 shows a wavelength scan of the molecular nitrogen laser's output from 3300 to 3420 angstroms and shows that there are no other appreciable lines in the region. Likewise, at the same resolution other spectra have shown no other lines over the range of 2500 angstroms to 6500 angstrons, but these are not presented here for obvious reasons. However, if one goes to a much higher sensitivity it is possible to see other lines in the specrta even though they are of very weak intensity. Thus, for very specialized applications it may

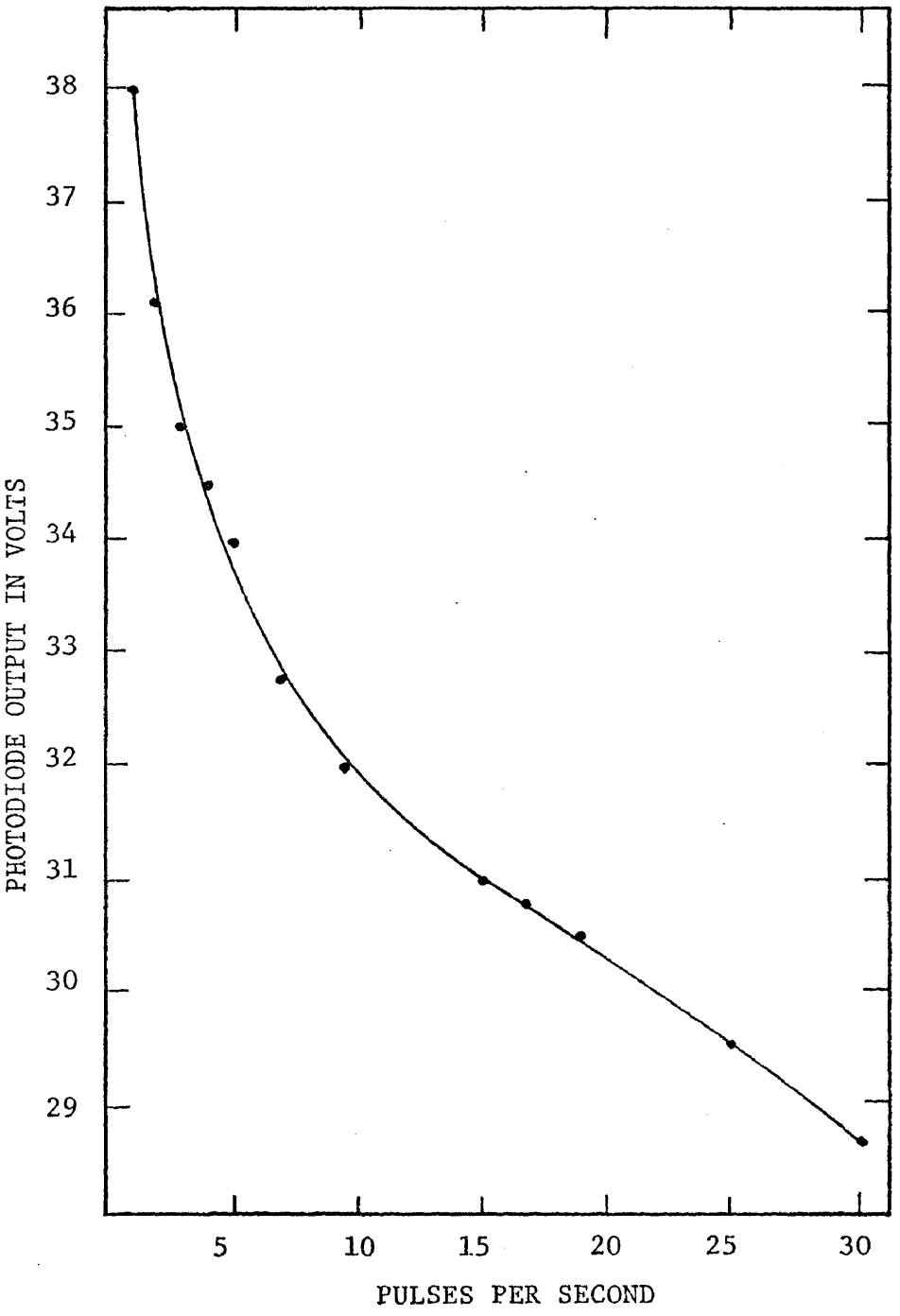

Figure AI-7. Peak laser output as a function of pulse rate.

be necessary to use a narrow band pass filter which allows only the 3371 angstrom line to be transmitted.

Figure AI-9 is a higher resolution scan of a section of fig. AI-8 but only over the region from 3364 angstroms to 3378 angstroms and clearly shows the separation of the two lines. The main nitrogen laser line is at 3371 angstroms, and there is a smaller line at 3367 angstroms. The output of a molecular nitrogen laser consists of approximately 41 separate lines centered at 3371 angstroms, with a band width of approximately 1 angstrom at full-width-half-maximum. From figure AI-9 it is seem that the width of the 3371 band at FWHM is measured to be 1.25 angstroms. Therefore, it is seen that the molecular nitrogen laser offers a very clear spectrum as compared to other sources such as mercury and xenon arcs and has a very high intensity essentially concentrated into one line at 3371 angstroms.

Absolute power measurments of the nitrogen laser were made using a potassium ferrioxalate actinometer[39]. In this method light sensitive potassium ferrioxalate is made and diluted to a known concentration, and then irriadiated with the laser beam. The reactions that take place are:

$$\left[Fe(C_2O_4)\right]^{+} \xrightarrow{h\nu} Fe^{+2} + (C_2O_4)^{-}$$

and

$$(C_2O_4)^{-} + \left[Fe(C_2O_4)\right]^{+} \longrightarrow 2CO_2 + Fe^{+2} + (C_2O_4)^{=}$$

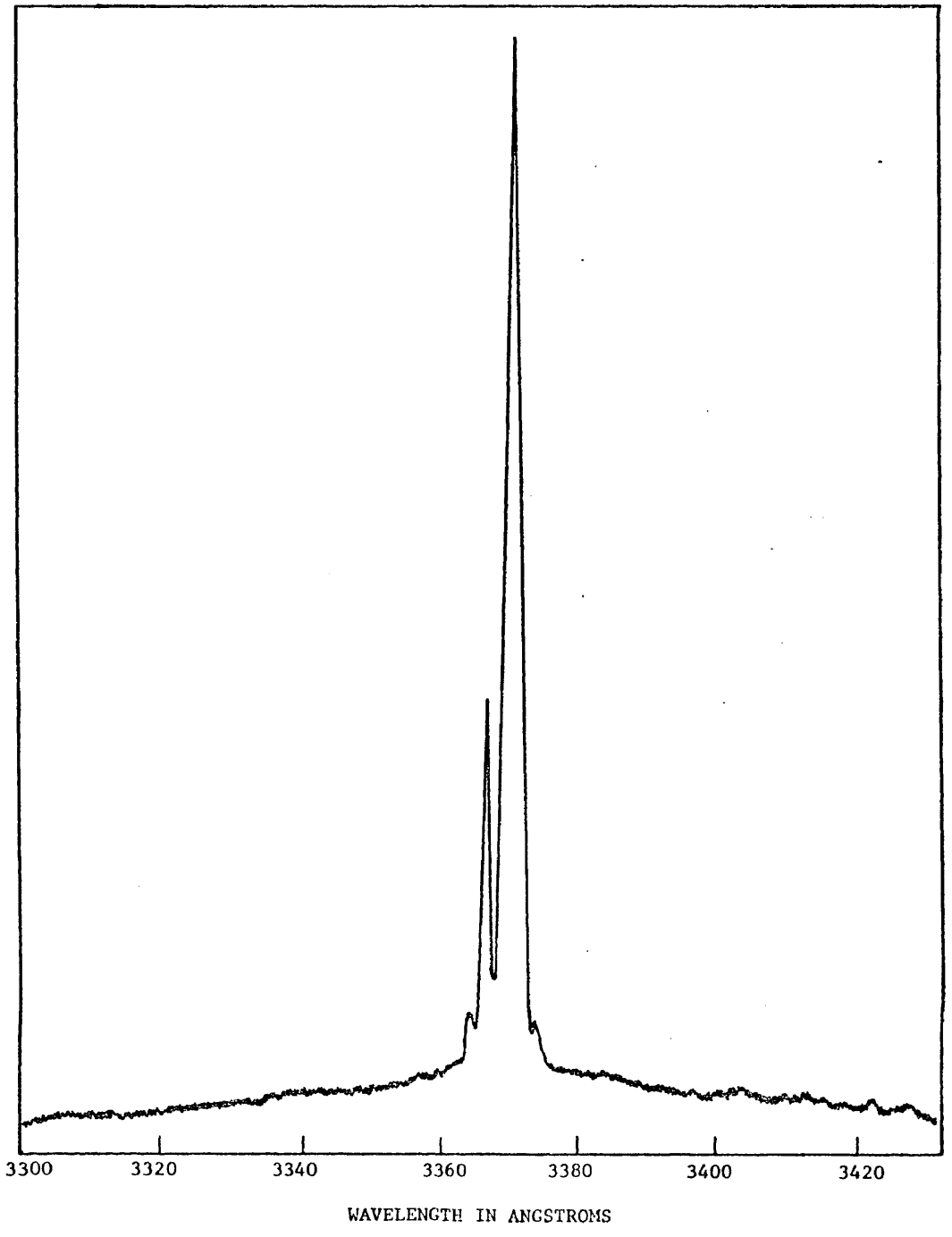

Figure AI-8. Wavelength scan of the N_2 laser line.

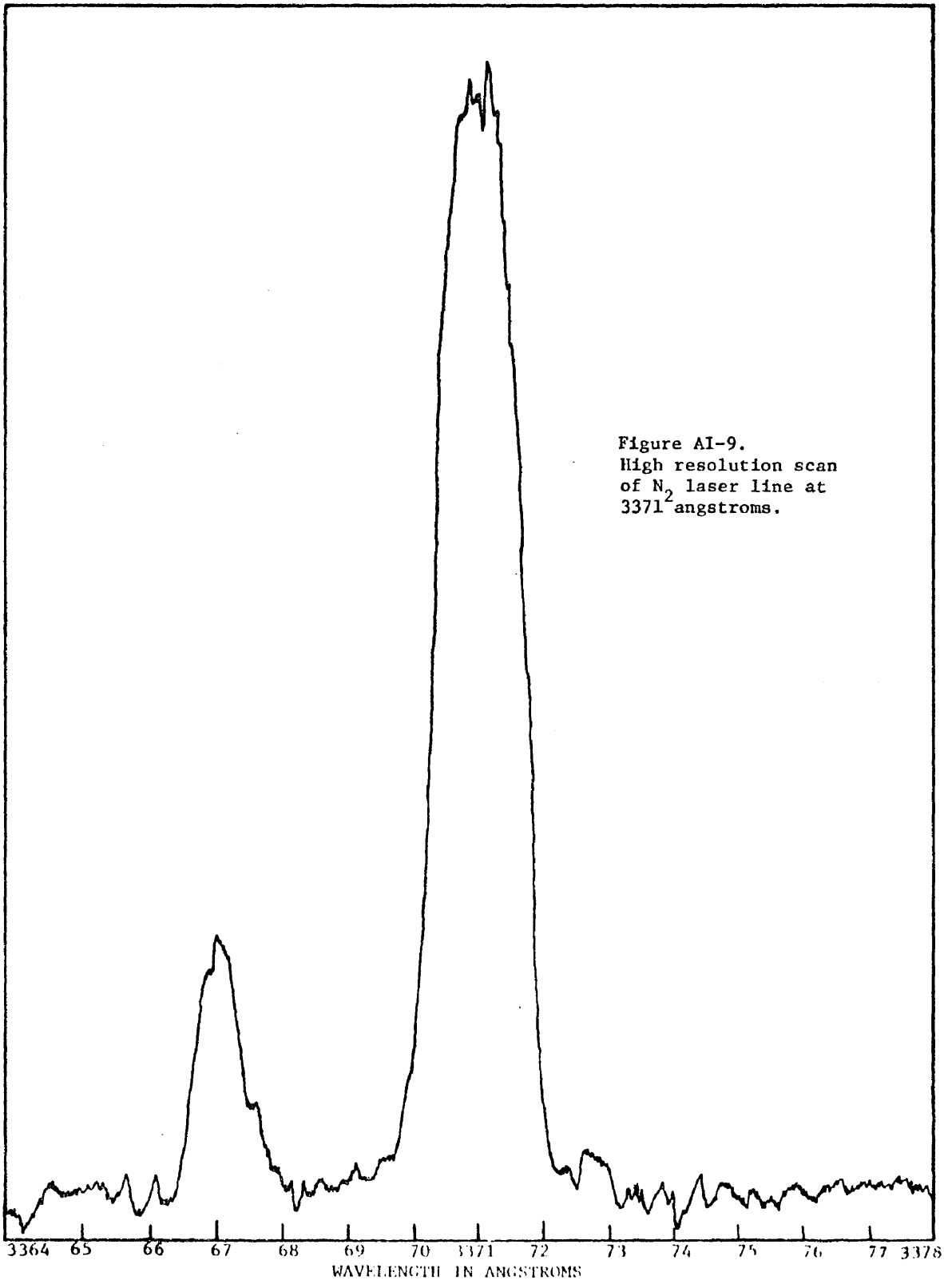

Figure AI-9.
High resolution scan of N_2 laser line at 3371 angstroms.

Next, the Fe^{+2} is complexed with 1,10-phenanthroline, left to stand in the dark for one half hour, and the absorbance read on a Heath model 703 filter spectrometer. The absorbance read on the spectrometer in then related to the amount of iron produced.

Since the quantum efficiency is the number of moles produced divided by the number of einsteins absorbed, the number of einsteins may be calculated. (Number of moles of Fe^{+2} from the absorbance, and the quantum efficiency from ref. #39.) Realizing that one einstein equals the number of molecules produced times hv, and that this is the energy in joules, then knowing the pulse length, it is possible to calculate the energy per pulse i.e. the output power per pulse. Using this method, the power of the nitrogen laser was measured to be 160 KW, and this is in good agreement with the photodiode measurment made by Schenck[37]. At high pulse rates the power per pulse drops to around 130 KW, but it must be remembered that the average power increases due to the higher pulse rate.

Another Gas System

It has been reported that such a system as the molecular nitrogen gas system should also work with neon[30-32]. Therefore, tests were made using neon gas instead of nitrogen, at a pressure of 30 torr and a voltage of 15 KV. According to previous experiments[32] at these conditions, one is very near the threshold condition for neon and indeed superradiant laser action was

observed, but only at low repetition rates. Thus, while in some circumstances it may be possible to use the 5401 angstrom line of the neon laser in this system, it does not seem as reliable as nitrogen. The pulse to pulse uniformity was poor (as to be expected near threshold), and according to other experiments,[31] the experimental power attainable in this system is about one kilowatt. Thus, for present applications it is much more practical to use nitrogen as the excitation gas and approach the 5400 angstrom region of the spectrum by other means.

APPENDIX II

TUNABLE ORGANIC DYE LASER

Introduction

The tunable dye laser shares the intensity, monochromaticity, coherence, and collimation characteristics of the fixed frequency lasers and in addition has the unique feature of tunability. What differentiates an organic dye molecule from other laser materials is the fact that a dye has a broad continuous fluorescence spectrum, rather than one or a series of narrow discrete fluorescence emission lines. Lasing can occur only at wavelengths where natural fluorescence is amplified, and thus continuous tunability requires a continuous emission spectrum from the laser active medium.

If a population inversion had been induced in the lasing material so that there are more molecules in a higher energy level than a lower one, trapped radiation with a frequency ν equal to the energy difference divided by h will be amplified by stimulated emission during each pass through the active region. The population inversion is essential for amplification since the cross sections for stimulated emission and absorption are equal.

Dye Laser Theory and Performance Parameters

When one considers the conjugated chain that comprises the chromophore of a dye, it is useful to approximate this complex

system as a core plus a π-electron cloud. The core is comprised of the constituent atomic nuclei plus the tightly bound, inner-shell electrons, all bound together by σ-bonding electrons. In addition to valence electrons localized in bonding σ orbitals there are other valence electrons in π orbitals. The π orbitals of adjacent atoms overlap, forming in essence large (molecule sized) wave functions that are delocalized over most of the molecule. These electrons in the delocalized π wave functions are not so tightly bound as the σ electrons and they are the electrons that are involved in the near uv, visible, and near ir optical transitions.

To a fair degree of approximation, the π electrons can be thought of as a one-dimensional electron gas of more or less free electrons. Thus a (spatially) longer chromophore (i.e. a longer conjugated chain with its associated π electrons) can be considered a longer "box" for the π electron wave functions, and the energy-level spacing is correspondingly reduced. Everything else being equal, absorption and fluorescence will occur at longer wavelengths for longer chromophores. Figure AII-1 demonstrates the relationship between types of dyes, structure, and their wavelength tuning range.

Because the molecule is so large and has so many constituents, i.e. so many bonds and internal degrees of freedom, there is a great deal of opportunity for vibration and rotation along different bonds, and the simple "electron-in-a-box" energy levels are split

NO.	DYE	FAMILY	STRUCTURE
1	3,3' DIETHYLTHIA-TRICARBOCYANINE IODIDE	POLYMETHINE	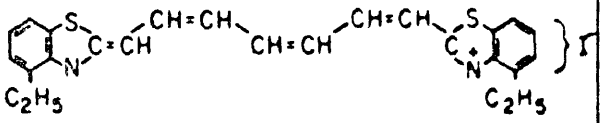
2	RHODAMINE 6G	XANTHENE	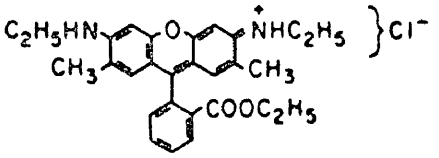
3	4-METHYL-UMBELLIFERONE	COUMARIN	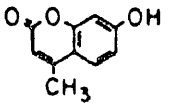
4	2,5 DIPHENYL-OXAZOLE	OXAZOLE	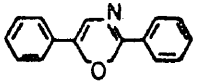

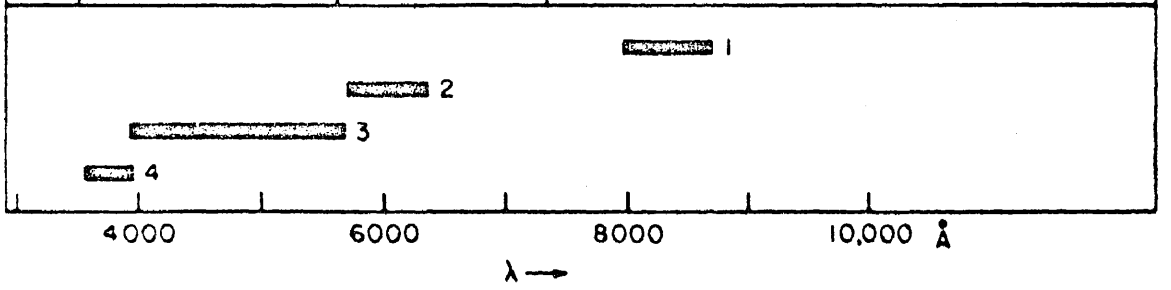

Figure AII-1. Examples of some laser dyes with their respective wavelength tuning range.

into many, virtually continuous levels. Figure AII-2 is a schematic representation of the π-orbital energy levels of a dye molecule. The dye laser operation is basically a four-level process as shown by the heavy lines labeled excitation and emission, but, in addition, there are other levels of interest which are: the molecular ground state (singlet), the first excited singlet state, the lowest triplet state, and the first excited triplet state.

Although this process has been known for some time, a detailed theory of dye laser operation has only recently been developed for two reasons[40]. First, emission from optically fluorescing organic dyes occurs over a spectral band that may be as wide as 1500 angstroms; furthermore, the molecular triplet state, which is not radiatively connected to the ground state, may play a critical role in the lasing process. Therefore, it is desirable to consider the development of the gain equations (performance parameters) of organic dyes in some detail.

The only allowed radiative transitions are between the singlet pair and between the triplet pair, and it is the singlet-singlet transition that is needed for lasing. However, because the nonradiative intersystem crossing from the excited singlet to the lower triplet is energetically allowed, and because the subsequent decay to the ground state is relatively slow, the triplet state plays an important part in laser action. This population of the triplet state removes molecules from the lasing channel and also provides for resonant absorption of the laser

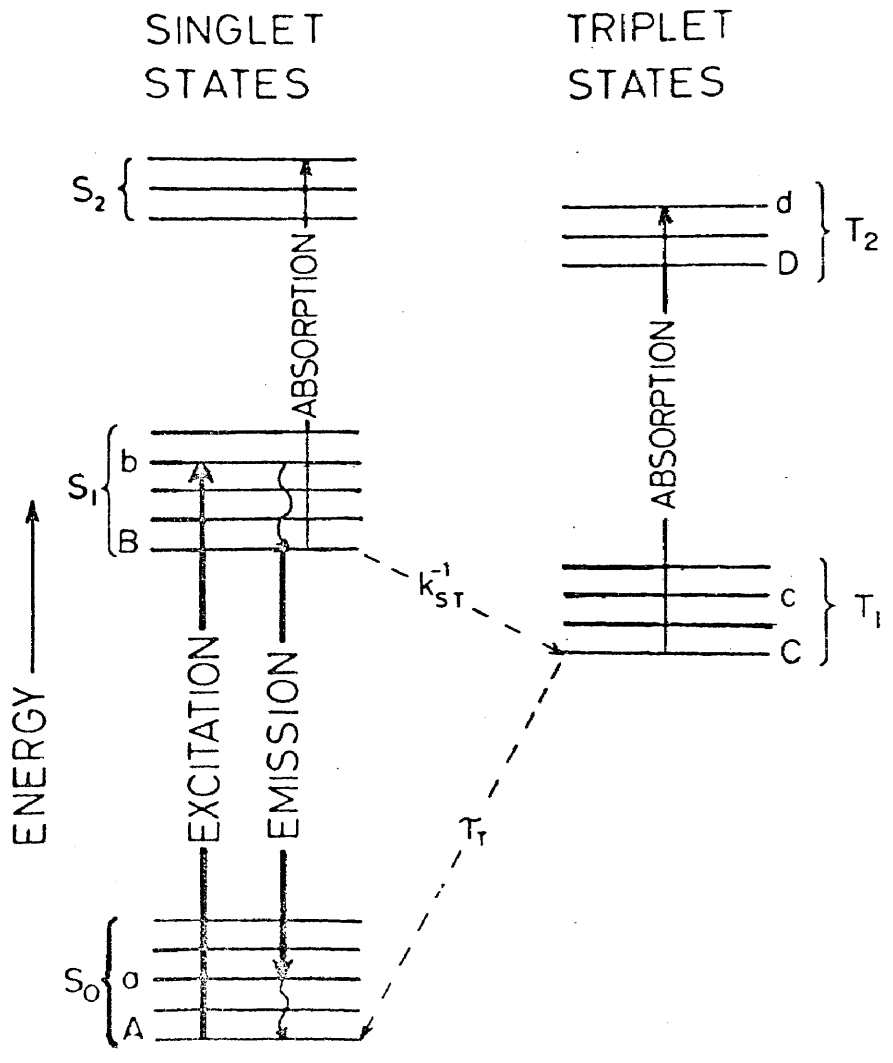

[40]

Figure AII-2. Schematic representation of the energy levels of a dye molecule. Excitation and laser emission are represented by the transitions A→b and B→a respectively. Other transitions represent losses in the laser process

light by excitation to the upper triplet state.

One may define the gain as the rate at which photons are being produced in, or removed from the laser cavity. Photons are lost primarily by induced transitions, and are gained by stimulated emission from the excited singlet state. With this in mind it should be possible to write an expression for the gain in terms of useful (measurable) quantities.

The transition rate between descrete states $|I\rangle$ (initial) and $|F\rangle$ (final) is:

$$W_{FI}=(2\pi/\hbar)\,|\langle F|V|I\rangle|^2\delta(E_{FI}) \qquad (1)$$

V = perturbing term in the Hamiltonian

E_{FI} = energy between initial and final states

The initial state has N_m photons in mode m[41] and a molecule excited to state (B) in figure AII-2. The final state has one more photon in mode m and the molecule in one of the states (a). The states are:

$$|I\rangle=|N_m;B\rangle \qquad (2)$$

$$|F\rangle=|(N+1)_m;a\rangle \qquad (3)$$

In the electric dipole coupling between (B) and (a), the matrix element of V is:

$$|\langle F|V|I\rangle|^2 = 1/2(\hbar\omega_m)[(N+1)_m/\upsilon n^2]\,|\mu_{Ba}\cdot\varepsilon_m|^2 \qquad (4)$$

ω_m and ε_m = frequency and polarization vector of m^{th} mode

υ = cavity volume

μ_{Ba} = dipole transition matrix element

n = refractive index of the medium

Since there are many possible states (a), we must sum over all the contributing final states.

$$\sum_a W_{FI} = [(N+1)_m/v] \sum_{Ea} M_{Ba} \delta(E_{FI}) \tag{5}$$

where

$$M_{Ba} = \sum_a \omega_m \pi |\mu_{Ba} \cdot \varepsilon_m|^2 / n^2$$

and the delta function allows for only energy conserving transitions, ie. $E_a + \hbar\omega_m = E_B$.

Since the states are densly distributed in energy, $\rho_a dE_a$ equals the number of states in the energy range dE_a (ie. $\rho_a = dN_a/dE_a$). The total emission from (B) is now:

$$N_B \cdot \sum_a W_{FI} = [(N+1)_m/v] \, N_B \bar{M}_{Ba} \bar{\rho}_a \tag{6}$$

N_B = the assumed pressence of molecules in state (B),

and bars indicate that ρ_a and M_{Ba} are evaluated at $E_a = E_B - \hbar\omega$. By similiar notation the absorption is:

$$dN_m/dt|_{absorp.} = (N_m/v)[N_C \bar{M}_{Cd} \bar{\rho}_d + N_A \bar{M}_{Ab} \bar{\rho}_b] \tag{7}$$

The gain may now be defined as the rate of emission minus the rate of absorption plus an additional loss term for dispersive losses (mirrors, windows, etc.). Denote this as the product of photon density and the dispersive loss function ie. $(N_m/v)(d\lambda_m)$.

Thus, the gain is:

$$dN_m/dt = (N_m/v)[(1+N_m^{-1})N_B \bar{M}_{Ba} \bar{\rho}_a - N_C \bar{M}_{Cd} \bar{\rho}_d - N_A \bar{M}_{Ab} \bar{\rho}_b - d(\lambda_m)] \tag{8}$$

Now one only has to relate these to measurable quantities.

The first term may be related to the fluorescence lifetime, ie. the rate at which a molecule in state (B) decays to one of the states (a) times the probability that the decay is accompanied by a photon emission in the wavelength range λ to $d\lambda$; thus:

$$\bar{M}_{Ba}\bar{\rho}n(\lambda)d\lambda = (1/\tau)E(\lambda)d\lambda \qquad (9)$$

τ = the lifetime of (B)

and

$E(\lambda)$ = the probability of emission

$E(\lambda)$ is also called the line shape function.

Since not all de-excitations are radiative, the sum of the photon emission probabilities is less than unity. The same is true for the quantum yield, which is defined as the integral over the emission band of the line shape function:

$$\phi = \int_0^\infty E(\lambda)d\lambda \leq 1 \ . \qquad (10)$$

From equation (9) replace $n(\lambda)d\lambda$ by the density of states factor $(8\pi n^3/\lambda^4)d\lambda$ and reduce the first term in (8) to measurable quantities, and we have:

$$N_B\bar{M}_{Ba}\bar{\rho}_a = N_B[\lambda^4 E(\lambda)/8\pi\tau n^3] \qquad (11)$$

The second and third terms are treated in the same manner.

To simplify things further, the dye may be described by a linear absorption coefficient; that is, the photon number decays exponentially with path length.

$$dN_m/dl = -(\alpha_S + \alpha_T)N_m$$

where the absorption cross sections (extinction coefficients) are:

$$\alpha_S = n_S\sigma_S \quad , \qquad \alpha_T = n_T\sigma_t$$

and $$n_S = N_A/v \quad , \qquad n_T = N_C/v$$

Multiply the first term in (11) by n/c to express the rate of change with path length rather than with time, and one has:

$$dN_m/dl = N_m\{[\lambda^4 E(\lambda)/8\pi c\tau n^2]n^* - \sigma_S n_S - \sigma_T n_T - r\} \qquad (12)$$

r = losses due to mirrors, etc. and if only mirrors and cell windows are important loss sources, then:

$$r = -(1/2l)\ \ln R_1R_2T_1T_2 \qquad (13)$$

where σ_S and σ_T are the singlet-singlet and triplet-triplet absorption cross sections and,

R = reflection coefficient

T = transmission coefficient

l = cavity length

n^* = excited singlet concentration

Thus, the gain = the average growth rate per unit length per photon,

$$G(\lambda) = (1/N_m)(dN_m/dl) \ . \qquad (14)$$

Explicitly, the gain function is:

$$G(\lambda) = \sigma_{em}n^* - \sigma_T n_T - \sigma_S n_S - r \qquad (15)$$

where σ_{em} = the emission cross section = $\lambda^4 E(\lambda)/8\pi n^2 c\tau$.

Figure AII-3 plots the absorption and emission cross sections for 7-diethylamino-4-methylcoumarin. Note that the total dye

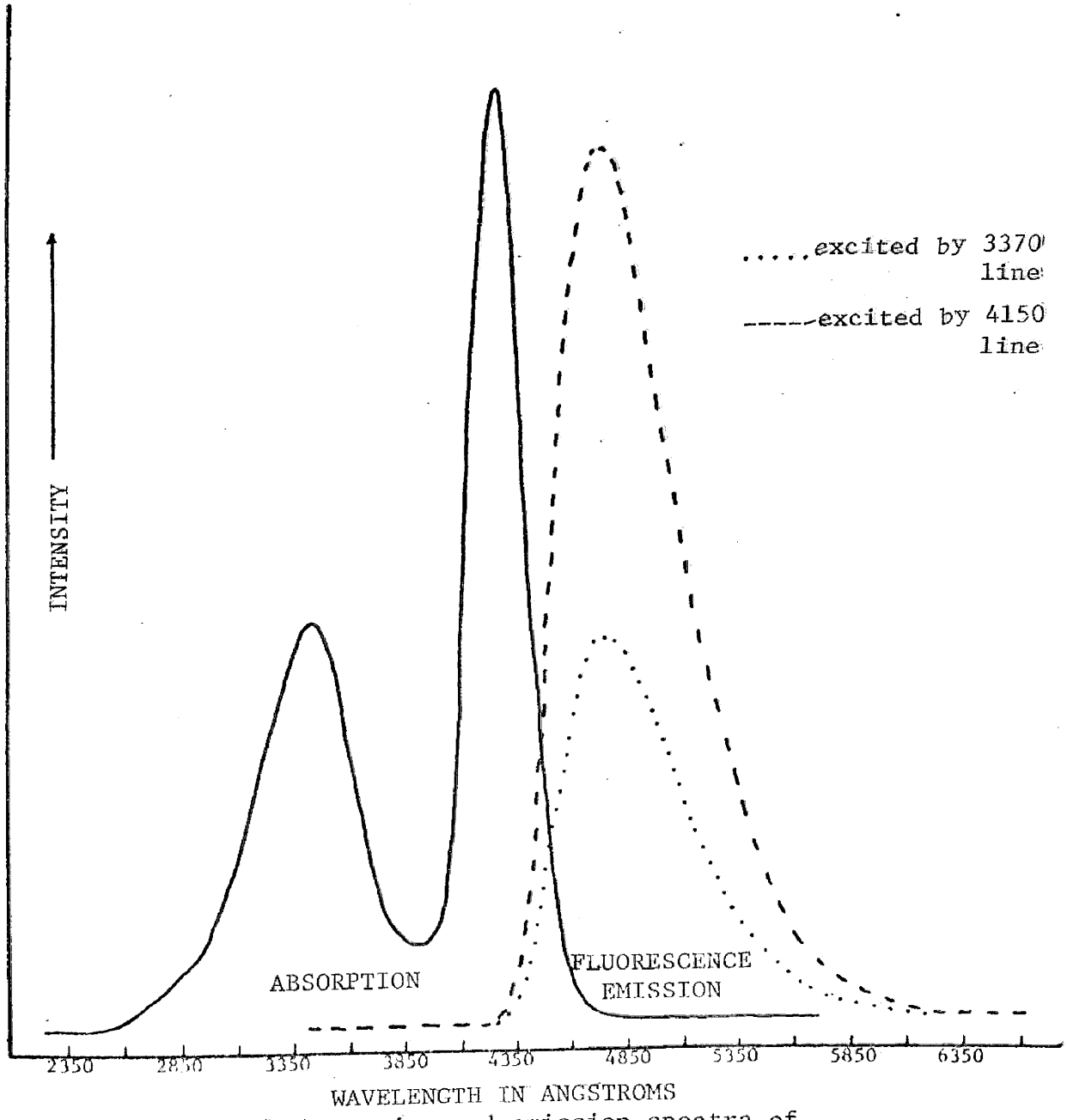

Figure AII-3. Absorption and emission spectra of 7-diethylamino-4-methylcoumarin in ethanol.

concentration n is equal to the sum of n_o, n*, and n_T. Thus, equation (15) may be re-written as:

$$G = n^*(\sigma_g + \sigma_S) - n_T(\sigma_T - \sigma_S) - n\sigma_S - r \qquad (16)$$

The lifetime of the molecule in the triplet manifold (τ_T) may be typically 100 nsec., and if one assumes a time scale for threshold studies several times longer than τ_T, one may assume that electrons are leaving the triplet state as readily as others are entering it. Where this equilibrium is valid, (It should be clear that where the equilibrium triplet approximation is not itself valid, its consequence is still true. That is, n_T and n* can be proportional to each other with a proportionally constant different from $K_{ST}\tau_T$.) the rate equation for the triplet population is:

$$\dot{n}_T = n^*K_{ST} - n_T/\tau_T$$

and if the equilibrium exists, then $\dot{n}_T = 0$ and

$$n_T = n^*K_{ST}\tau_T \; . \qquad (17)$$

Now eliminate the triplet and ground state singlet concentrations in favor of n* and n. The gain equation is now,

$$G(\lambda) = \gamma n^* - \sigma_S n - r \qquad (18)$$

where the growth coefficient is

$$\gamma = \sigma_{em} + \sigma_S + K_{ST}\tau_T \; (\sigma_S - \sigma_T). \qquad (19)$$

Immediately, we see that the triplet state enters through $K_{ST}\tau_T$ and through the wavelength dependence of the triplet cross section $\sigma_T(\lambda)$.

The gain as a function of wavelength for zero extrinsic loss for several values of $K_{ST}\tau_T$ is shown in figure AII-4 for rhodamine 6G assuming $n^*/n = 0.01$ and $\mu=K_{ST}\tau_T$. ($n^*/n = 0.01$ is a reasonably typical threshold value[40].) It should be clear from figure AII-4 that the triplet state has a very significant influence on the gain.

One should also notice that G=0 has the characteristic of a threshold condition and this can be inverted to give the threshold excited state population.

$$n^*\big|_{G=0} = n^*(r/n,\ K_{ST}\tau_T,\ \lambda)\big|_{G=0} \qquad (20)$$

It is very interesting in itself, to be able to calculate the excited state population but, in addition, laser threshold is defined by G=0, and the threshold inversion, which is really the criteria in question, is trivially derived from equation (16):

$$(n^*/n)_{G=0} = \frac{(\sigma_S + r/n)}{(\sigma_g + \sigma_S) - (\sigma_T - \sigma_S)n_T/n^*} \qquad (21)$$

This equation is to be evaluated at the wavelength where laser emission occurs, and this will occur at some wavelength greater than that of the singlet-singlet absorption maximum, where generally $\sigma_S(\lambda) << \sigma_g(\lambda)$ and $\sigma_T(\lambda) \lesssim \sigma_g(\lambda)$.

Since the triplet state is populated at a rate equal to $K_{ST}n^*$ and spontaneously empties at a rate equal to n_T/τ_T, n_T can be expressed in terms of n^*, K_{ST}, and τ_T. The relative triplet-excited-singlet ratio $n_T(t)/n^*(t)$ depends on the time

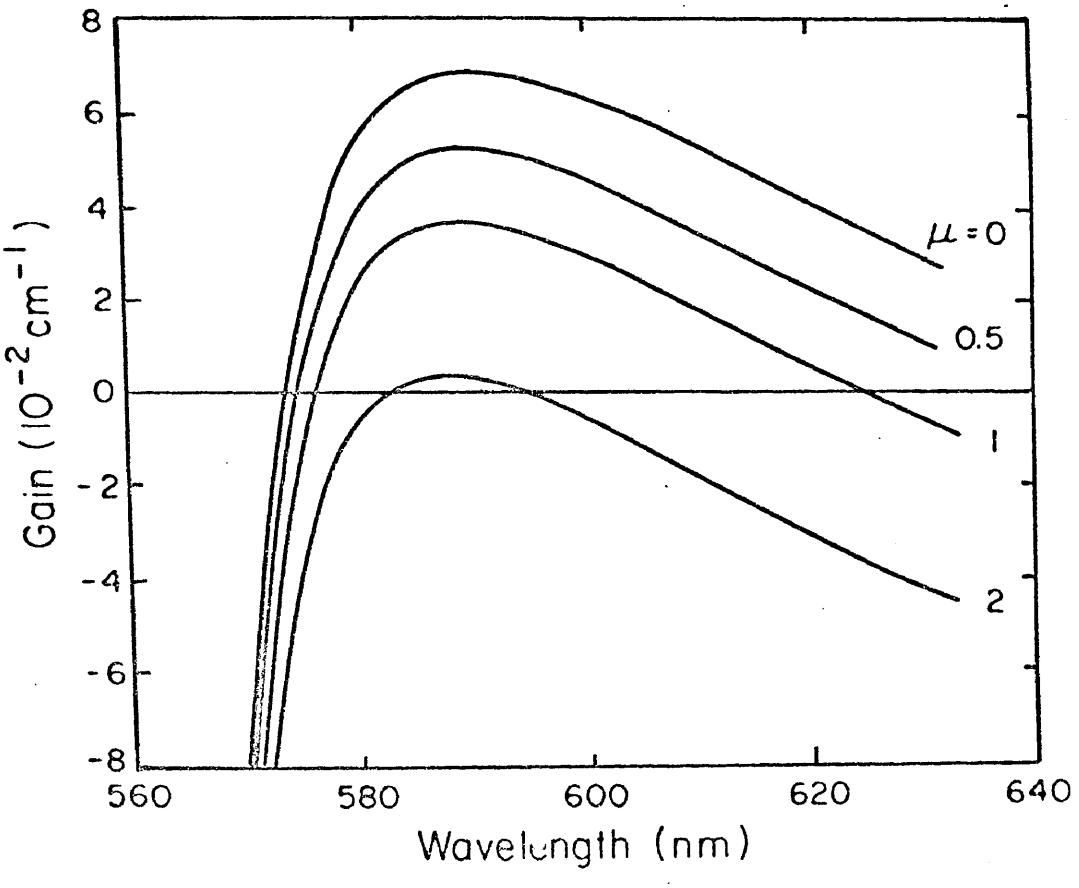

Figure AII-4.[40] The intrinsic gain per unit length in the dye for rhodamine 6G as a function of wavelength for an arbitrary value of $n^*/n = 0.01$ for several values of $\mu = K_{ST}\tau_T$.

history of excitation, but is of the order of $K_{ST}T$ where $T=\tau t/(\tau T+t)$, and t is the time since inception of excitation.

For times $t>>\tau T$, $n_T/n^* = K_{ST}\tau_T$, and threshold inversion is a function of two variables, λ and the normalized extrinsic loss r/n, plus the parameter $K_{ST}\tau_T$ which is essentially determined by the dye, solvent, and triplet quencher used if any[42].

Figure AII-5 shows the threshold inversion, $(n^*/n)_{G=0}$ as a three dimensional surface plotted as a function of λ and r/n for rhodamine 6G in this "long-time" equilibrium triplet limit. The value used for $n_T/n^* = K_{ST}\tau_T$ is 1.0 which is close to the value of $0.9\pm.2$ experimentally determined by Snavely[43].

The increased threshold at shorter wavelengths reflects the increase in singlet-singlet self-absorption (σ_S is the numerator of equation 21) as λ decreases. Toward longer wavelengths, σ_S becomes negligible, but the extrinsic loss r/n remains finite in the numerator, and σ_g also decreases toward longer wavelengths, generally more rapidly than σ_T, so $(\sigma_g-\sigma_T n_T/n^*)$ can vanish. This is the origin of the long wavelength "triplet wall" in figure AII-5. The slope and location of this triplet wall depend strongly on n_T/n^* and hence can be time dependent for excitation times short compared to the triplet life time. If $n_T/n^* \sim K_{ST}T$ is large enough, the triplet wall can be displaced into the short-wavelength, high singlet absorption loss domain, and threshold inversion will be unattainable. The time

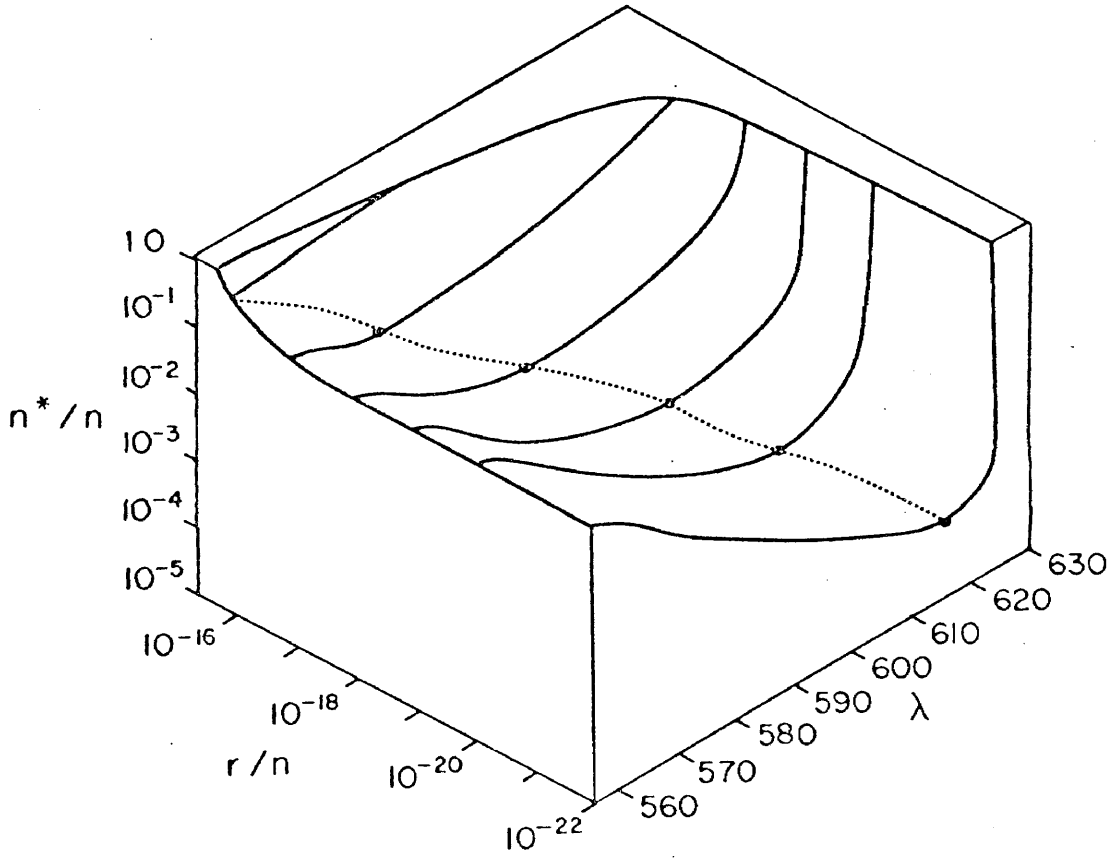

Figure AII-5.[40] The relative excited state population at threshold (n*/n) in rhodamine 6G for $K_{ST}\tau_T=1.0^{1}$ as a function of lasing wavelength λ(nm), and normalized extrinsic loss r/n. The iso-loss contours are the intersections of constant loss planes with the zero gain surface, and the dotted line representing the locus of minima of the intersections is the critical threshold inversion for self-tuning.

dependence of T, for excitation times << τ_T, explains the requirement for fast exciatation for many dyes; under sufficiently fast excitation threshold inversion can be obtained before the triplet wall has had time to build up to its equilibrium value.

In principle, lasing can occur at any wavelength and any extrinsic loss for which a physically realizable fraction of dye molecules can be excited to the zero gain surface. In a given experimental configuration, however, r/n is fixed by mirror reflectivity, scattering losses, etc. For example, a non-dispersive extrinsic loss can be represented in figure AII-5 by a plane orthogonal to the r/n axis. The intersection of such a plane with the zero gain surface defines an "iso-loss" line on the surface.

Self-tuned laser threshold occurs at the wavelength of the minimum $(n^*/n)_{G=0}$ point on the physically relevant iso-loss line, and the excited state population is fixed at the value by stimulated de-excitation. The dotted line in figure AII-5 is the locus of the iso-loss minima. Clearly, the locus of minima occurs at shorter wavelengths and larger values of n^*/n as the normalized extrinsic loss is increased.

Figure AII-6 shows the self-tuned wavelength for 7-diethylamino-4-methylcoumarin. The larger peaks over the emission range are due to the mirror effects of the flat quartz windows of the dye cell.

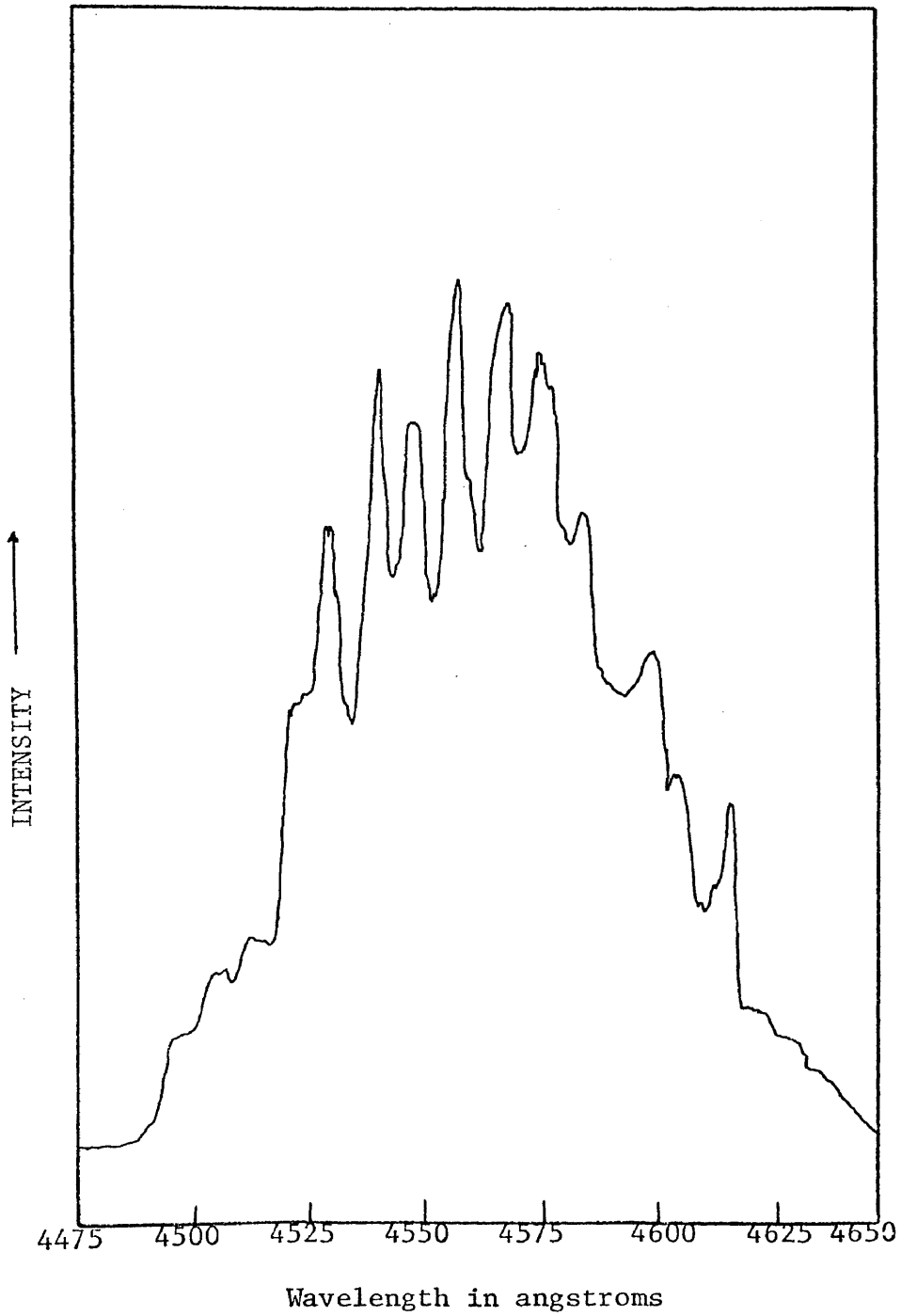

Figure AII-6. Wavelength scan of a self-tuned (superradiant) dye laser using 7-diethylamino-4-methylcoumarin.

In contrast to a self-tuned system, the loss can be made to be wavelength dependent. If a diffraction grating is replaced for one of the laser-cavity mirrors, for a given grating setting light of only one wavelength will be reflected back upon itself to retraverse the active medium. The extrinsic loss is then effectively infinite for wavelengths that are not retroreflected. Constraining the laser action to this specified wavelength is equivalent to choosing a specific constant wavelength plane in figure AII-5. The value of the loss associated with the dispersive element at that wavelength then acts to specify an iso-loss line on the surface. The intersection of the iso-loss line with the constant wavelength plane then determines the point on the zero gain surface where lasing occurs. It is important to note that this point need not, and typically does not, lie on the locus of minima.

This configuration with a dispersive loss element in the cavity is denoted as "externally tuned" since threshold is no longer constrained to appear on the locus of iso-loss minima. Tuning is accomplished simply by rotating the grating so that a different wavelength will become the retroreflected, low-loss wavelength for the dispersive cavity. Figure AII-7 shows the tuning range of a grating tuned, nitrogen laser pumped 7-diethylamino-4-methylcoumarin laser.

Introduction of a dispersive loss element in the cavity not only provides for tuning, but also narrows the spectral width

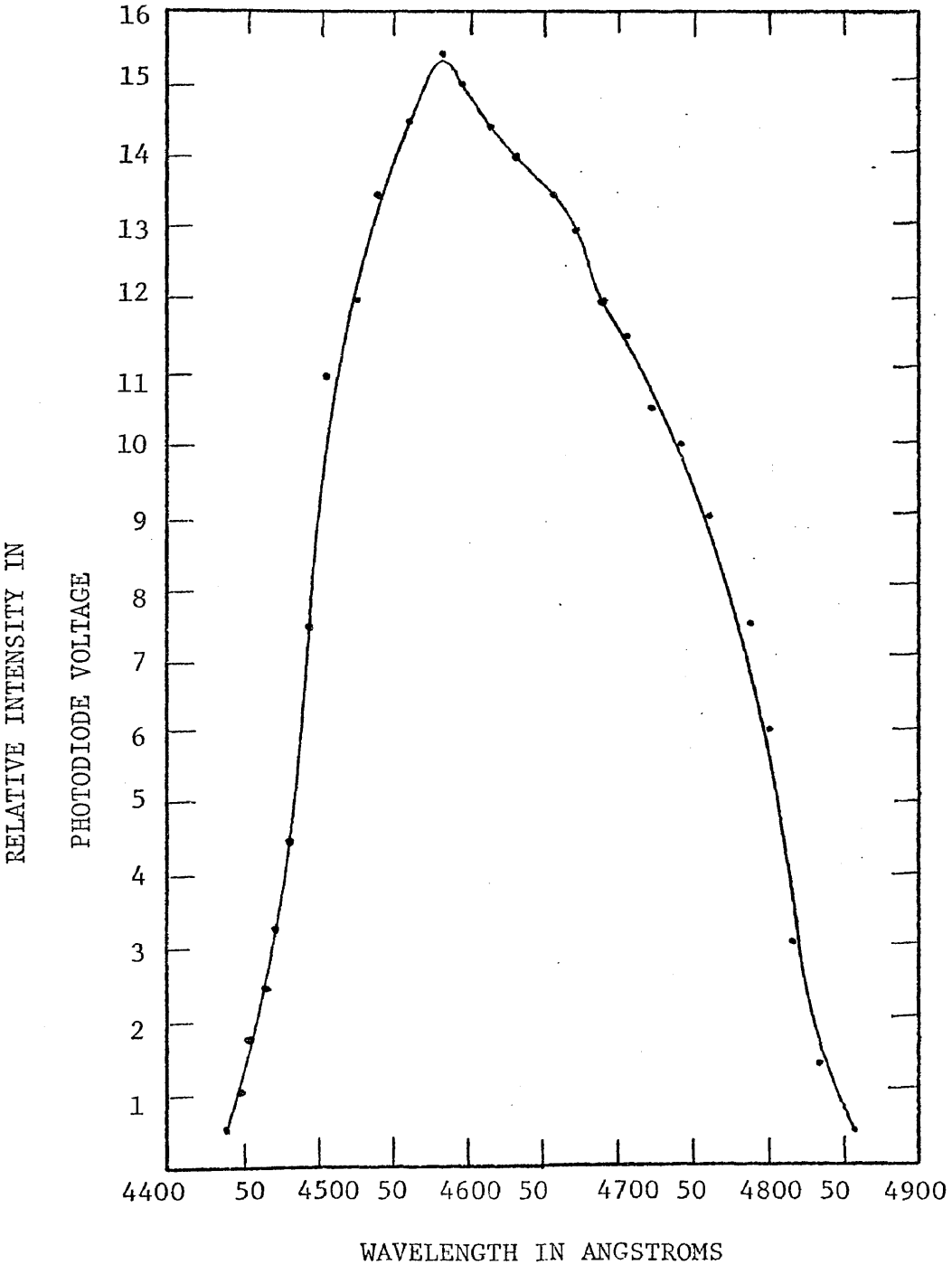

Figure AII-7. The wavelength tuning range of the a dye laser using 7-diethylamino-4-methylcoumarin in ethanol.

of the laser. The spectral width (FWHM) of a self-tuned laser is inherently quite wide (100 angstroms) while the externally tuned wavelength may be typically 30-40 angstroms. Figure AII-8 shows one line from an externally tuned coumarin laser and figure AII-9 shows a higher resolution scan of the same line (note that the line width is about 15 angstroms at FWHM).

Other experimenters[44,45] have inserted other types of elements such as beam expanding telescopes and laser Fabry-Perot etalons and have achieved even further reduaction in line widths. Hänsch reports 0.03 angstroms at FWHM with a beam expanding telescope alone, and 300 MHz (less than 0.004 angstroms) with an etalon inserted into the cavity[44].

From studies of the gain equation[46] it is very clear that in order to limit the built up of the triplet state, which is detrimental to laser action, that pump sources with extremely short pump times are desirable so that $K_{ST}\tau_T \approx 0$. The pulsed molecular nitrogen laser is an excellent pump source since it has high intensity in the ultraviolet, high peak power, and a very short pulse length. The pulse length of the nitrogen laser as indicated in Appendix I is 10 nsec., which is of the same order as the fluorescence lifetimes of most organic dyes. Thus, a very good match between pump and dye laser is possible.

Several dye laser designs have been devised[44,45,47,48] by different workers, and the one used in these experiments is similiar to that proposed by Myer[48] (See figure AII-10), but with

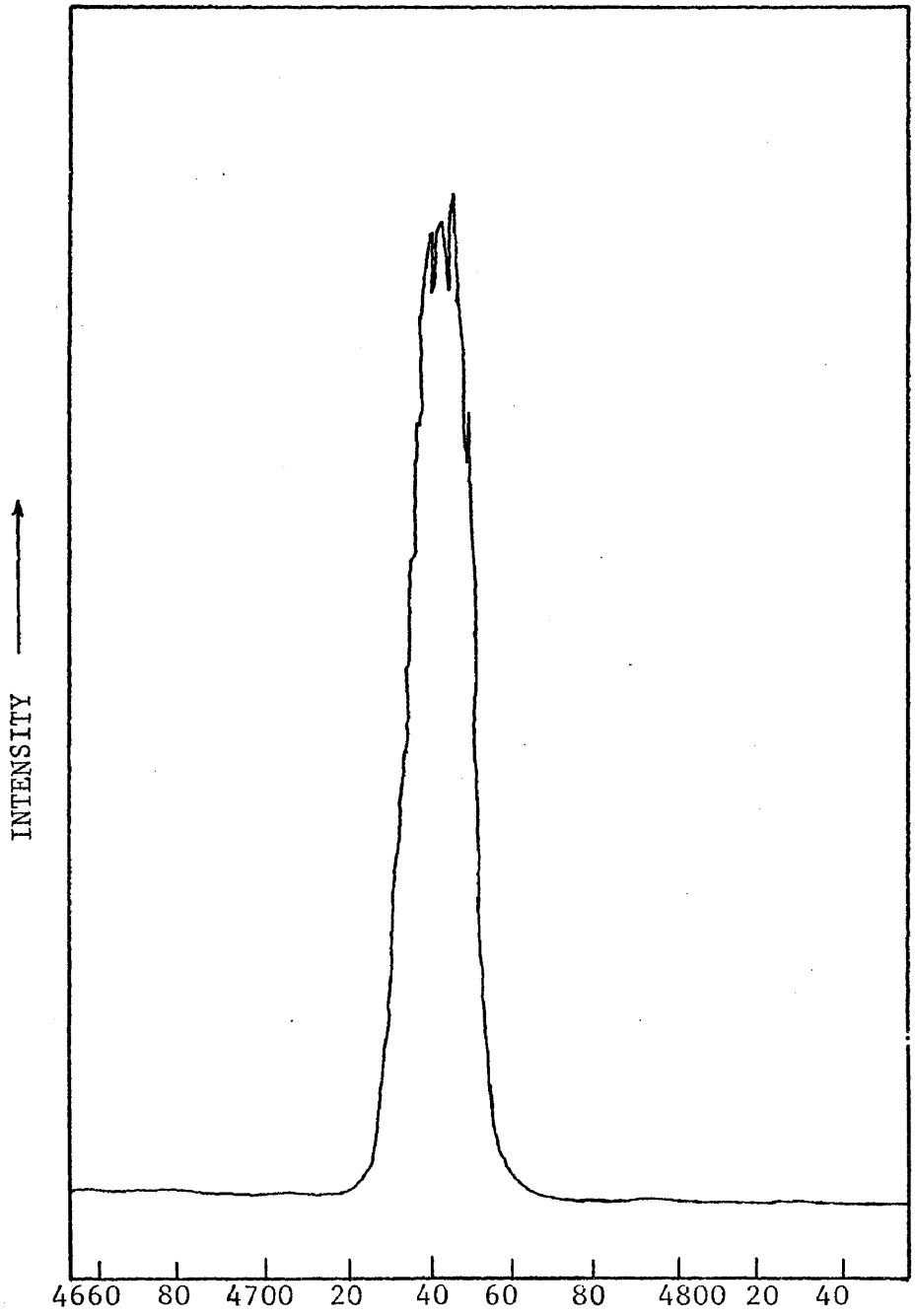

Figure AII-8. Wavelength scan of a line of a grating tuned laser using 7-diethylamino-4-methylcoumarin.

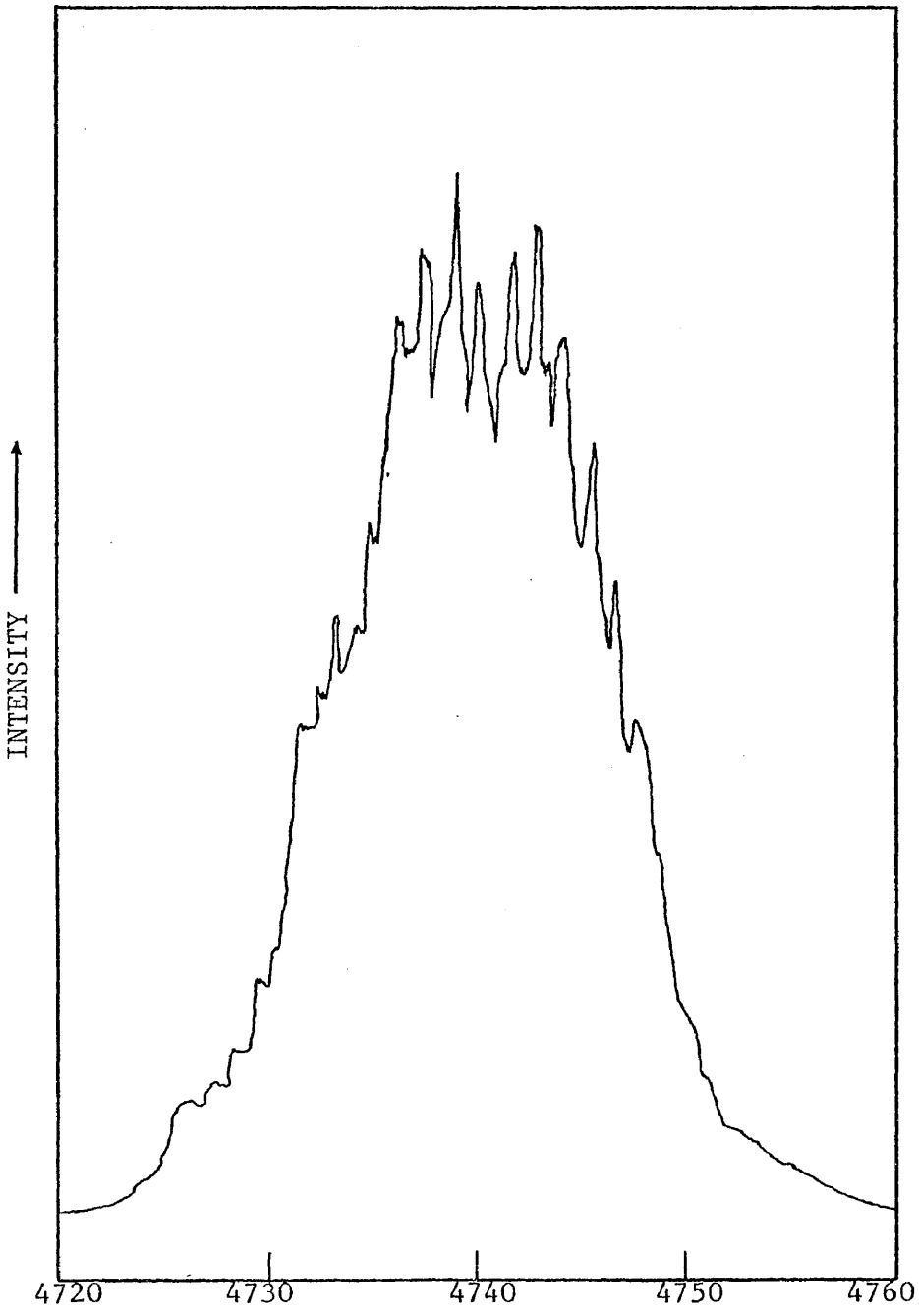

Figure AII-9. Higher resolution scan of the laser line in figure AII-8 showing a width of 15 angstroms at FWHM.

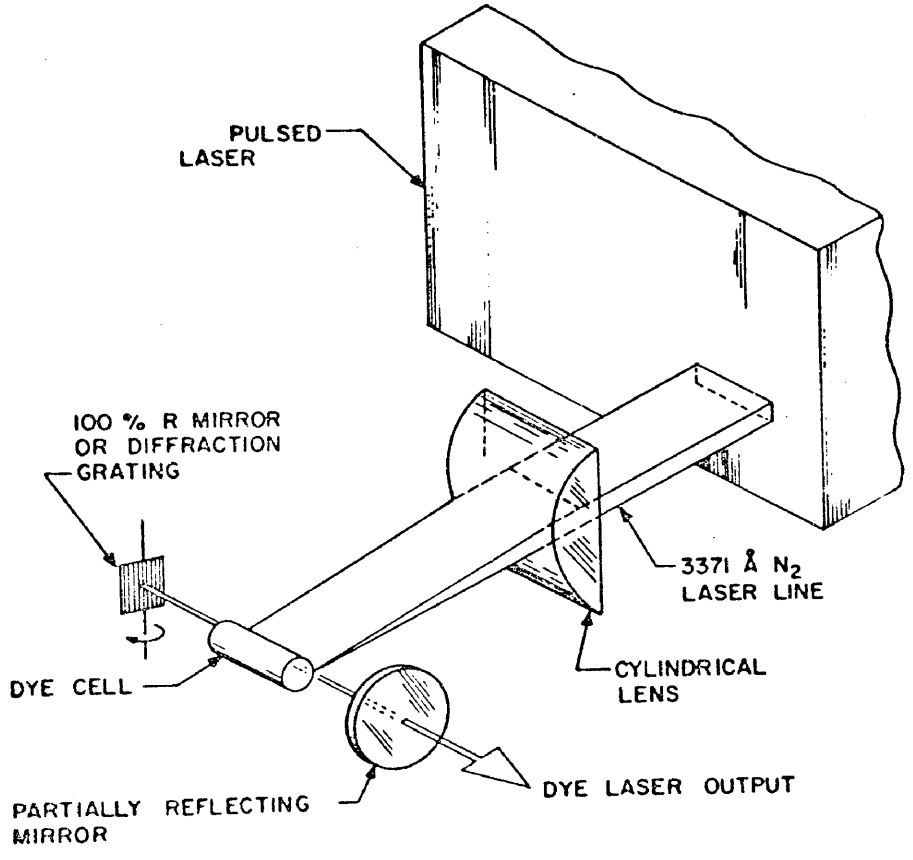

Figure AII-10. Schematic diagram of a tunable dye laser [48].

provision for adding a beam expanding telescope as proposed by Hänsch.[49,50] Tunable wavelengths from 3550 angstroms to 6500 angstroms[47] are possible using a nitrogen laser pump and longer wavelengths to the near infrared (1.2μm)[49] are possible using fast flashlamps or Q switched ruby lasers as the pump source. Table AII-1 shows the characteristics of dyes pumped by a nitrogen laser. The list is by no means complete as many more compounds are known which lase, and new ones are being developed as research in this area continues.

Probably the only real limitation of the dye laser is that it cannot be Q switched to give tremendously high peak powers. This limitation is intrinsic to dyes because their high spontaneous fluorescence rates preclude any integrated pumping of excited-state population for times greater than their spontaneous lifetimes (a few nanoseconds). Ruby and neodymium have millisecond lifetimes during which excited state populations can be pumped up, thus, dyes obviously do not provide the energy storage capacity for extremely energetic pulses. That is, for pumping times longer than a few nanoseconds, the dye laser output will be in equilibrium with the pumping intensity.

In addition to the low cost of the laser-active material, the potential impact of the dye laser is further emphasized by its inherent simplicity, which is made possible by the large gain of organic dye solutions pumped by a pulsed nitrogen laser.

TABLE AII-1

Characteristics of dye laser excited by pulsed N_2 laser.

Dye	Spectral Range (Angstroms)	Peak Power Ratios	Pulse Width (nsec)
Rhodamine 6G	6200-5650	0.22 at 6000A	4
7-diethylamino-4- methylcoumarin	4900-4450	0.25 at 4650A	5
		0.27 at 4500A	5
POPOP	4450-3900	0.13 at 4650A	8
		0.18 at 4500A	8
Fluorescein	6000-5200	0.20 at 6000A	4
		0.03 at 5500A	7
Diphenyl-anthracene	4500-4350	0.08 at 4500A	2
Diphenyl-stilbene	4200-4000	0.23 at 4050A	8
alpha-NPO	4135-3925	0.12 at 3950A	8

POPOP is 2,2'-p-Phenylenebis (5-phenyloxazole)

alpha-NPO is 2-(1-naphthyl)-5-phenyloxazole

p-quaterphenyl lases from 3960 to 3620 angstroms and[51]

p-terphenyl lases in the region of 3410 angstroms[52]

The high spectral purity, near diffraction-limited beam divergence, and convenient reproducible wavelength tunability render this laser as a powerful tool for optical spectroscopy. The short pulse width makes the laser particularly well suited for dynamic studies such as measurments of life times and relaxation rates.

REFERENCES

1. M. Kasha, Disc. Faraday Soc. 9, 14 (1950).

2. T. Deinum, C. J. Werkhoven, J. Langelaar, R.P.H. Rettschnick, and J. D. W. Van Voorst, Chem. Phys. Lett. 27, 210 (1974).

3. A. Nitzan, J. Jortner, and P. M. Rentzepis, Proc. R. Soc. London 327, 367 (1972).

4. A. Nitzan, Molecular Physics 28, 559 (1974).

5. William Rhodes, J. Chem. Phys. 4, 259 (1974).

6. P. Wannier, P. M. Rentzepis, and J. Jortner, Chem. Phys. Lett. 10, 102 (1971).

7. T. Deinum, C. J. Werkhoven, J. Langelaar, R. P. H. Rettschnick, and J. D. W. Van Voorst, Chem. Phys. Lett. 28, 51 (1974).

8. Akira Nakajima, Bul. Chem. Soc. Japan 45, 1687 (1972).

9. P. A. Geldof, R. P. H. Rettschnick, and G. J. Hoytink, Chem. Phys. Lett. 4, 59 (1969).

10. Bernard Nickel, Chem. Phys. Lett. 27, 84 (1974).

11. T. Deinum, C. J. Werkhoven, J. Langelaar, R. P. H. Rettschnick, and J. P. W. Van Voorst, Chem. Phys. Lett. 12, 189 (1971).

12. P. Wannier, P. M. Rentzepis, and J. Jortner, Chem. Phys. Lett. 10, 193 (1971).

13. C. E. Easterly, L. G. Christophorou, and J. G. Carter, Chem. Soc. Faraday Trans. II 69, 471 (1973).

14. P. A. Geldof, R. P. H. Rettschnick, and G. J. Hoytink, Chem. Phys. Lett. 4, 59 (1969)

15. J. B. Birks, "Organic Molecular Photophysics", John Wiley and Sons, New York, 1973.

16. Richard N. Zare and Paul L. Dagdigan, Science 185, 739 (1974).

17. P. A. M. van den Bogaardt, R. P. H. Rettschnick, and J. D. W. Van Voorst, Chem. Phys. Lett. 18, 351 (1973).

18. G. J. Hoytink, Chem. Phys. Lett. 22, 10 (1973).

19. F. B. Dunning and R. F. Stebbings, Optics Comm. 11, 112 (1974).

20. G. E. Busch, P. M. Rentzepis, and J. Jortner, J. Chem Phys. 56, 361 (1972).

21. R. M. Hochstrasser and J. E. Wessel, Chem. Phys. Lett. 19, 156 (1973).

22. J. B. Birks, "Photophysics of Aromatic Molecules", John Wiley and Sons-Interscience, New York, (1970).

23. I. B. Berlman, H. O. Wirth, and O. J. Steingraber, J. Am. Chem. Soc. 90, 566 (1968).

24. Josef Michl, J. Mol. Spec. 30, 66 (1969).

25. E. W. Thulstrup and J. H. Eggers, Chem. Phys. Lett. 1, 690 (1968).

26. Ronald E. Brown, K. D. Legg, M. W. Wolf, L. A. Singer, and J. H. Parks, Analytical Chem. 46, 1690 (1974).

27. Ivan Isenberg and Robert Dyson, Biophysical Journal 9, 1337 (1969).

28. W. R. Ware, Sai K. Lee, Gary J. Brant, and Peter D. Chow, J. Chem. Phys. 54, 4729 (1971).

29. W. R. Ware, L. J. Doemeny, and T. L. Nemzek, J. Phys. Chem. 77, 2039 (1973).

30. D. A. Leonard and W. R. Zinky, Applied Phys Lett. 12, 113 (1968).

31. D. A. Leonard, IEEE Jour. of Quantum Electronics 3, 113 (1967).

32. D. A. Leonard, R. A. Neal, and E. T. Gerry, Applied Phys Lett. 7, 175 (1965).

33. W. T. Walter, M. Piltch, N. Solimene, and G. Gould, Bul. Am. Phys. Soc. 11, 113 (1966).

34. G. R. Fowles and W. T. Silfvast, Applied Phys. Lett. 6, 236 (1965).

35. D. A. Leonard, Applied Phys. Lett. 7, 4 (1965).

36. D. A. Leonard, Laser Focus 3, 26 (1967).

37. Peter Schenck and Harold Metcalf, Applied Optics 12, 183 (1973).

38. E. T. Gerry, Applied Phys. Lett. 7, 6 (1965).

39. C. Parker, "Photoluminescence of Solutions", Elsevier Pub. Co., (1970).

40. O. G. Peterson, J. P. Webb, W. C. Colgin, and J. H. Eberly, Jour. of Applied Phys. 42, 1917 (1971).

41. J. S. Kruger, Electro Optical Systems Design 4, 12 (1972).

42. R. Pappalardo, H. Samelson, and A. Lempicki, Applied Phys. Lett. 16, 267 (1970).

43. B. B. Snavely, Proc. IEEE 57, 1374 (1969).

44. T. W. Hänsch, Applied Optics 11, 895 (1972).

45. S. A. Myers, Optics Comm. 4, 187 (1971).

46. J. Pierce Webb, Analytical Chemistry 44, 30 (1972).

47. G. Capelle and D. Phillips, Applied Optics 9, 2742 (1970).

48. J. A. Myer, C. J. Johnson, E. Kierstead, R. D. Sharma, and Irving Itzhan, Applied Phys Lett. 16, 3 (1970).

49. Theodore W. Hänsch, "Atomic Physics" 3, 579 (1972).

50. H. P. Broida and S. C. Haydon, Applied Phys. Lett. 16, 142 (1970).

51. J. T. Warden and Lucille Gough, Applied Phys. Lett. 19 345 (1971).

52. J. A. Myer, I. Itzhan, and E. Kierstead, Nature 225, 544 (1970).